

# **Study of Protein Organization in Phospholipid Bilayers with Inserted Synthetic Lipid Droplets**

Dissertation  
zur Erlangung des Grades  
des Doktors der Naturwissenschaften  
der Naturwissenschaftlich-Technischen Fakultät  
der Universität des Saarlandes

von  
**Sevde Puza**

Saarbrücken

2023

Tag des Kolloquiums: 25.05.2023

Dekan: Prof.Dr.Ludger Santen

Berichterstatter/in: Prof.Dr.Ralf Seemann

Prof.Dr.Jochen Hub

Vorsitzende/r: Prof.Dr.Albrecht Ott

Akademischer Mitarbeiter/in: Dr. Anne Holtsch

# Table of Contents

List of Figures .....	i
List of Tables .....	iv
Acknowledgements.....	v
Abstract.....	vi
Zusammenfassung .....	vii
1 Introduction .....	1
2 Overview And Connectivity.....	2
BACKGROUND AND STATE OF THE ART.....	4
3 Background and State of the Art .....	5
3.1 Membrane Phospholipids .....	5
3.2 Lipid Packing Defects.....	8
3.3 Mobility in a Membrane.....	11
3.4 Lipid Droplet Biogenesis.....	12
3.4.1 Structure and Formation .....	13
3.4.2 Equilibrium Shape of the Lipid Droplets.....	14
3.5 Lipid Droplet Associated Proteins .....	17
3.5.1 Insertion and Trafficking.....	17
3.5.2 Overview of the Studied Proteins.....	19
3.5.3 Effect of Lipid Packing on Localization .....	23
3.6 Model Systems in Literature For Studying Lipid Droplets.....	26
MATERIALS AND METHODS .....	30
4 Materials and Methods.....	31
4.1 Materials .....	31
4.1.1 Lipids and Oil .....	31
4.1.2 Fluorescence Probes.....	33
4.2 Preparation Methods .....	34
4.2.1 Microfluidic Device Preparation.....	34
4.2.2 Bilayer Formation .....	36
4.2.3 Formation of Lipid Droplets.....	37

4.2.4 Formation of PLDs containing UBXD8 Protein .....	38
4.2.5 Formation of PLDs containing Cav1 <sub>1-17</sub> Peptides.....	39
4.2.6 Formation of PLDs containing ADRP Proteins .....	40
4.2.7 Artificial Lipid Monolayer Formation.....	40
4.2.8 Droplet Interface Bilayer (DIB) Formation .....	41
4.3 Microscopy .....	42
4.3.1 3D Imaging .....	42
4.3.2 FRAP .....	43
4.4 Patch Clamp Recordings.....	45
4.5 Interfacial Tension Measurements .....	47
4.6 Molecular Dynamics Simulations .....	48
RESULTS and DISCUSSION.....	49
5 Results and Discussion .....	50
5.1 Bilayer Characterization .....	50
5.2 Insertion of LDs and Proteo-LDs.....	53
5.3 Studying Wetting Phenomenon for LDs and PLDs .....	59
5.4 Lipid Diffusion Barrier.....	65
5.5 Molecular Dynamic Simulations.....	70
5.6 Protein Partitioning Due To Lipid Packing.....	72
5.7 Exchange Kinetics of Proteins and Phospholipids.....	79
SUMMARY .....	83
6 Summary .....	84
CONCLUSION and OUTLOOK.....	86
7 Conclusion and Outlook.....	87
REFERENCES .....	89

## LIST OF FIGURES

---

Figure 1 Schematic structure of a cell membrane with membrane proteins .....	6
Figure 2 Lipid composition of different membranes in cell. The blue and light blue colors in graphs represent the mammalian and yeast cells, respectively .....	7
Figure 3 Critical packing parameter due to the molecular shape and resulting self-assembly entities. ....	9
Figure 4 Schematic demonstration of LD biogenesis steps .....	14
Figure 5 Schematic representation of contact angles for (A) bilayer (B) all stages of the formation of a lipid droplet considering the wetting theory.....	17
Figure 6 Schematic representation of the insertion of Class I and Class II proteins shows that Class I proteins bind LD monolayer through the bilayer, and Class II proteins bind to the surface directly from cytosol. ....	18
Figure 7 Schematic description of proposed membrane topology of UBXD8.....	20
Figure 8 Schematic description of SRP-mediated targeting (left) for most bitopic or polytopic membrane proteins and PEX-19 mediated targeting (right) for UBXD8 proteins.....	21
Figure 9 Schematic description of Caveolin-1 domains that let interaction with membrane and other proteins (A). Anchored shape of Cav1 via membrane insertion (B) .....	22
Figure 10 Differences in lipid packing between a bilayer and LD monolayer. The yellow area shows neutral lipid core of the LD (A). Amphipathic helices (AH) interaction with the bilayer (left) and LD monolayer (right) in presence of packing defects (B). Interaction of AH containing protein (C). Interaction of hairpin protein with the bilayer and the lipid droplet (D) .....	24
Figure 11 Example systems to study lipid droplets and associated proteins A) Giant unilamellar vesicle (GUV) and Droplet-embedded vesicle (DEV) systems. (B) Double interface bilayer (DIB) Systems .....	27
Figure 12 Example MD simulation systems to study the accumulation of triolein in the bilayer. (A) Side view of triolein accumulation trend depend on increasing amount of triolein in POPC bilayers. (B) Side view of the in silico-model (upper view) and top view showing the accumulation of triolein due to the increasing PC bilayer surface tension.....	28
Figure 13 Chemical Structures of Lipids, Cholesterol and Squalene oil used in the experiments	33
Figure 14 Schematic representation of steps of photolithography (A) and soft-lithography (B).	35
Figure 15 Combination of Aluminum based cone and channel on silicon wafer (left). Positioning the cone at the middle of the channel (upper right image). Final device (lower right image) (A). Schematic representation of the device from top (left) and side (right) view (B). The two inlets are used to introduce the components for the experiments. ....	36
Figure 16 Steps of bilayer formation (A). Oil drainage by the walls of PDMS before the bilayer is formed (B) .....	37
Figure 17 In vitro translated UBXD8 proteins are reconstituted in the protein-free liposomes composed of POPC:DOPS (1:9 mol%). A biphasic of triolein/buffer is formed and sonicated. The product is protein containing lipid droplets. ....	38

Figure 18 Predicted IDDT per position for Cav1 <sub>1-17</sub> by AlphaFold2 IA (A). Sequence by Heli Quest analysis (B). .....	39
Figure 19 Scheme of the microfluidic device to form the artificial LD monolayer by decorating the phospholipids on the triolein-buffer interface .....	41
Figure 20 Schematic representation of DIB experiments.....	42
Figure 21 Representation of the principle of FRAP experiments and explanation of the steps by schematic drawing and graph.....	44
Figure 22 Positioning of Ag/AgCl electrodes into the microfluidic device (A) and the principle of patch clamp measurements of the bilayer (B). .....	46
Figure 23 A typical drop image and schematic description of how the geometry of the droplet is fitted to obtain surface tension value (A). A typical drop image where the buffer phase (0.1 M NaCl) is formed in a mixture of squalene and phospholipids DOPC:DOPE:DOPS (60:30:10 mol%) (B). Corresponding change of IFT (Interfacial tension) by time until the fixed surface tension value is obtained (C). .....	48
Figure 24 Capacitance measurement of a bilayer formation with bright-field images. ....	51
Figure 25 FRAP experiments on the bilayer for the bilayer composition DOPC:DOPE:DOPS (60:30:10 mol%) labelled with Atto DOPE-647N. Scale bars with arrows denote 15 $\mu$ m for x and y (A). FRAP data for three equivalent areas presented with dots in green, blue and red. The Soumpasis equation fitted to the data presented by the black line (B).....	52
Figure 26 Lipid droplets labelled with BODIPY 493/503 on a non-fluorescent bilayer with a composition of DOPC:DOPE:DOPS (60:30:10 mol%). .....	53
Figure 27 Fluorescence microscopy images of the lipid bilayer (left image) and LDs (middle two images) in bulk. Scale bars are 100 $\mu$ m, 10 $\mu$ m, and 1 $\mu$ m for bilayer, LDs, and single LD images, respectively (A). z-stack images of LD before (upper image, t $\approx$ 5 min) and after (bottom image, t $\approx$ 10 min) touching the bilayer (B). Lipid bilayer before and after LD insertion (C). Scale bars with arrows, 5 $\mu$ m for x and z .....	54
Figure 28 3D representation of a lipid droplet (in yellow) inserted in the 40 mol% cholesterol including bilayer (in red). Scale bars with arrows show 10 $\mu$ m in the upper panel (A). The xz plane of a lipid droplet insertion. Scale bars for the lower panel; 10 $\mu$ m for x and 2 $\mu$ m for z (B).....	55
Figure 29 Schematic representation of the PLD-UBXD8 insertion pathway (A). Fluorescence images of the bilayer (red signal, Atto DOPE) containing PLDs (green signal, Atto488). The scale bar shows 15 $\mu$ m (B). z-stacks from the bilayer core through the PLD top (upper row). Scale bars denote 15 $\mu$ m and 10 $\mu$ m (x,y) for upper and lower rows, and z-arrows show 1 $\mu$ m for the lower left two images and 700 nm for the right image (C) .....	56
Figure 30 3D confocal images of an bilayer inserted PLD containing Cav1 <sub>1-17</sub> . Channels are shown for LD and proteins in green and red colors, respectively. Scale bars with arrows denote 5 $\mu$ m (x,y, and z) (A) and 5 $\mu$ m (B) and 2 $\mu$ m (C) for (x and z).....	57
Figure 31 The typical pancake shape of Proteo-LDs containing ADRP proteins inserted into the bilayer. Scale bar denotes 5 $\mu$ m for x,y, and z. ....	58

Figure 32 2D surface plot projections (left two rows) and corresponding confocal images (right rows) of LDs for bilayer-cholesterol compositions 40%, 30%, and 20% from top to bottom. Scale bars denote 5 $\mu\text{m}$ and 200 nm for x and z planes, respectively .....	59
Figure 33 Schematic representation of surface forces acting on the bilayer (A) on a LD in the bilayer for the symmetric (upper) and asymmetric (lower) case (B) .....	60
Figure 34 Comparison with the wetting theory for bilayer embedded LDs for 20%,30% and 40% cholesterol, and PLDs containing UBXD8 protein for 0% cholesterol .....	62
Figure 35 3D confocal images of bilayer embedded PLDs for 0%, 20% and 40% cholesterol, and bilayer embedded LD for 0% cholesterol (A). Comparison with the wetting theory (B) .....	64
Figure 36 Area selection in the area of lipid droplet and bilayer. For bleaching the molecules on LD surface, entire surface of the lipid droplet, and for the bilayer, a bleaching area at the center of the entire bilayer is selected. ....	65
Figure 37 FRAP measurements on the neutral core of the lipid droplet with a size of 5 $\mu\text{m}$ inserted into a bilayer. The area is bleached for 20 seconds .....	66
Figure 38 3D representation of the selection of areas for LD and bilayer before bleaching. Scale bars are 10 $\mu\text{m}$ for all directions (A). FRAP experiments on the bilayer (upper row) and the entire LD (lower row) for the bilayer composition DOPC/DOPE/DOPS (60:30:10 mol%) labelled with Atto DOPE-647N. The scale bar shows 25 $\mu\text{m}$ and 10 $\mu\text{m}$ , respectively (B).....	67
Figure 39 FRAP curves for LD and bilayer after bleaching an area labelled with Atto-DOPE with a diameter of 30 $\mu\text{m}$ for 20 sec .....	69
Figure 40 FRAP curves after bleaching an area labelled with Cy5-PC with a diameter of 30 $\mu\text{m}$ for 20 sec in the LD monolayer.....	70
Figure 41 Equilibrated CG simulation of an LD. The red color is the neutral lipids and phospholipids are shown as green/blue/white sticks in the simulations. The detailed simulation of the side view consists of DOPC in blue, DOPE in orange, and DOPS in pink.....	71
Figure 42 Coarse-grained numerical simulations representing the lateral lipid densities on a LD monolayer and surrounding bilayer. The lipid composition is set to DOPC:DOPE:DOPS (60:30:10 mol%) for bilayer. TAG composition is set to 537 triacylglycerol.....	71
Figure 43 Schematic description of the insertion of PLDs consist of Cav1 <sub>1-17</sub> into the bilayer ....	73
Figure 44 Confocal images of the lipid droplets inserted on the bilayer by 2D and 3D representations. Scale bars with the arrows are 5 $\mu\text{m}$ for x,z (2D images) and 10 $\mu\text{m}$ for x,y and z (3D images) for DOPC/DOPE experiments. Lipid droplet core and the Cav1 <sub>1-17</sub> proteins are shown in green and red, respectively. ....	74
Figure 45 Schematic representation of how protein partitioning can be explained by the evaluated P value.....	75
Figure 46 Confocal images of protein partitioning between the LD (in green) and bilayer (in red) to show the distribution of proteins with respect to increased lipid packing in the bilayer (A). Partition coefficients for the bilayers composed of DOPC/DOPE and POPC/POPE (B).....	76
Figure 47 DIB examples of bilayer intensities for DOPC/DOPE and POPC/POPE for the molar ratios 1:1, 1:2 and 1:3. ....	77

Figure 48 Relative bilayer intensity due to PC/PE ratio for all bilayer compositions for DIB experiments. .... 78

Figure 49 FRAP data obtained for Cav1<sub>1-17</sub> proteins and DOPE lipids in the bilayer with a composition DOPC:DOPE:DOPS (60:30:10 mol%). .... 79

Figure 50 (A) Area of Cav1<sub>1-17</sub> proteins on LD area (dashed circle) and DOPE in the bilayer area composed of DOPC:DOPE:DOPS (60:30:10 mol%) for FRAP experiments. Scale bar shows 10 μm. (B) Schematic of FRAP in the LD area (C) FRAP data obtained for proteins and lipids in the LD monolayer. .... 80

Figure 51 (A) FRAP experiments on the lipid monolayer with a composition of DOPC:DOPE (3:1). The images correspond to DOPE-Cy5 (2% mol) (upper row) and ADRP-Alexa488 (lower row). (B) FRAP data obtained for LD monolayer and bilayer embedded LD experiments..... 82

## LIST OF TABLES

---

Table 1 Characterization of a bilayer including embedded LDs and PLDs containing UBXD8 protein ..... 61

Table 2 Characterization of a bilayer including embedded LDs and PLDs containing ADRP protein by using the values obtained by Interfacial Tension measurements ..... 63

Table 3 Comparison of lateral diffusion of lipids from the LD surface to the bilayer and in pure lipid bilayer by coarse-grained MD simulations ..... 72



## **ACKNOWLEDGEMENTS**

---

I would like to thank my advisor Prof. Ralf Seeman, for giving me the opportunity to be a part of the team, for the guidance, and for being family-friendly throughout my study. I will also always be grateful to Dr. Jean Baptiste Fleury for the endless support, for leading me, and for always creating suitable time for scientific discussions. I would like to express my appreciation to Jun. Prof. Bianca Schrul and Prof. Jochen Hub for the helpful meetings and collaboration. I appreciate my lab mates, who always helped me when I needed. My special thanks to Dr. Michael Jung and Pegah Shakeri, whose support and friendship added a lot to my life.

Last but not least, overcoming all the difficulties during that time would not be possible without my husband, Dr. Fatih Puza. I would like to thank him for his love and understanding and for being a great dad. I am grateful to my daughter, Defne Puza, for being my life energy and being with me when I was completing the tough steps of PhD. I would like to thank my parents who always guided me professionally with their engineer identities, and also took care of my daughter as grandparents. I am thankful to all my family for teaching me how to cope with difficult situations and also enjoy life.

This thesis is dedicated to my beloved daughter, Defne Puza...

## ABSTRACT

---

Lipid droplets (LDs) are the main fat storage organelles of the cell that originates from the endoplasmic reticulum (ER) membrane. They are composed of a neutral lipid core surrounded by a phospholipid monolayer that is decorated by proteins. These proteins have an important role in regulating lipid storage and consumption, which is directly the source of several metabolic diseases like obesity. A key question about these proteins is, how they are partitioning between a phospholipid bilayer and LD monolayer membranes. To address this question, a free-standing bilayer with a physiologically relevant composition is produced in a 3D microfluidic device. Afterward, the artificially formed LDs with and without proteins are introduced to the device and waited until they are inserted into the bilayer and equilibrated. The 3D geometries of LDs and the distribution of proteins in the monolayer and bilayer are explored as a function of bilayer composition. For the protein UBXD8<sub>71-132</sub> with a hydrophobic domain, it has been found that the accumulation of proteins on the LD monolayer induced an asymmetric bulged lipid droplet. The protein ADRP, which has an affinity to surfaces of LDs, enriched non-homogenously all over the LD's surface and displayed a pancake shape, however, the hairpin-like peptides Cav1<sub>1-17</sub> are freely diffused through the LD core which resulted in a symmetric shape. Fluorescence recovery after the photobleaching (FRAP) technique is applied and the following insights about the dynamics of proteins and phospholipids are obtained. The existence of a phospholipid diffusion barrier at the interface of the bilayer and monolayer is observed and rationalized by coarse-grained molecular dynamic simulations by revealing the lipid-specific density distributions along the pore rim. The dynamics of the proteins and phospholipids show that in presence of hairpin-like proteins in the system, the lipid diffusion barrier is weakened. However, when there are ADRP proteins on the lipid droplet, the lipid diffusion barrier is destroyed which means that the transport of lipid molecules is facilitated. Further studies with Cav1<sub>1-17</sub> peptide have demonstrated that the partitioning of the proteins is regulated by the lipid bilayer packing. Hence, hairpin-like proteins are partitioned more on the lipid droplet when there are more defects in the bilayer. The results about the dynamics of proteins and phospholipids, and the effect of lipid packing give new insight into the possible mechanisms controlling the partitioning of proteins.

## ZUSAMMENFASSUNG

---

Lipidtröpfchen (LDs) sind die wichtigsten Fettspeicherorganellen der Zelle, die aus der Membran des endoplasmatischen Retikulums (ER) stammen. Sie bestehen aus einem neutralen Lipidkern, der von einer Phospholipid-Monoschicht umgeben ist, die mit Proteinen verziert ist. Diese Proteine spielen eine wichtige Rolle bei der Regulierung der Speicherung und des Verbrauchs von Lipiden, die direkt die Quelle mehrerer Stoffwechselerkrankungen wie Fettleibigkeit sind. Eine Schlüsselfrage zu diesen Proteinen ist, wie sie sich zwischen einer Phospholipid-Doppelschicht und LD-Monoschicht-Membranen aufteilen. Um diese Frage zu beantworten, wird eine freistehende Doppelschicht mit einer physiologisch relevanten Zusammensetzung in einem 3D-Mikrofluidikgerät hergestellt. Danach werden die künstlich gebildeten LDs mit und ohne Proteine in das Gerät eingeführt und gewartet, bis sie in die Doppelschicht eingefügt und äquilibriert sind. Die 3D-Geometrien von LDs und die Verteilung von Proteinen in der Monoschicht und Doppelschicht werden als Funktion der Doppelschichtzusammensetzung untersucht. Für das Protein UBXD8<sub>71-132</sub> mit einer hydrophoben Domäne wurde festgestellt, dass die Akkumulation von Proteinen auf der LD-Monoschicht ein asymmetrisch gewölbtes Lipidtröpfchen induzierte. Das Protein ADRP, das eine Affinität zu Oberflächen von LDs hat, reicherte sich inhomogen über die gesamte Oberfläche der LD an und zeigte eine Pfannkuchenform, jedoch diffundieren die haarnadelartigen Peptide Cav1<sub>1-17</sub> frei durch den LD-Kern, was zu einer Symmetrie führte gestalten. Die Fluoreszenzwiederherstellung nach Anwendung der Photobleichtechnik (FRAP) und die folgenden Erkenntnisse über die Dynamik von Proteinen und Phospholipiden werden erhalten. Die Existenz einer Phospholipid-Diffusionsbarriere an der Grenzfläche von Doppelschicht und Monoschicht wird beobachtet und durch grobkörnige molekulardynamische Simulationen erklärt, indem die lipidspezifischen Dichteverteilungen entlang des Porenrandes aufgedeckt werden. Die Dynamik der Proteine und Phospholipide zeigt, dass in Anwesenheit von Haarnadel-ähnlichen Proteinen im System die Lipid-Diffusionsbarriere geschwächt wird. Wenn sich jedoch ADRP-Proteine auf dem Lipidtröpfchen befinden, wird die Lipiddiffusionsbarriere zerstört, was bedeutet, dass der Transport von Lipidmolekülen erleichtert wird. Weitere Studien mit dem Peptid Cav1<sub>1-17</sub> haben gezeigt, dass die Partitionierung der Proteine durch die Lipiddoppelschichtpackung reguliert wird. Daher werden Haarnadel-ähnliche Proteine mehr auf dem Lipidtröpfchen verteilt, wenn mehr Defekte in der Doppelschicht vorhanden sind. Die Ergebnisse über die Dynamik von Proteinen und Phospholipiden und den Effekt der Lipidpackung geben neue Einblicke in die möglichen Mechanismen, die die Partitionierung von Proteinen steuern.

# 1 INTRODUCTION

---

Cells are the building blocks of living organisms. The observation of the first cell is dated to the 17<sup>th</sup> century by Robert Hooke by his simple microscopy technique of reflecting the light by using three different lenses and stage light. With the development of microscopy techniques over the centuries, it has been realized that cells are complex systems, which are constituted by organelles and nanometer-size structures including membranes, lipid droplets, or vesicles which consist of lipids and proteins. One main responsibility of the lipids is to store the energy in form of “lipid droplets,” which originate after the accumulation of neutral lipids in the Endoplasmic reticulum membrane, where the membrane lipids and proteins are synthesized. Disproportionate lipid storage is the source of several metabolic diseases such as obesity and diabetes [1]. As many proteins take part in the correct functioning of lipid droplets (LDs), the questions about how the proteins target lipid droplets and how they relocate between the bilayer and lipid droplets become important. The remaining questions about the protein movement between the bilayer and the lipid droplet, so-called partitioning, caught our attention to mimic each component in a model membrane platform.

The very first platforms to create an artificial bilayer were black lipid membranes (BLMs) and supported lipid bilayer membranes which brought some limitations such as low diffusivity of the membrane components due to underlying substrate or low stability [2]. To overcome these limitations, an alternative method was created via the fusion of the two free-standing lipid monolayers to create a bilayer [3]. The fluidity of the bilayer components could be mimicked closer to a physiological situation with a fluidity similar to a cell membrane without any undesired boundary effects from the solid support. If the bilayer is formed in a 3D microfluidic device, a full view of the bilayer area in all directions can be achieved [4]–[6]. The electrophysiological measurements (patch-clamp) can be performed on these bilayers, while the device allows contacting the sample by electrodes.

In this thesis, a 3D microfluidic system has been created for the studies of bilayers, lipid droplets, and protein interactions. The model system enables obtaining a free-standing bilayer in a fluid state like an ER membrane with a composition that can be freely adjusted. The artificial LDs were inserted into the bilayer and their shape differences were observed. The role of different bilayer compositions on the geometry of lipid droplets was explained by wetting theory. By using LD-associated proteins (UBXD8<sub>71-132</sub>, Cav1<sub>1-17</sub>, ADRP), the obtained results reveal that the lipid droplet symmetry and partitioning of the proteins between the LD and the bilayer could be crucially related to the protein type as well as the bilayer packing.

## 2 OVERVIEW AND CONNECTIVITY

---

The purpose of this thesis is to present a new perspective to study lipid droplets and associated proteins to extend the current knowledge about protein partitioning from a biophysical point of view. The main motivation to build up a simple microfluidic system was to create a stable free-standing bilayer to study membrane components such as phospholipids, lipid droplets, proteins, or ion channels. For analyzing the components of the bilayer, this platform should also be compatible with 3D fluorescence imaging. Considering these, a 3D microfluidic device was developed to create a horizontal bilayer to investigate each component with a full area view of the bilayer with the desired composition. The bilayer was formed via the fusion of two monolayers by trapping the oil and lipid mixture between two buffer phases, and the formation was demonstrated by two techniques. The patch-clamp technique was used to prove the bilayer thickness is similar to the thickness of a biological membrane, which should be around 3-5 nm when the formation is completed. As the membrane structure is in a fluid state in cells, the Fluorescence Recovery After Photobleaching (FRAP) technique was used to show the fluidity of the bilayer is similar to the fluidity of an ER membrane. To evaluate the functionality of 3D fluorescence imaging, the first study aimed to image the bilayer in the case of silicon oil inclusion. In the publication by *Tawfik et al. in Frontiers in Cell & Developmental Biology 2020*, the increased intensity of the silicon oil between two leaflets of the bilayer due to increasing silicon oil concentration in the bilayer could be measured precisely in all directions [7], which proved that the microfluidic device serves as a useful tool for 3D imaging of the bilayer with the desired composition.

Therefore, the artificial lipid droplets were inserted into the lipid bilayer in the desired composition to study their properties as shown in the publication by *Puza et al. Small 2022* [6]. Insertion angles of lipid droplets were investigated by 3D imaging. By applying the equilibrium wetting theory, it has been found that the reduction of insertion angle is driven by the increased bilayer tension which has been tuned by changing the membrane composition. The symmetry of the lipid droplets was broken when the UBXD8<sub>71-132</sub> hairpin protein was accumulated only on the lipid droplet monolayer. Finally, the FRAP measurements revealed a significant diminishment of phospholipid transfer at the LD monolayer-bilayer interface and it exhibits that there is a diffusion barrier at the LD rim which is confirmed by MD Simulations.

In the continuation of this study, a hairpin-like peptide Cav<sub>1-17</sub> was studied to follow the partitioning by tuning the PE amount and the packing of the bilayer. Cav1 protein presents a dynamic partitioning by freely diffusing between the ER membrane and LD monolayer surrounding. For simplicity, the Cav<sub>1-17</sub> peptide with a hairpin-like structure is selected as a model peptide to study the controlling mechanisms for protein partitioning. Proteo-LDs consisting of Cav<sub>1-17</sub> were introduced to the system after the bilayer formation. In addition to

biologically relevant lipid combinations (DOPC/DOPE, POPC/POPE), some other high-packing characteristic lipid combinations (DPhPC/DPhPE) were studied that allowed to test of different lipid packing characteristics. Increased packing defects in the bilayer related to the increased amount of PE caused a high preference for the LD monolayer compared to the bilayer. In the case of fewer packing defects in the bilayer, the hairpin-like peptides distribute uniformly. The results of mobility measurements have shown that the proteins and phospholipids are moving freely in the bilayer and nearly freely at the bilayer-LD monolayer interface. Although, the phospholipid diffusion barrier still exists but does not strong enough to block the partitioning of the proteins. This provides strong proof that partitioning is mainly controlled by bilayer packing.

The experiments have been performed by ADRP protein which is known to be associated with the surfaces of LDs as shown in the publication by *Puza et al. International Journal of Molecular Sciences 2023* [8]. After Proteo-LDs consisting of ADRP proteins were inserted into the bilayer, it has been observed that the non-homogeneous distribution of the ADRP protein caused the bilayer-embedded LDs to take a pancake shape which corresponds to an equilibrium wetting theory. The shape could be controlled by increasing the bilayer tension by increasing cholesterol concentration, which results in the increment of the insertion angle. The measurements of diffusion properties have shown that the ADRP molecules can diffuse freely on the LD surface as expected. Moreover, the ADRP proteins enable the transport of lipids and proteins along the LD rim by destroying the hypothesized phospholipid ring.

This thesis is sectioned into four main chapters as follows:

- In the chapter “**Background and State of Art**” membrane phospholipids, their organization, lipid droplets, and associated proteins are explained in the scope of the thesis. A brief overview is given about the insertion and trafficking ways of proteins, and the studies in artificial bilayer systems.
- The chapter “**Materials and Methods**” introduce the methods applied in the experiments, instruments, and materials used.
- The chapter “**Results and Discussion**” focuses on the results of the lipid droplet studies on the model membrane and summarizes the key findings.
- In the “**Conclusion and Outlook**” chapter, the results are summarized and presented as a guide for future research.

## **BACKGROUND AND STATE OF THE ART**

---

### 3 BACKGROUND AND STATE OF THE ART

---

Structures of cell and organelle membranes are important to ensure a protected interior by controlling the exchange of molecules through the membrane. The main components responsible to organize the structure of the membranes are phospholipids and proteins, and the distribution and interaction of these molecules determine the physical properties. In this chapter, a general introduction to the organization of phospholipids in cellular membranes and some of their key features such as fluidity and packing due to this dynamic organization will be introduced. The origination of lipid droplets from the lipid bilayer will be explained by defining the equilibrium shape of the droplets to demonstrate the insertion of synthetic lipid droplets into the bilayer. The factors taking a role in the partitioning of proteins between the lipid bilayer and lipid droplets are aiming to be clarified, and an overview about the proteins used in this thesis is given. As many model systems are used to mimic the lipid droplets in the bilayers for years, some examples of these systems from the literature will be given for the further understanding of the microfluidic system used in this thesis to study the proteins partitioning on the lipid droplet inserted bilayers.

#### 3.1 MEMBRANE PHOSPHOLIPIDS

One of the theories regarding the origin of life can be expressed as the “membrane-first” hypothesis. To ensure a proper life, the prior condition is to create a safe environment for each organelle in the cell, which is formed by membranes [9]. Membranes are everywhere in cellular systems to determine the boundaries between cells by separating each organelle from the interior. They are highly selective and semi-permeable gatekeepers, which are crucial for osmotic and electrical gradients for activities like neuron signal transduction and bioenergetics [10]. Further for all cells and organelles, membranes control the exchange of the type and number of substances that come in and go out. For instance, while small hydrophobic molecules like oxygen can cross a cell membrane easily, polar molecules like water and ethanol can pass in a slower way, whereas highly charged molecules such as ions diminish diffusion in the membrane. The cell membrane was first described as a continuum fluid-mosaic model by Singer and Nicolson in 1972. It is defined as a combination of lipids, cholesterol, and proteins, where proteins are partially or fully embedded in the lipid bilayer (**Figure 1**) [11], [12].



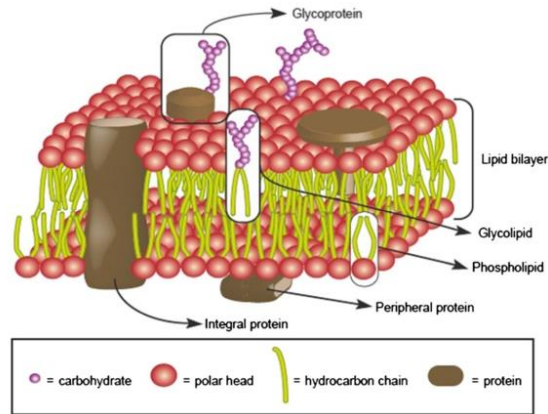


Figure 1 Schematic structure of a cell membrane with membrane proteins. Reproduced by permission of publisher [13].

In eukaryotic organisms, there are four major classes of lipids: glycerophospholipids, sphingolipids, glycerol glycolipids, and sterols. A typical cell uses 5% of its genes to synthesize thousands of these lipids to fulfill the specific functions of the cellular processes [18]. ER-localized enzymes take the role to synthesize the majority of these cell membrane phospholipids and cholesterol as well as triacylglycerol and cholesteryl esters. Lipids as well as proteins, are found in different quantities in the two leaflets of the biological membrane, and the lipid composition of each organelle membrane differs as shown in **Figure 2**. While the plasma membrane contains prominent levels of saturated lipids, cholesterol, and negatively charged lipids, the endoplasmic reticulum (ER) membrane is described by the high amount of monounsaturated acyl chains, a low amount of charged lipids, sterols, and complex sphingomyelins. For a yeast cell, the most significant lipids are PC and PE, which are forming in total around 90% of the membrane, whereas the rest are various kinds of lipids such as PI and PS [14].

The three main functions of the phospholipids should be categorized briefly to understand lipids' main roles. Firstly, lipids are serving as the energy storage organelles in the form of "lipid droplets" by storing the triacylglycerols and sterol esters in their cores. Before biogenesis, they are the neutral lipid accumulations in the ER membrane, which are serving as sufficient reservoirs to provide energy to the cell when needed for cellular processes. The second role of the lipids is to form the cellular membranes by self-organization which is necessary to create physical boundaries between the internal components of the cell and the external environment. This selective barrier is also crucial for the processes like budding, fission, fusion, cell division, and intracellular membrane trafficking. Finally, the ion channels in membranes take the role of signal transduction and molecular recognition process by forming pores with transmembrane proteins. This is crucial to transmitting a message out of the membrane [14]–[17].

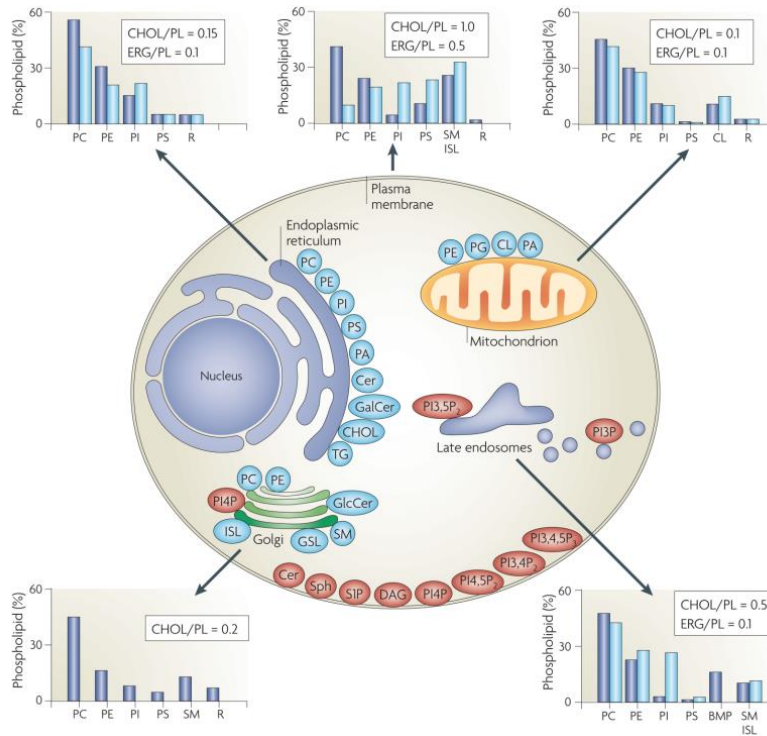


Figure 2 Lipid composition of different membranes in cell. The blue and light blue colors in graphs represent the mammalian and yeast cells, respectively. Reproduced by permission of publisher [14].

The composition of the membrane is dynamically regulated by the self-organization of lipids and other components. The amphiphilic molecular structure of the phospholipids led them to be organized to form the membrane structure. The head of the phospholipid consists of a glycerol unit which is attached to the fatty acids which can be called the tail part. The attachment is done by the binding of the fatty acids to the first two carbons of the glycerol unit. However, the common synthetic phospholipids are produced by further esterification of the phosphate group with an alcohol, such as choline, ethanolamine, serine, glycerol, or inositol for research studies. The resulting lipids can be listed as phosphatidylcholine (PC), phosphatidylethanolamine (PE), phosphatidylserine (PS), phosphatidylglycerol (PG) and phosphatidylinositol (PI). These lipids are either charged (like PS, PI, and PG) or dipolar (like PC and PE). A phospholipid molecule is identical to a triglyceride up to the phosphoric acid unit. These chemical properties of phospholipids lead to an association between the hydrophobic tails by the means of dispersion forces where the organization is entropically driven by water. The hydrophilic head of the lipid immerses in water, and the rest which is the hydrophobic tail, therefore immerses in nonpolar substances. As the hydrophilic heads tend to cooperate with each other, they orient through the aqueous environment, and the hydrophobic tails orient simultaneously in the opposite direction. This

dynamic organization ends up with a two-dimensional liquid system which is called a “bilayer.” As the hydrophobic tail is composed of some unsaturated fatty acids, so the components in the membrane are free to move, this feature helps to describe the membrane as fluid.

Maintenance of a stable membrane asymmetry is assured by specific proteins called ATPases by facilitating the transport of phospholipids between the two leaflets with simultaneous energy [18]. Specific membrane transport proteins permanently embedded in the membrane take part in molecular recognition and transportation. These transmembrane proteins are embedded in the membrane as a single  $\alpha$ -helix, multiple  $\alpha$ -helices, or  $\beta$ -barrels [19]. They organize their domains by facing the cytosolic side towards the cytoplasm, and the exoplasmic domain towards the exterior domain, and by interacting with the hydrophobic membrane core with the membrane-spanning domain. So, these membrane proteins can interact both with hydrophilic and hydrophobic structures due to their amphipathic nature.

The structures of lipids and proteins have an impact on the insertion of the proteins into the membrane. For example, a hydrophobic domain-containing protein prefers to be on the hydrophobic regions, and removal of these proteins from the membrane can be only done by detergents or non-polar solvents which results in damaging the membrane. Receptor proteins are another type of transmembrane protein and responsible to transmit information across the membrane. These proteins bind to the membrane by their extracellular domains when they recognize the specific ligands. By this, the conformation of the protein changes and carries the signal into the cell which is defined as the “signal transduction”. These receptors can be in the cytoplasm, nucleus, or membrane. The receptors that bind to cells are mainly categorized as ligand-gated ion channels, G-protein-coupled receptors, and receptor tyrosine kinases [20]. Contrary to transmembrane proteins, peripheral proteins attach to the membrane temporarily either from the cytosol or exterior domain without inserting into the membrane core due to their hydrophilic nature, while creating attachment sites for transmembrane proteins or openings for ion channels [21]. Peripheral proteins can be removed from the membrane by changing the salt levels or pH. Another class of proteins are lipid-anchored proteins. These proteins covalently bind to phospholipids from one leaflet without being fully embedded into the membrane. These anchors include phenyl groups, long-chain acyl, glycosyl-phosphatidylinositol (GPI), or cholesterol.

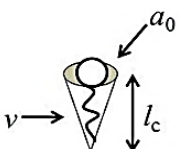
### **3.2 LIPID PACKING DEFECTS**

The geometry of lipids in the membrane has a key role in biomolecular interactions, especially with various classes of proteins. Here, it is aimed to clarify the meaning of packing defects for further understanding of the influence of lipid packing on protein localization. The term “defects”

originates from the imperfections created by the different geometry of lipids in the membrane. The packing parameter determines the curvature and the shape of a membrane, which is originating from the different geometry of the molecules such as cone, truncated cone, inverted cone, or cylinder (**Figure 3**). The packing parameter ( $P$ ) can be defined as:

$$P = \frac{V}{a_0 l_c} \quad (1)$$

Where  $V$  and  $l_c$  are the volume and length of the hydrophobic tail and  $a_0$  is the hydrophilic head cross-section area. Different geometrical structures formed by distinct critical packing shapes can be summarized as shown in **Figure 3**.



$$CPP = v/a_0 l_c$$

Critical Packing Parameter ( $v/a_0 l_c$ )	Critical Packing Shape	Structures Formed
$< 1/3$	Cone	Spherical micelles
$1/3 - 1/2$	Truncated cone	Cylindrical micelles
$1/2 - 1$	Truncated cone	Flexible bilayers, vesicles
$\sim 1$	Cylinder	Planar bilayers
$> 1$	Inverted truncated cone or wedge	Inverted micelles

Figure 3 Critical packing parameter due to the molecular shape and resulting self-assembly entities. Reproduced by permission of publisher [22].

Due to the packing parameter, the assorted sizes of polar head groups can be used for the comparison of various lipid arrangements in the membrane. When we consider the difference between DOPC and DOPE as an example, even in the case when they have the same fatty acid tails, their head groups are different (-choline and -ethanolamine). The polar head of phosphatidylethanolamine (PE) is smaller compared to phosphatidylcholine (PC), which creates

a difference in their geometry [23]. DOPC is considered geometrically as a cylinder where the shape of DOPE is more like a conical shape between a cylinder and a cone, which can be described as a truncated cone. A planar membrane composed of cylindrical shaped phospholipids like DOPC creates a well-packed planar membrane. The non-lamellar lipids which are the secondary lipid structures including hexagonal or cubic phases forms molecular structures due to their geometry. For example, if there are only DOPE phospholipids in the buffer, they create inverted hexagonal phase micelles due to the spontaneous organization. Therefore, the presence of non-lamellar lipids in the planar membrane creates void areas available for acyl chain tails, in the assembly of acyl-chain tails which are larger compared to their head groups. This effect causes the lipids to not tightly come together and creates less-packed regions in the bilayer called “packing defects.”

Due to the interactions between lipid molecules, the bilayer owns a lateral pressure profile which is the distribution of lateral stresses across the width of the bilayer. The net lateral pressure on a lipid bilayer is zero when that is not under tension. The truncated or inverted cone shapes of the non-lamellar lipids in the bilayer change the local curvatures, which alters both the head group spacing and the entropy of the hydrophobic chains. For the lipid molecules with an inverted cone shape, like PE, as a result of the negative membrane curvature and due to the non-lamellar lateral pressure profile, the bilayer also becomes less stable. The stability and packing defects together influence pore formation and membrane fusion processes. This lipid geometry and the related bilayer curvature are key factors for the protein and peptide interactions in the bilayer. Numerous proteins and peptides are reported as being sensitive to the membrane curvature [24]–[28] with the effect of lipid composition as a factor for the partitioning [29], [30].

Another factor affecting the packing of the bilayer is the saturation of acyl chains of phospholipid molecules. When we compare two phospholipids with the oleyl chain (C18:1) and palmitoyl chain (C16:1), the oleyl chain has a larger volume due to the double bond at the middle of the chain by inducing the “kink” structure at this point. The presence of unsaturated acyl-chain in a well-packed membrane eventually causes packing defects. The binding preference of the specific proteins depends on their structure. For soluble proteins like amphipathic helix-containing proteins, increasing the lipid packing defects in a bilayer result in enrichment on the lipid droplet monolayer rather than the bilayer. For the hydrophobic domain-containing proteins such as  $\beta$ -hairpins, this effect still exists, and they also barely relocated to the bilayer. This preference can change for the monotopic proteins depending on the amino acid composition or the presence of charged residues in their hydrophobic domain [31]. To summarize, the proteins recognize the phospholipid packing defects, neutral lipids, and surface charges. Due to the packing defects, the proteins can cluster more in the void areas of less-packed bilayers. This effect can be reduced by creating well-packed bilayers.

### 3.3 MOBILITY IN A MEMBRANE

The absence of covalent linkages between the lipids and the protein in the membrane makes them freely move by conformational, rotational, or translational motions. These molecules are free to diffuse in the two-dimensional bilayer, and asymmetrically distributed within the membrane. Only some of the proteins are not free to diffuse due to their attachment to the cytoskeleton [32]. The membrane proteins are able to move laterally and rotationally in the membranes. The proteins diffuse laterally in the bilayer with a typical diffusivity between  $10^{-3}$  and  $2 \mu\text{m}^2/\text{s}$  [33]. Lateral diffusion of the integral and peripheral proteins takes a role in controlling the dynamics and functioning of the membrane as well as the motion of lipids. Lipids can transversally move between the two leaflets by enzymatic reactions which are called the “flip-flop”, which is catalyzed by enzymes called flippase, floppase, and scramblase, which takes the role of the bilayer to stay asymmetric. A lipid can also do the rotational movement on its axis while interacting with other neighbors in the bilayer laterally around one leaflet. The lateral motion of the lipids depends on their chemical structure, physical state, and lipid-protein and lipid-cholesterol ratios in the membrane. As the phospholipids in ER membrane are free to move, they are expected to be in a fluid state with a typical diffusivity of  $\approx 10 \mu\text{m}^2/\text{s}$ . Investigating the lateral motion of lipids and proteins provides information about the fluidity of the overall membrane which is one of the main characteristics that shows if the movement of the proteins are favorable within the membrane.

Several continuum theories have been developed to describe the diffusion of lipids and proteins in the bilayer. Brownian motion is explained by Robert Brown (1827) as the particles suspended in a liquid or gas environment fluctuate randomly without any preferred direction. Due to this no preference for the direction of these particles, they separate evenly in the medium over time. If there is a concentration difference in the system, the particles move from the high concentration to the low concentration region, so-called “diffusion.” The diffusion is driven by Gibbs free energy, which is the maximum amount of work in a closed system when both the pressure and temperature are constant. The chemical potential of the molecules is defined as the partial molar Gibbs free energy, and the particles are moving from the higher to lower chemical potential to reduce this free energy. According to the kinetic theory of Boltzmann, the temperature of a substance is depending on the average kinetic energy of the molecules in it, which are vibrating or moving. This theory describes the motion of the particles as reversible in agreement with Newtonian mechanics. Due to the second law of thermodynamics, not all energy is transferred or transformed to work, but some of it is transformed into heat during the conversion, and many processes are irreversible. The kinetic theory and the second law of thermodynamics were combined and formulated by Einstein in 1905 [34]. Einstein’s quantitative theory of Brownian motion is described as:

$$D = \mu k_B T \quad (2)$$

Here  $D$  is the diffusion coefficient,  $k_B$  is the Boltzmann's constant,  $\mu$  is the mobility of the particle and  $T$  is the absolute temperature, respectively. For the diffusion of spherical particles through a liquid which is dominated by laminar flow, Stokes-Einstein equation can be written as follows:

$$D = \frac{k_B T}{6\pi\eta r} \quad (3)$$

where  $r$  defines the radius of the particle and  $\eta$  is the dynamic viscosity of the liquid. The Stokes friction coefficient  $f = 6\pi\eta r$ , and the relation with the mobility of a particle can be defined as:

$$f = 1/\mu \quad (4)$$

The diffusion of a particle in the membrane is described in more detail by Saffman and Delbrück [35]. By this model, the classical Brownian motion is applied to a hydrodynamic model by the assumption of cylindrical particles, here the proteins, displaced freely in the membrane. The size of an object embedded in a membrane can be extracted from its translational diffusion coefficient. The model comprises an approximate solution for the translational motion of the inclusions in a membrane surrounded by a viscous fluid, and it was originally developed to explain the protein mobility in membranes, where the proteins are small compared to the characteristic length scale. Hence, this model is developed to predict the self-diffusion of small membrane-spanning objects [36]. To study the motion of a wider range of molecules in the bilayer, another model is created to describe the diffusion which is called the "free volume model." This model is based on the concept of redistribution of the molecules taking place in presence of open voids for diffusive displacement [37], [38], [39]–[41]. The free volume is  $v_f = a' v_m (T - T_0)$ , where  $a'$  is the thermal expansion coefficient and  $v_m$  is the mean molecular volume where the free volume does not exist anymore. This free volume model is the first to be used for long-range diffusion of lipids and proteins by measuring them with the Fluorescence Recovery After Photobleaching, so-called "FRAP" technique.

### 3.4 LIPID DROPLET BIOGENESIS

In this subchapter, the steps of lipid droplet formation from the ER membrane are introduced by including the roles of the proteins. Then the equilibrium shape of lipid droplets is explained biophysically by the three-phase wetting phenomenon. For this aim, a lipid droplet inside the

bilayer is demonstrated as an oil phase (neutral lipid) in between two water phases (ER lumen and cytosol) which results in the budding of the oil phase from the bilayer.

### 3.4.1 Structure and Formation

The major metabolic energy storage in cells is maintained by lipid droplets in the form of neutral lipids (i.e., triacylglycerols (TAGs) and sterol esters) which can be used for cellular processes if needed. The neutral lipid core is covered by a phospholipid monolayer which includes several integral and peripheral proteins (Class I and Class II proteins) [42]. Storing the lipids in an inert form and providing reservoirs of sterols, fatty acids, and phospholipids make the LDs important for cellular survival. Their role in energy metabolism also makes them crucial for cell homeostasis by maintaining stability in terms of energy maintenance. Lipid droplets are also establishing contact with other cellular organelles such as peroxisomes, mitochondria, and lysosomes.

The typical formation of LDs from ER membrane follows three steps, including neutral lipid synthesis, lens formation, and budding (**Figure 4**). Firstly, the neutral lipids (triacylglycerols and sterols) are synthesized in between two leaflets of the ER membrane. This biosynthesis is an enzyme-catalyzed esterification of an activated fatty acid to diacylglycerol or a sterol. Even if the neutral lipids are dispersed in between the two monolayers at low concentrations, when the concentration increases up to a certain value (5-10 % mole), the accumulation of the neutral lipids results in an oil inclusion with a lens-like shape. This is due to the demixing and reduced interaction of neutral lipids with other components, such as proteins and lipids [43]. The membrane curvature before budding is induced by proteins (i.e., COPII) to transform from the lens-shape to the bulged shape which results in lipid droplet budding [44]–[46].

The membrane phospholipid composition is determining the membrane tension. Minimizing the surface tension is crucial to come to the state of the formation of a bud. While molecules like diacylglycerol (DAG) and PE are disfavoring the budding due to their conical shape, contrarily molecules like lysophospholipids promote budding. The budding can occur in both directions, either towards the cytosol or ER lumen. The direction depends on the lipid/protein composition balance between two membrane monolayers. Although it generally occurs in the direction of the cytosol. Several proteins have roles in LD budding including fat storage induced transmembrane proteins (FIT1, FIT2), perilipin-1 (Pln1), Seipin with different molecular mechanisms, which are still being studied for further understanding. FIT (fat-storage-inducing transmembrane proteins) promotes LD budding by triggering the accumulation of neutral lipids between the two leaflets of the bilayer. In mammals, the Pln1 (also known as Pet10) protein binds to LD in the process of biosynthesis. Seipin is another responsible protein of the LD formation, which promotes the accumulation of TG molecules that are crucial for the LD to reach the lens shape with a certain concentration before budding [47]. As a LD life cycle has an importance on both membrane



synthesis and cell biology, the molecular details of the biological processes need to be further investigated and understood as most of the fundamental questions about LD biology have not yet been solved [48], [49].

The equilibrium shape of the lipid droplet in the membrane is also a result of the partitioning of the protein, as the shape can be determined by the localization of the protein whether on the lipid droplet surface or in the bilayer. In this thesis, one of the aims is to contribute the answer to the question of how this equilibrium shape of the lipid droplets changes in presence of different classes of proteins.

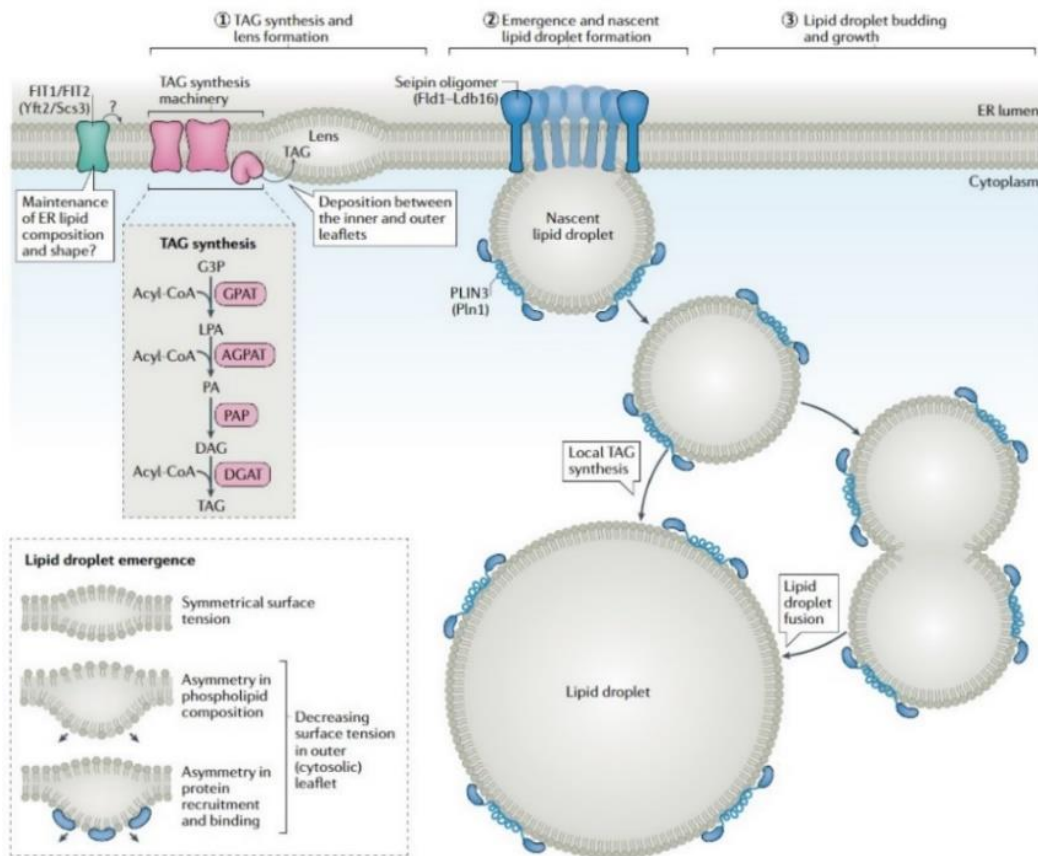


Figure 4 Schematic demonstration of LD biogenesis steps. Reproduced by permission of publisher [43].

### 3.4.2 Equilibrium Shape of the Lipid Droplets

The interface between the neutral lipid in two leaflets of the bilayer, cytosol, and the ER lumen has a high energy cost to be generated during budding. Therefore, phospholipids in cell membranes organize together with proteins to minimize energy while minimizing the contact

area between oil and water [49]–[51]. The shape of a LD in the membrane can be defined by the balance between surface tensions which are expected to play an important role for budding.

For this aim, the stage of lipid droplet budding towards the cytosol can be defined as a three-phase wetting phenomenon which will be explained by the difference in surface tensions. The origination of a lipid droplet starts with the spreading of the oil (triglycerides and sterol esters) between the cytoplasm and the ER lumen, which indicates the “wetting phase.” When this oil starts to have a lens-shape by the increased concentration of the neutral lipids between two leaflets of the bilayer, a contact angle forms between the LD and the bilayer, where the “dewetting” process starts. The surface tensions acting on the neutral phase of the lipid droplet in the two leaflets of the bilayer are in equilibrium, where the balance between different surface tensions defines the budding angle by the Young equation, the bilayer tension  $\Gamma = 2\gamma_{LB}\cos(\theta)$  as shown in **Figure 5** [50]. Here,  $\gamma_{LB}$  is the surface tension of one of the monolayers which are forming the bilayer,  $2\theta$  is the contact angle of the plateau border. Complete dewetting occurs when the lipid droplet completely forms and buds off from the bilayer. This formation can be defined as a spontaneous “emulsification” as the surface tension lowers and at the end approaches a value close to zero. For the physical characterization, the three phases are determined by interfacial tensions to achieve droplet budding. In the dewetting process of a lipid droplet, the three phases are defined by interfacial tensions as  $\Gamma$  (tension between cytosol and ER lumen),  $\gamma_{ULD}$  (tension between the upper leaflet of the LD and cytosol) and  $\gamma_{LLD}$  (tension between the lower leaflet of the LD and ER lumen) (**Figure 5**), which create the angle at the end. For the ER membrane and monolayers, the surface tensions are expected to be in the order of  $\Gamma = 10^{-2}mN/m$  and  $\gamma_{ULD} = \gamma_{LLD} = 0.1 - 1 mN/m$  [51], [52]. For the case of a symmetric droplet, the contact angle of the upper monolayer should be equal to the lower monolayer, where  $\alpha_U = \alpha_L = \alpha$ . The contact angle can be defined by the surface tensions as follows:

$$-\cos\alpha = \frac{\gamma_{LLD}^2 - \Gamma^2 - \gamma_{ULD}^2}{2\Gamma\gamma_{ULD}} \quad (5)$$

For the small values of  $\alpha$  (close to 0), the oil is still spreaded between the two phases and wetting remains. For the larger values, a spherical droplet is formed. In the partial wetting phase, the contact angle can be measured.

The balance between contact angles ( $\alpha_U, \alpha_L$ ) of the droplet gives the main information about the symmetry of the lipid droplet. It is expected to have a symmetric shape when there are only the forces of two symmetric monolayers in the system. For the small contact angles, the LDs remain connected with the bilayer, and the proteins can still reach the LDs [53], [54], whereas for the larger contact angle on one leaflet, the budding can eventually occur. The proteins take a

role in LD formation and influence the contact angle by modulating the surface tensions as already reported in Section 3.2.1. The symmetry of a lens-shaped lipid droplet in the bilayer can be broken by the accumulation of proteins on only one side. When the membrane curvature is induced, the biogenesis of the lipid droplet occurs, which can be defined as direct emulsions in the cytoplasm. However, as lipid droplets are oil emulsions and are still metastable, they are still open for destabilization by coalescence or ripening in the long term [55]. In the case of LDs, phospholipids ensure stability in cooperation with the proteins decorated on the lipid droplet monolayer. Even if the lipid droplets are originating from the Endoplasmic Reticulum bilayer, the type of phospholipids in the LD monolayer differs from the bilayer where they originated from. Compared to the bilayer composition, lipid droplets have more phosphatidylcholine (PC) and free cholesterol. In addition to that, there is phosphatidylethanolamine (PE) and to some lesser extent phosphatidylinositol (PI) and lysophospholipids in the lipid droplet monolayer. PC is the key phospholipid with its cylindrical geometry which results in well-packed coverage at the surface area which lowers the surface tension and provides good stability.

The stage of a droplet can be also described by the entering coefficient ( $E$ ) and the spreading coefficient ( $S$ ) by using the tensions, where  $E = \Gamma - \gamma_{ULD} - \gamma_{LLD}$  and  $S = \Gamma + \gamma_{ULD} - \gamma_{LLD}$ . Here, the entering coefficient ( $E$ ) predicts whether the droplet will be in the membrane or remain submerged in the water phase, where the spreading coefficient ( $S$ ) can indicate the spreading tendency. The droplet stays in the membrane when  $E > 0$ , and either forms a lens shape or spread along the bilayer. Entering and spreading coefficients together predicts whether the neutral lipid will stay in the bilayer ( $S > 0$ ), or will be in the state of forming a lens-shape ( $S < 0 < E$ ), or will become a nascent LD via budding ( $E < 0$ ) based on the balance of tensions in the system (**Figure 5**) [52], [56].

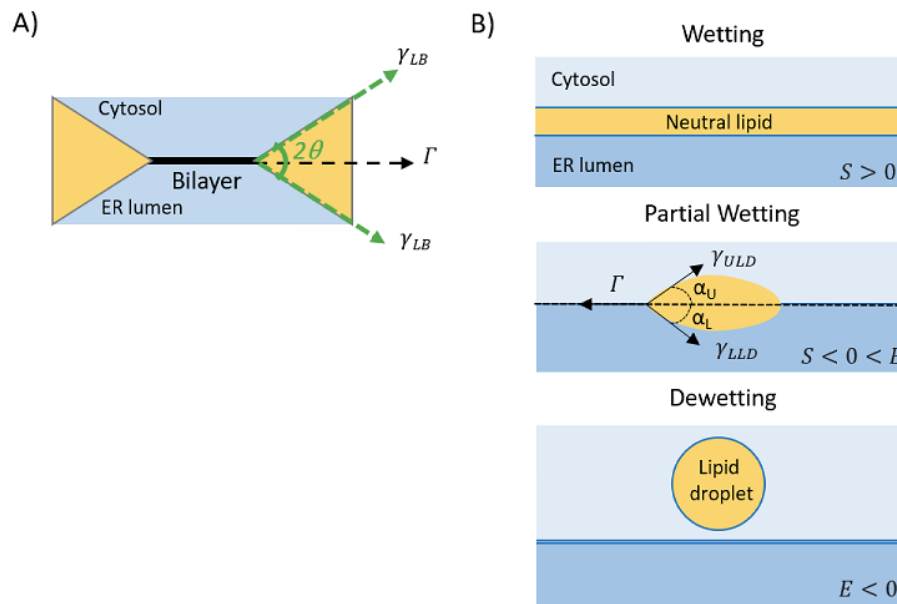


Figure 5 Schematic representation of contact angles for (A) bilayer (B) all stages of the formation of a lipid droplet considering the wetting theory.

### 3.5 LIPID DROPLET ASSOCIATED PROTEINS

Lipid droplet-associated proteins are classified as Class I and Class II proteins according to the different pathways they follow to insert into the lipid droplets. The insertion takes place either directly from the cytosol or by diffusing from the bilayer through the LD monolayer depending on the functional parts of the proteins. In this chapter, the insertion and trafficking of lipid droplet associated proteins, effect of lipid packing on the localization of these proteins and several microfluidic model systems developed over years to understand the regulation phenomenon of LD-associated proteins will be introduced.

#### 3.5.1 Insertion and Trafficking

Lipid droplet-associated proteins diversify between cell types, and the lipid droplet proteome consists of 100-150 proteins in mammalian cells [43]. Proteins can access the LD surface in two different pathways: through hydrophobic domains (Class I proteins) or through amphipathic helices (Class II proteins) [57]. Class I proteins are the proteins which localize both in the ER and in the LD and can also be found in ER in absence of LD. Class I proteins are typically attached to the membranes by hydrophobic sequences often with a hydrophobic 'hairpin' motif and

accommodate both the ER membrane and LD surface. The hairpins with hydrophobic domains first insert into the ER membrane, and then freely diffuse from the membrane through the surface of the lipid droplets via membrane bridges. For the proteins translocate from ER to LDs via membrane bridges, it might be expected that these proteins would equilibrate between ER and LD surface, but for many proteins, such as GPAT4, they excessively accumulate on LD surfaces compared to ER [58]. Hence, even if the membrane bridges provide the path for proteins, the mechanism led to the accumulation of proteins on lipid droplets are still unknown [59]. The insertion of the proteins happens via the insertion of the hydrophobic hairpins/helices into the membrane that finally get a V-shape with its ends (N- and C- termini) facing through cytosol which is shown in **Figure 6**. Several examples of proteins with hairpins can be classified as ACSL3, GPAT4, AUP1 and UBX domain-containing protein 8 (UBXD8), and Caveolin-1 [60]. Class II proteins bind straight to the LD surface without diffusing in the bilayer, which shows a different behavior than Class I proteins. Class II proteins either bind through amphipathic  $\alpha$ -helices, or some of them use both amphipathic and hydrophobic helices for binding. When these proteins bind with amphipathic helices, the hydrophobic part is embedded in the LD monolayer and the hydrophilic part positions through the polar head groups of the lipids (**Figure 6**). Some examples of Class II proteins can be classified as Perilipins, CCT $\alpha$ , and Cidea.

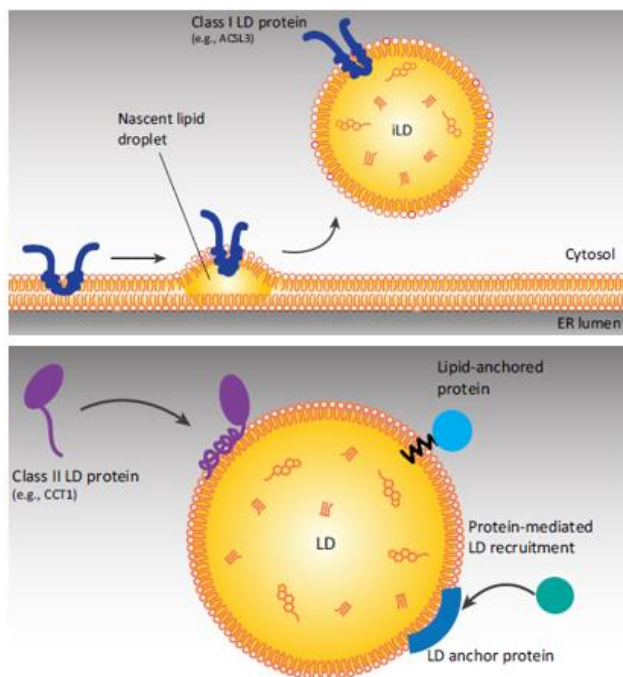


Figure 6 Schematic representation of the insertion of Class I and Class II proteins shows that Class I proteins bind LD monolayer through the bilayer, and Class II proteins bind to the surface directly from cytosol. Reproduced by permission of publisher [58].

There are two main hypotheses for the dynamic localization of the proteins. The first way includes the diffusion of these proteins in the outer leaflet of the bilayer and transferring the proteins to the lipid droplet monolayer during the LD formation [61]. Another proposed way is the trafficking from ER to mature LDs through membrane bridges, which is combining two organelles [54]. As the Class I proteins first bind to ER, this binding can follow two pathways: the signal recognition particle (SRP) pathway and the guided entry of tail-anchored proteins (GET) pathway. The proteins, which are inserted via the SRP pathway contain N-terminal sequences or transmembrane domains. The insertion of the hydrophobic integral, bitopic or polytopic proteins takes place co-translationally via the protein conducting channels such as Sec61 channel which mediates protein translocation across the ER membrane by forming pores in the membrane for the passage of soluble domains through the hydrophobic part of the membrane. Besides, they can assist the lateral integration of hydrophobic membrane-spanning segments [62]. On the contrary, the proteins which have C-terminal transmembrane domains follow the GET pathways for post-translational insertion due to their tail-anchored (TA) topology.

One main factor for the proteins to specifically target the lipid droplet monolayers is their content. Proteins insert into the surface monolayer lipids and further embed into the hydrophobic core of the bilayer embedded lipid droplet if their hydrophobic residues allowing them to, whereas the proteins with hydrophilic regions cannot insert into the core, which is energetically unfavorable. The proteins select a conformational organization for binding by minimizing the energy at the bilayer interface, which is possible by decreasing overall stress. The binding site preference of each protein class originates from the difference between the interaction-free energy of the bilayer and the monolayer. Even if the lipid droplets are the continuation of the bilayer, lipid droplets have much higher surface tensions due to the thickness of the neutral lipid accumulation, which is more than the thickness of the hydrophobic core of the bilayer. Compared to the hydrophobic thickness of a bilayer (3-4 nanometers), the thickness of the lipid droplet is infinitive (a few micrometers). This hydrophobic domain creates a greater surface for the binding of proteins with hydrophobic domains. The proteins including AUP1, GPAT4, AAM-B, UBDX8 and Caveolin-1 specifically bind to the ER membrane from the cytoplasm via their hairpin domains before localization towards LDs.

### **3.5.2 Overview of the Studied Proteins**

Related to the fact that hairpin proteins are primarily localized in ER, it is still a question of how the partitioning between ER and LD is organized. To answer this question, protein-protein combinations by various amino acid residues were studied in the literature [62]–[65]. Despite the

well-characterized pathways, the insertion machinery of hairpin proteins can also show unique set of biophysical features [57]. In the following section, the features and known partitioning pathways of proteins studied in this thesis will be briefly introduced to contribute the understanding of controlling mechanisms of protein partitioning.

### *Protein UBXD8*

UBXD-domain-containing proteins are mainly ubiquitin-regulatory proteins [66], and the molecular mechanism of the partition between ER and LD membranes of these proteins is still unknown. UBXD8 is a fusion protein that is known as a Class I intrinsic membrane protein, and it firstly localizes in the ER membrane via binding with hairpin domains. Both NH<sub>2</sub> and COOH terminus of UBXD8 protein orient towards the cytoplasm and forms a hairpin loop in the membrane by insertion via its membrane domain (amino acid 90-118) which is a typical insertion of hairpin proteins into the membrane (**Figure 7**). This binding is actualized specifically to the cytoplasmic leaflet of the ER membrane prior to the localization towards LDs. UBXD2 protein organizes the ER-associated protein degradation (ERAD) machinery, and it can dynamically localize to ER and LDs. In the case of defects in the UBXD2 protein, the UBXD8 protein functions in the conservation of lipid homeostasis by complementing the defect [67].

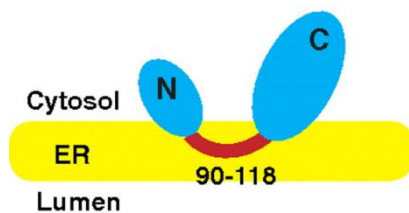


Figure 7 Schematic description of proposed membrane topology of UBXD8. Reproduced by permission of publisher [68].

UBXD8 is studied in literature to investigate the underlying mechanism of the insertion and dynamics of the hairpin proteins [68]–[71]. A study done by *Schrul et al., 2016* [72] shows that the partitioning of UBXD8 proteins requires a peroxisomal biogenesis factor. It is reported that hairpin domain-specific binding partners like PEX19 and BAG6 have a role in targeting UBXD8 to ER membranes [72]. The insertion pathway of UBXD8 protein into the ER is affected by the interrupted interaction of the PEX19-PEX13 pathway independent of all other pathways such as SRP and GET. While in the case of this uninterrupted interaction, UBXD8 inserts into the ER membrane but when there is interrupted interaction it inserts into the mitochondria [72]. So far, UBXD8 is the only LD protein that employs the PEX19-PEX3 pathway for the insertion (**Figure 8**).



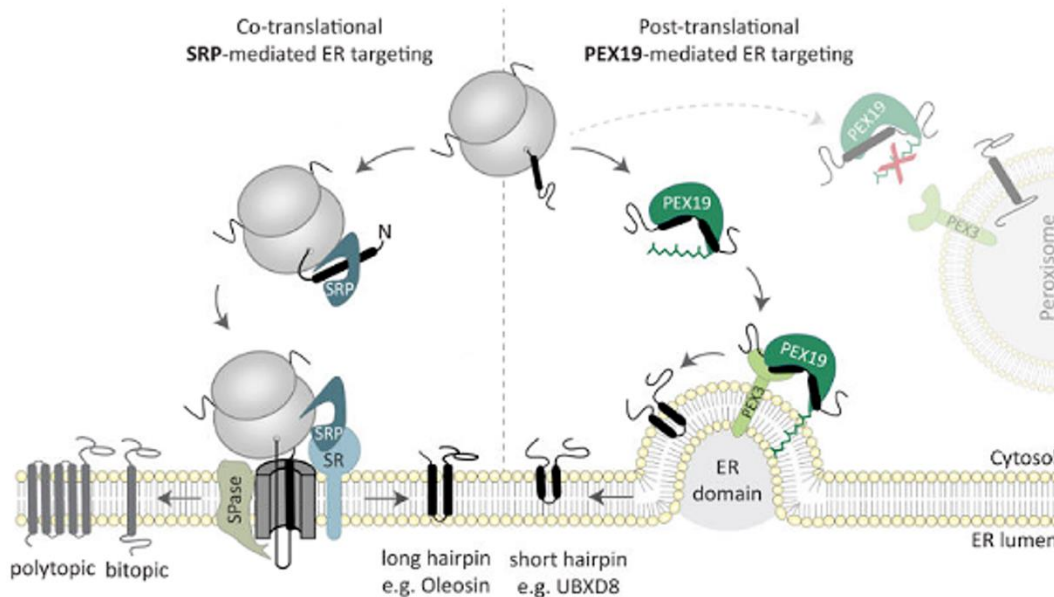


Figure 8 Schematic description of SRP-mediated targeting (left) for most bitopic or polytopic membrane proteins and PEX-19 mediated targeting (right) for UBXD8 proteins. Reproduced by permission of publisher [62].

The peroxisomal proteins and LD-hairpin proteins are associated and coupled to balance lipid storage/consumption together with ER, which questions the role of UBXD8 protein on neutral lipid storage. The study by *Wang et al., 2012* addresses that the UBXD8 might have an impact on the conversion of diacylglycerols (DAGs) to triacylglycerols (TAGs), [67] by inhibiting the synthesis of TAGs. Another interaction of UBXD8 proteins is with valosin-containing proteins (belonging to the AAA ATPase family of proteins) for the removal of UBXD8 from ER membrane [70], [67], [69]. In the cell, UBXD8-p97 and associated proteins prefer to be in the droplets. Other class I proteins such as ALDI, AAM-B and Cyb5r3, which are targeting both ER and LDs, have N-terminal hydrophobic sequences rather than hairpins, and the structure of these domains is likewise not known [58].

### *Protein Caveolin-1*

The caveolin family proteins were first identified as curvature-inducing monotopic proteins in the plasma membrane [73]–[75]. The caveolin protein family has three members: caveolin-1, caveolin-2, and caveolin-3 which are mostly found in the plasma membrane but also in the Golgi, endoplasmic reticulum, and vesicles [76]. The name caveolin comes from the proteins' function



of marking the cave-like invaginations, which are called “caveolae”, in the plasma membrane. It also regulates the transport of cholesterol in caveolae, ER, and Golgi [73]. High levels of Caveolin-1 (Cav1) are mostly found in adipocytes, endothelial, and smooth muscle cells. The absence of Cav1 protein can be linked to several diseases such as lipid metabolism disorders, decreased life span, and vascular abnormalities [77]. It has been shown in the literature that Cav1 is a soluble protein and can move to multiple compartments with caveolae-vesicles to fulfill its role in lipid traffic and signal transduction [61], [78]. They are relatively small proteins (18-24 kPa) but form oligomeric complexes with more than 14-16 monomers [76]. The chemical structure of cav1 protein is a membrane-spanning hairpin-like structure with N- and C- groups both directed against cytoplasm (**Figure 9**). As caveolae contain amphipathic lipid binding domains, they interact with lipids and related proteins to bind to lipid droplets [69], [73], [79]. In the caveolae protein family, cav1 and cav2 are specifically found in lipid droplets. The in-vitro insertion study of cav1 protein shows that it employs the SRP-Sec61 insertion pathway for the insertion of heterogeneously expressed oleosin [78], [80]. Localization between diverse membrane organelles is also observed for caveolin-1 proteins [61],[78][73]–[78], [81], [82].

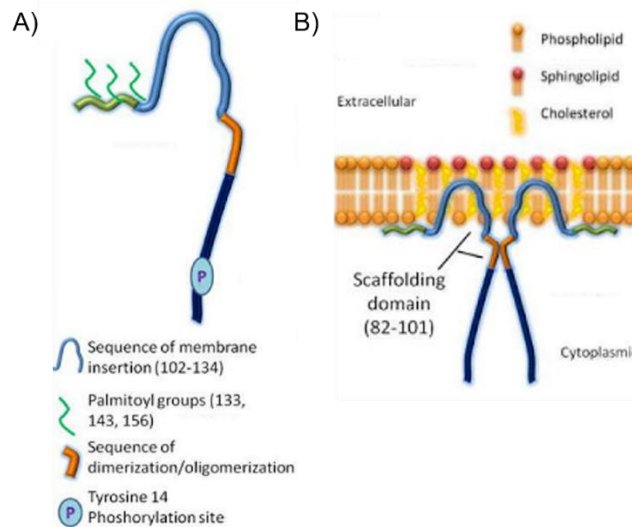


Figure 9 Schematic description of Caveolin-1 domains that let interaction with membrane and other proteins (A). Anchored shape of Cav1 via membrane insertion (B). Reproduced by permission of publisher [83].

### *Protein ADRP*

The perilipin proteins (PLINs 1-5) are the major Class-II LD-associated proteins, and PLIN1 and PLIN2 proteins are considered as markers of the LD surface. PLIN2 has originally named the Adipose differentiation-related protein (ADRP), which is ubiquitously expressed and takes the role in the stabilization of LDs, adipocyte differentiation, and generation of small LDs [84], [85].

ADRP is responsible for lipid accumulation by displaying in the adipocytes in the early stage of origination. The overexpression of ADRP induces the accumulation of LDs in fibroblasts [85], which is directly related to their role in the protection of Triolein from lipolysis and the promotion of LD formation. Therefore, ADRP has a key role in the management of neutral lipid storages. ADRP is considered a Class II LD-associated protein, and the studies show that alpha helices of Class II proteins are unfolded in the cytosol and fold into the helical structures by their alpha-helices when they contact and bind to the LD surface [86]. In literature, it has been shown that the disruption of the hydrophobic face of the predicted AH diminishes the localization of the amino terminus of ADRPs on the LD surface [87], and ADRPs bind to the LD monolayers via their C-terminal four-helix bundle with the 11-aa [62]. The live cell analysis of ADRP protein displays that they do not rapidly diffuse along the membranes and barely affect the mobility of phospholipids [88]. Even if it is known that alpha helices play an important role in targeting the LDs and the ADRPs are stable on lipid droplet surfaces, it is a remaining question how the ADRP proteins target and bind to lipid droplets.

### 3.5.3 Effect of Lipid Packing on Localization

The geometry of lipids in the membrane has a key role in biomolecular interactions, especially with various classes of proteins. Due to the hydrophobic part of a protein, the protein might prefer the LD monolayer which has an effective underlying hydrophobic region (neutral lipids) thickness compared to the thickness of phospholipid acyl chains in the bilayer (**Figure 10A**). Monotopic membrane proteins embed into one face of the membrane, and the  $\beta$ -hairpin proteins embed into and across the membrane due to their membrane-associated domains, which are the widely used model motifs. As lipid packing is much lower at the lipid droplet monolayer compared to the bilayer, the monotopic and  $\beta$ -hairpin proteins generally prefer the monolayer. This also shows that proteins bind to a specific area of the membrane via the recognition of the polar head group when the area is less packed. In the case where the lipids are not equally accessible for the protein due to imperfections in the membrane, the detection of the defects becomes crucial.

As the lipid droplet monolayer is the continuation of the bilayer, the lipid packing defects which originate from the composition of the bilayer may contribute to the protein's preference for LD monolayer rather than ER. Increasing lipid packing defects contribute to the formation of hydrophobic packing voids in the bilayer and monolayer. The nature of these voids within a membrane controls the binding level of the amphipathic helices on the LD surface (**Figure 10B**) [63]. Normally these proteins bind to lipid bilayers by interacting with the acyl chains. Their preference changes if the neutral lipids become more accessible due to the reduced packing of the phospholipids. This means that the amphipathic helices bind to the neutral lipids by creating

less interaction with water and folding in the monolayer. In cells, the packing of a lipid droplet monolayer is around 90% smaller compared to a bilayer [62]. By this, hairpin proteins are expected to move from the bilayer to the LD monolayer (**Figure 10C**). As mentioned before in Section 3.1.2, this packing defect can be regulated artificially by increasing the amount of cone-shaped lipids (such as DOPE) in the composition. This type of non-lamellar lipid has a negatively curved morphology different from the planar morphology of the lamellar phase. This curvature results in a less stable bilayer with a less uniform lateral pressure profile, in contrast to the uniform pressure profile of cylindrical phospholipids in the bilayer. Here, the lateral pressure profile of the bilayer depends on the distribution of lipids in nanometric scale. Besides, for few nanometer size droplets, a lens-shaped LD has a larger curvature compared to the planar bilayer. As a result, the proteins may constitute more on the LD surface due to the lipid composition and packing defects at these sites.

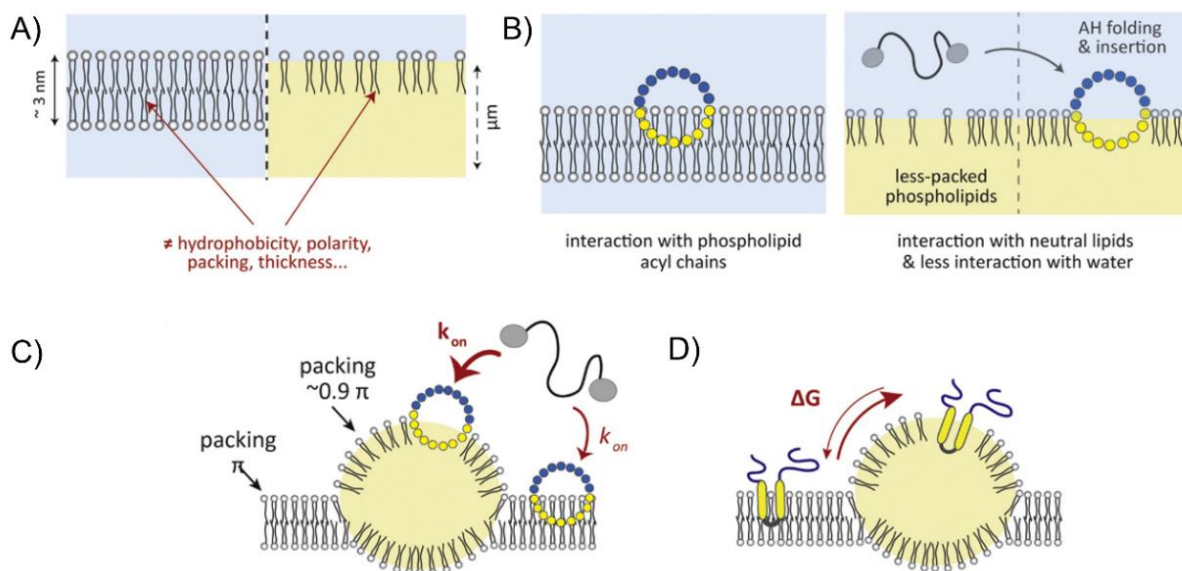


Figure 10 Differences in lipid packing between a bilayer and LD monolayer. The yellow area shows neutral lipid core of the LD (A). Amphipathic helices (AH) interaction with the bilayer (left) and LD monolayer (right) in presence of packing defects (B). Interaction of AH containing protein (C). Interaction of hairpin protein with the bilayer and the lipid droplet (D). Reproduced by permission of publisher [62].

For example, a guiding study is done by *Caillon et al. (2020)* to study the partition of different proteins by creating GUVs as a model system for ER membranes containing lipid droplets [31], [89]. Several monotopic integral membrane proteins including Cav1 are assessed. The study shows that independent of the PC/PE ratio, there was more partition through the monolayer compared to the bilayer and increasing the PE amount further favors the monolayer partition. When the amount of PE in the bilayer increases, the hydrogen bonding with the amine head

group of PE will increase the membrane tension. The tension variation due to membrane composition is also a factor for proteins to be dispersed or co-organized. For instance, under some cellular membrane tension, caveolae tend to group into clusters at the plasma membrane. Another study is done by *Mani et. al (2006)* by beta-hairpin antimicrobial peptide to show the effect of packing on a different protein structure. The oligomeric structure of PG-1 is changed due to the membrane composition and headgroup charge of the phospholipids in the membrane. Even if the PG-1 could be inserted in an anionic membrane, no insertion is observed for densely packed POPC/cholesterol membranes due to the negative curvature strain created by cholesterol inserted in the hydrophobic and glycerol regions of the bilayer. Besides, the rigid sterol ring structure of cholesterol causes a reduction in membrane elasticity which makes the membrane more difficult to deform for the accumulation of PG-1 [90].

Class II proteins can also have lipid composition dependence for binding. CCT $\alpha$  (CTP: phosphocholine cytidyltransferase  $\alpha$  isoform) is a class II amphipathic helix protein, which has binding properties depending on the lipid PC:PE ratio. When the PC amount is lacking on the LD surface, due to the higher surface tension, CCT $\alpha$  molecules perceive this insufficient covering as “PC deficiency.” As a result, CCT $\alpha$  operates to ensure the efficient amount of the PC in the LD monolayer to achieve a complete coating of phospholipid monolayer around the LD. Further, the binding of class II proteins also depends on the amount of diacylglycerol which promotes the binding [91]. Protein crowding on the LD surface is another factor that determines how much additional class II protein can bind to the surface. When the surface is fully covered with proteins, class II proteins cannot find enough space to bind to the LD surface. Some other proteins can bind to the LD by both amphipathic and hydrophobic helices, such as perilipin/ADRP/PLIN4 (PAT proteins). Perilipins bind to the LD surface by transforming their amino acid repeats from disordered to bounded. This means that in the cytosol, the amino acid repeats are disordered and at the LD surface it folds into an amphipathic helix [92]. In the literature, the results show that PLIN4 is directly binding to the neutral lipids by replacing the phospholipids on the LD monolayer [93].

In the literature, it was demonstrated that the mobility of these proteins depends on their surrounding (composition of the membrane) and thus it is expected that is also varied in the bilayer and on the LD, but it was not shown up to date. It is reported that the mobility and diffusion coefficient of the caveolae depend on the location (in the plasma membrane, in Golgi, or in the cytoplasm) and the type of caveolae (cav1, cav2, wild type, or mutant) [94], [95]. In addition to that, the length of the amino acid sequences and the location (apical membrane or basolateral membrane) of caveolae cause a significant change in diffusion coefficient [96]–[98]. Caveolin-1 specifically shows high immobility once it has arrived in the plasma membrane, which results in a very limited lateral diffusion [99]. As the different motion characteristics of these proteins in the bilayer and lipid droplets are still a question, investigating the mobility or

diffusivity of these proteins caught our attention. Hence, in this thesis, the dynamics of hairpin-like Cav1 and ADRP proteins in the lipid bilayer and on the LD surface will be explored.

### 3.6 MODEL SYSTEMS IN LITERATURE FOR STUDYING LIPID DROPLETS

As natural pathways in cells show the complexity and fast transitions of lipids and proteins, model systems are widely used to investigate lipid droplet biogenesis and lipid droplet-protein interactions, which enable compositional changes of lipids and proteins [31], [100]–[102]. All model systems such as GUVs, DIBs, and molecular dynamic simulations have some general advantages such as giving an ease to tailor the lipid composition and the type of proteins for the purpose of the research. Here, some of the examples for these systems from literature will be introduced. The most used components to study LD biogenesis are Droplet-embedded vesicles (DEVs), which are combined with several proteins to study the emergence of LDs (**Figure 11**). DEVs are prepared by embedding the oil droplets from an emulsion into the Giant unilamellar vesicles (GUVs) [64] to mimic a lipid droplet in physical contact with the ER membrane. Using those systems, bilayer asymmetry and budding kinetics are studied [63], [64], [101]–[103].

According to the hypothesis about LD emergence, the asymmetry between two monolayers that are forming the bilayer is sufficient to complete the budding. The effect of asymmetry on LD biogenesis has been investigated by *Chorlay et al. (2019)* via the incorporation of LDs between the monolayer leaflets of Giant Unilamellar Vesicles (GUVs) [102]. The study focuses on how protein crowding promotes the direction of budding. An asymmetry between two leaflets was created by increasing the number of PC molecules in one leaflet and the budded shape is observed in that direction. The proteins Arf1 and Cav1<sub>59-178</sub> were observed to accumulate on the leaflet with more coverage and thus reduced surface tension, and this determines the budding direction. The study shows that hydrophobic residues containing amphipathic helix proteins, in general, prefers the lipid droplet monolayer compared to the phospholipid bilayer. Another study has been done by *Ben M'barek et al. (2017)* by combining different ratios of phospholipids for bilayer formation including PC, Lyso-PC, PE, PA, and Cholesterol [103]. Here, droplet-embedded vesicles (DEVs) were used as model systems to investigate the budding. The results show that increasing the bilayer tension has an impact on the triolein accumulation inside the bilayer. Triolein spreads more in the bilayer and does not desire to form a lens-like shape if the bilayer tension value exceeds 0.1 mN/m. For the tensions lower than this value, LD budding takes place. These systems were also used to study both classes of LD-associated proteins to investigate the impact of the proteins in the budding. When the proteins are adsorbed from the cytosol side, the surface tension decreases at this side and LD emerges towards cytosol and vice versa for ER lumen side adsorption.

A guiding study to contribute to the investigation of protein partition between ER membrane and LDs has been done by *Caillon et al. (2020)* by using Droplet Interface Bilayers (DIBs) as a model system. In this study, two phospholipid monolayers of droplets are contacted in a neutral lipid environment (TG) to form the bilayer [31]. By altering the PC/PE ratio, the distribution of several monotopic integral membrane proteins such as Plin1 and caveolin were studied. These hydrophobic membrane association domains (HD) containing proteins highly partition in the monolayer rather than in the bilayer. This partition was observed for all PC/PE ratios and increasing the PE amount in the bilayer favors this partition. As DOPE and DOPC have conical and cylindrical shapes respectively, increasing the DOPE amount decreases the phospholipid packing and results in more HD-TG contact. All the selected proteins in this study showed that the hydrophobic domains such as helical hairpins, hydrophobic helices, and transmembrane domains preferably be at the lipid droplets rather than the bilayer [31]. Some examples of the systems introduced in this section are shown in **Figure 11**.

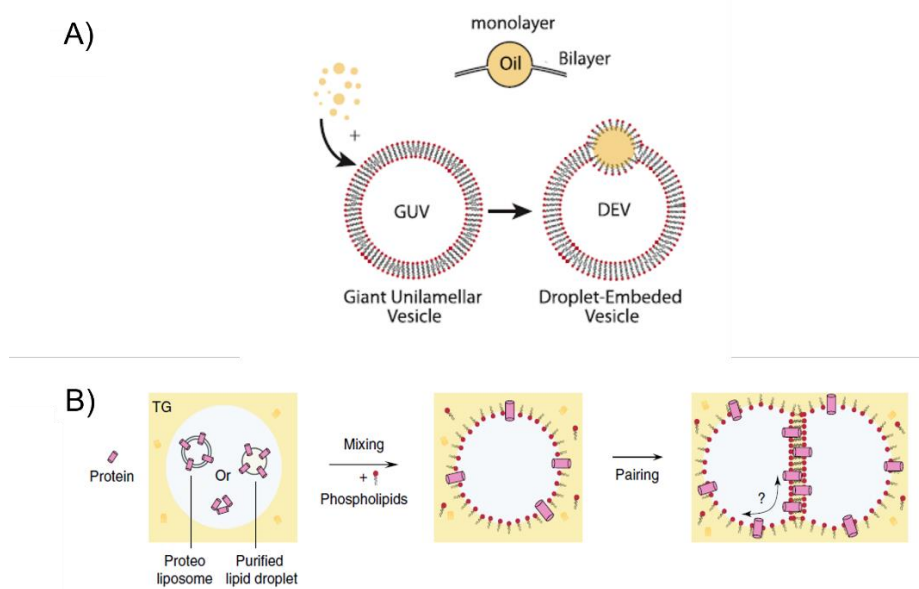


Figure 11 Example systems to study lipid droplets and associated proteins A) Giant unilamellar vesicle (GUV) and Droplet-embedded vesicle (DEV) systems. Reproduced by permission of publisher [102] B) Double interface bilayer (DIB) Systems. Reproduced by permission of publisher [31].

Molecular conformation and shape of the triolein inside a bilayer have been also studied by conducting molecular dynamic simulations [6], [45], [46], [104]–[106]. The triolein concentration effect in a POPC bilayer is reported by *Khandelia et al. (2010)* [45]. At a sufficiently high concentration of triolein (5.2 mol%) in the bilayer, “blister” like structures were formed inside the bilayer by altering the molecular conformation of phospholipids in the bilayer. The introduced model system by *Khandelia et al. (2010)* is convenient to study a wide range of phospholipid-

protein combinations to further investigate the dynamics of lipid droplets. The study shows that the neutral lipid accumulation in the bilayer also depends on the bilayer stresses, which are determined by the lipid acyl chains which has already studied experimentally by *Ben M'barek et al. (2017)*. Simulations have shown that, when the phospholipid density is lower in one monolayer and thus the surface tension is higher, LD is budding in the direction of the monolayer with smaller surface tension. Due to the created asymmetry, the success rate of the formation increases simultaneously. A wide range of phospholipid compositions has been also studied to show that the accumulation of neutral lipids is promoted by diacylglycerol together with lipids such as phosphatidylethanolamine, which are enriched at sites of LD formation. On the contrary, saturated acyl chains promote the accumulation of neutral lipids in the bilayer [104] (**Figure 12**).

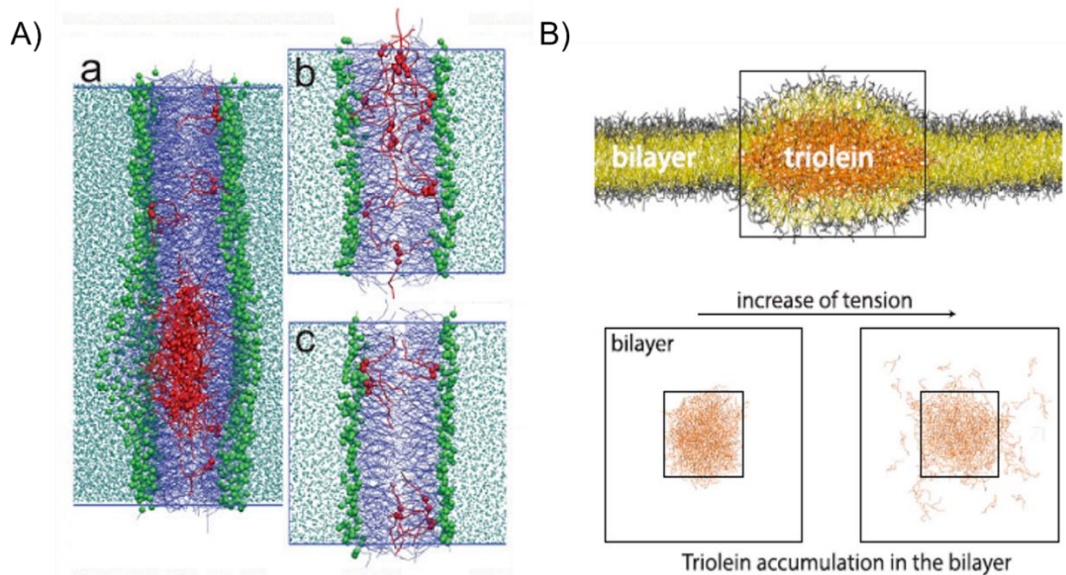


Figure 12 Example MD simulation systems to study the accumulation of triolein in the bilayer. (A) Side view of triolein accumulation trend depend on increasing amount of triolein in POPC bilayers. Reproduced by permission of publisher [45] B) Side view of the in silico-model (upper view) and top view showing the accumulation of triolein due to the increasing PC bilayer surface tension. Reproduced by permission of publisher [103].

Despite the fact that all the introduced systems have the advantages for lipid droplet studies, even if the fluidities of the GUV and DIB systems can be close to a free-standing bilayer (around  $10 \mu\text{m}^2/\text{s}$ ), the depth of the droplets limits the visualization of only one focal plane clearly and the signals are coming from the whole droplet. These extra signals are needed to be further processed to achieve a clear view of one focal plane. If we focus on a horizontal free-standing bilayer in a microfluidic system, its diffusivity is similar to a GUV vesicle. Nevertheless, the existing working area of the horizontal free-standing bilayer can be up to the order of hundred

micrometers which gives the opportunity to visualize more interaction and localization on the bilayer area with better resolution. In the other systems such as vertical lipid bilayers, the area is limited by the view direction which is parallel to the bilayer but perpendicular to its normal axis, and it is not possible to optically image the interior area. The cell membrane is in fluid state and dynamic. The components like lipid droplets or proteins inserted in a free-standing artificial membrane can be tailored closer to a real membrane. A free-standing bilayer gives the advantage to manipulate the system from both directions and is appropriate for 3D visualization of proteins and lipids on a solvent-free bilayer which will be introduced in the following chapter.



## **MATERIALS AND METHODS**

---

## 4 MATERIALS AND METHODS

---

In this chapter, the relevant experimental protocols and details are explained. The used molecules including lipids, oil and fluorescence probes are explained in subchapter 4.1. In subchapter 4.2, geometry and operation of the developed microfluidic device as well as preparation methods of lipid droplets, proteins, and proteo-lipid droplets are introduced. Applied characterization methods like 3D imaging and FRAP are introduced in subchapter 4.3. Following, patch-clamp recordings and the steps of interfacial tension measurements and molecular dynamic simulations are explained.

### 4.1 MATERIALS

The lipids 1,2-dioleoyl-sn-glycero-3-phosphocholine (DOPC), 1,2-dioleoyl-sn-glycero-3-phosphoethanolamine (DOPE), 1,2-dioleoyl-sn-glycero-3-phospho-L-serine (sodium salt) (DOPS), 1,2-diphytanoyl-sn-glycero-3-phosphocholine (DPhPC), 1,2-diphytanoyl-sn-glycero-3-phosphoethanolamine (DPhPE), 1-palmitoyl-2-oleoyl-sn-glycero-3-phosphocholine (POPC), 1-palmitoyl-2-oleoyl-sn-glycero-3-phosphoethanolamine (POPE) and cholesterol were purchased from Avanti Polar Lipids. Fluorescence dyes 4,4-difluoro-1,3,5,7,8-pentamethyl-4-bora-3a,4a-diaza-s-indacene (BODIPY 493/503, D3922, ThermoFisher), 1,2-dioleoyl-sn-glycero-3-phosphoethanolamine-N-(lissamine rhodamine B sulfonyl) (ammonium salt) (18:1 Liss Rhod PE), 1,2-dioleoyl-sn-glycero-3-phosphocholine-N-(Cyanine 5) (18:1 PC-Cy5), 1,2-Dioleoyl-sn-glycero-3-phosphoethanolamine labeled with Atto 647N (Atto-DOPE) were obtained from Avanti Polar Lipids. Human Caveolin peptide (MSGGKYVDSEGHLYTVP, Cav<sub>1-17</sub>), Alexa Fluor 488 Conjugation Kit (ab236553) and Alexa Fluor 647 Conjugation Kit (ab269823) were purchased from Abcam. Ultra-pure water was obtained from the ultra-pure filtration system by Thermo-Fischer. Sodium chloride was obtained from Sigma-Aldrich. The high-resolution transparency mask is ordered from Micro Lithography Services, Ltd, UK.

#### 4.1.1 Lipids and Oil

The phospholipids (DOPC, DOPE, DOPS, POPC, POPE, DPhPE, DPhPC) and Cholesterol were used to create the bilayers in microfluidic system. Triglyceride (so called Triolein) was used to create the artificial lipid droplets.

DOPC, DOPE and DOPS lipids were chosen as the main components while creating the artificial bilayer system, as they are also the main components of the ER membrane. *DOPC* (1,2-dioleoyl-sn-glycero-3-phosphocholine) is the most abundant phospholipid with a Choline

headgroup in the cell membrane and has a net charge of zero. Presence of DOPC in the membrane ensures a highly packed structure. *DOPE* (1,2-dioleoyl-sn-glycero-3-phosphoethanolamine) is another major phospholipid of the cell membrane which is a non-lamellar lipid with a head group of ethanolamine, which creates void areas in the membrane with its non-lamellar structure. DOPS increases the hydrogen bonding on the membrane and creates rigidity, and it is a key phospholipid for directing the protein binding. To mimic the artificial membrane close to the real one, the composition was set to DOPC:DOPE:DOPS (60:30:10 molar ratio) unless another composition is mentioned. By using the determined composition, the membranes were stable for at least for 2 hours and the measured phospholipid diffusivity was around  $10 \mu\text{m}^2/\text{s}$  which is very close to a biological free-standing membrane. Squalene oil was used in the artificial bilayer formation to carry the lipids into the system by dissolving. During the bilayer formation, squalene was absorbed by the walls of the microfluidic device which is made of PDMS [5]. All the lipid/squalene mixtures were prepared in the concentration of 5 mg/ml (phospholipids in squalene) for the bilayer formation. The chemical structures of lipids and oil used for the experiments are listed in **Figure 13**.

*POPC* (1-palmitoyl-2-oleoyl-sn-glycero-3-phosphocholine) is a diacylglycerol and phospholipid, and together with *POPE* (1-palmitoyl-2-oleoyl-sn-glycero-3-phosphoethanolamine) they create more packed structures compared to DOPC and DOPE, as well as *DPhPC* (1,2-diphytanoyl-sn-glycero-3-phosphocholine) and *DPhPE* (1,2-diphytanoyl-sn-glycero-3-phosphoethanolamine) [107], [108]. Here the combinations of these lipids (DPhPC/DPhPE, POPC/POPE or POPC/DOPE) were used to adjust the bilayer packing to study how it influences protein partitioning.

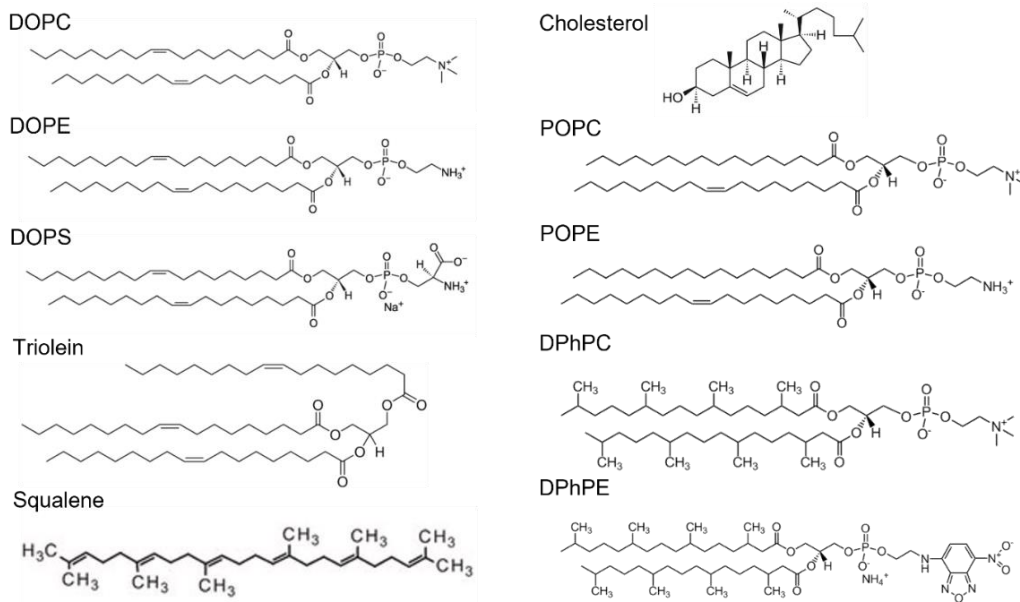


Figure 13 Chemical Structures of Lipids, Cholesterol and Squalene oil used in the experiments (Avanti Polar Lipids, n.d.).

#### 4.1.2 Fluorescence Probes

Two different labels Atto 647N DOPE or Rhodamine PE (1,2-dioleoyl-snglycero-3-phosphoethanolamine-N-(lissamine rhodamine B sulfonyl) (ammonium salt) were used to fluorescently label the lipid bilayer for the fluorescence microscopy depending on the exact experiment. In aqueous solution, Atto 647N DOPE shows high quantum efficiency which means that the fluorophores emit strong fluorescence even at low concentration. By replacing 2-4 mol% of DOPE with the fluorescent DOPE, a very good signal could be achieved. Without changing the natural bilayer composition, the fluorescence signal coming from the bilayer was enough to perform an efficient bleaching on the bilayer area for FRAP measurements.

Antibody Conjugation Kit (Alexa Fluor 488 or Alexa Fluor 647) was used to label the Cav1<sub>1-17</sub> peptides and Alexa Fluor 488 was used to label the ADRP proteins to follow the dynamics of the peptide by distinguishing the proteins, lipid droplets and bilayer. BODIPY (493/503) is widely utilized by scientists to stain neutral lipid droplets in literature. BODIPY binds to neutral lipid and emits green fluorescence signal but within a narrow wavelength range. This makes the BODIPY a very suitable probe for multi labelling experiments. In this thesis, it was used to stain the neutral lipid content (Triolein) inside the lipid droplets and for the identification in our system during the confocal microscopy experiments.

## 4.2 PREPARATION METHODS

Microfluidic tools were used to fabricate free-standing fluid lipid bilayers with both leaflets in contact with the buffer. The design principle allows to access the two sides of the bilayer to introduce additional components without rupturing the membrane. The 3D geometry design of the microfluidic device is aimed to be adaptable to a fluorescence microscope and patch-clamp amplifier. The details of the device preparation, bilayer formation, and preparation of LDs and PLDs will be explained in this section.

### 4.2.1 Microfluidic Device Preparation

The molds to create microfluidic devices have been done by combining photolithography and micromachining. Photolithography is a well-known technique to achieve microscale lateral structures [109]. In principle, the desired pattern is transferred from a transparent mask to a substrate by using a photosensitive chemical called photoresist.

The parameters of the negative photoresist spin coater were arranged to achieve a 100  $\mu\text{m}$  channel to allow a higher level of optical access. For this aim, 2 g of SU-8 was placed on a 2-inch silicon wafer that is placed on a spin coater, and the coating started with a rotational speed of 500 rpm with an acceleration of 100 rpm/second for 20 seconds, then 1500 rpm at 300 rpm/sec for 60 seconds to achieve the desired thickness of the photoresist on the surface. The coated wafer was put on a hot plate for 15 minutes at 65 °C for a pre-bake. Subsequently, the solvent was evaporated at 95 °C for 45 min to densify the film. A transparent mask with the desired channel pattern on it is carefully placed on the coated wafer and exposed to UV light. For UV exposure, the device was set to a wavelength of 400 nm with an intensity of 15 mW/cm<sup>2</sup> for 20 seconds. To cross-link the epoxy-based photoresist strongly with the silicon wafer, the wafer is post-baked for 1 minute at 65 °C, then at 95 °C for 5 minutes. Subsequently, the structure was washed with acetone, ethanol, and distilled water. The residues of the solvents are removed with a gentle stream of nitrogen gas. As the microfluidic device is aimed to be a combination of a channel and a cone, the obtained final structure is used as the channel part of the 3D mold. The cone was produced by micromachining from an Aluminum block by CNC machining. To create a 3D mold for the device fabrication, this cone was positioned at the center of the channel structure on the silicon wafer mold (**Figure 14**).

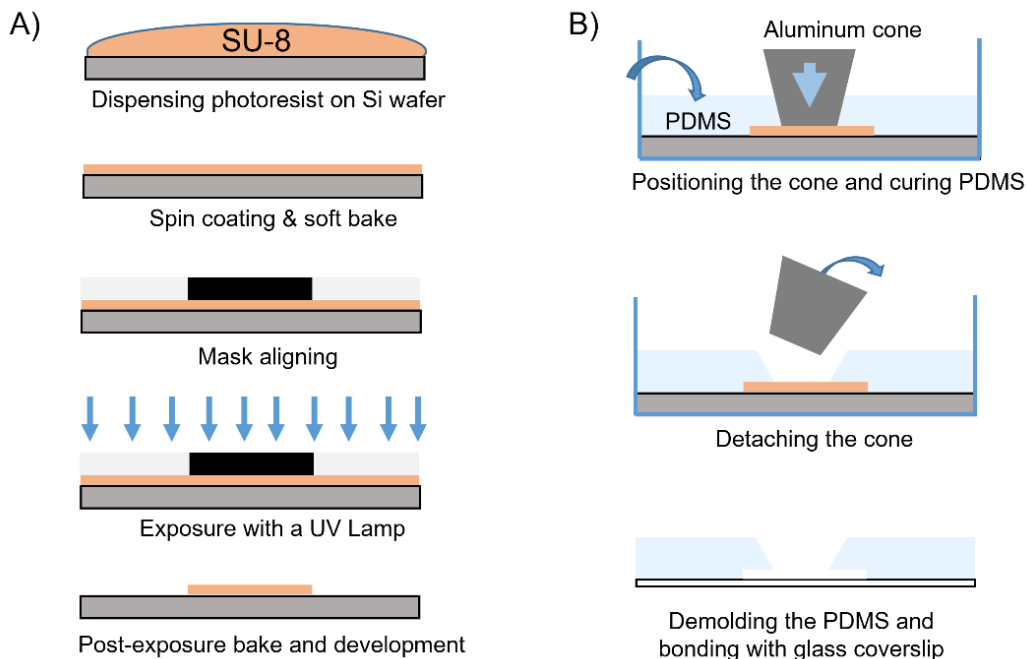


Figure 14 Schematic representation of steps of photolithography (A) and soft-lithography (B).

For the soft lithography, Sylgard 184 Silicone Elastomer Kit (Dow Corning) Silicone Elastomer Kit (PDMS) was used. PDMS is a member of organosilicon compounds called silicones. The chemical formula of PDMS is  $\text{CH}_3[\text{Si}(\text{CH}_3)_2\text{O}]_n\text{Si}(\text{CH}_3)_3$ . This widely used silicone is the main component for easy microfluidic device fabrication for a long time [110]. PDMS is transparent and optically creates a clear visualization for microscopy techniques. Due to its hydrophobic nature, it is also suitable to create a microfluidic device to form free-standing bilayers, where the hydrophobic oil is absorbed by the walls of PDMS, and the bilayer forms in between the walls. The microfluidic devices are produced via mixing two components Silicon Rubber Base and Cross Linker (catalytic agent) with a ratio of 10:1, respectively. Prior to pouring the mixture into the mold, the mixture was degassed in a desiccator under vacuum for 30 minutes. The cone and the bottom channel are positioned with ultimate contact, the hot plate was set at  $100\text{ }^\circ\text{C}$  and PDMS is cured for one hour (**Figure 14**). Then it is cooled down before detaching the Aluminum cone. The PDMS is removed from the mold, and it has the final shape of one channel connected to a conical hole that is opened toward the air. Two holes for the inlet and outlet were punched, and the prepared PDMS chip and a thin glass coverslip is treated by using a plasma cleaner (Plasma cleaner, Diener electronic GmbH) prior to bonding. Afterwards, to enhance the bonding quality, the device is kept at  $100\text{ }^\circ\text{C}$  for 1h on a hot plate. The set-up and final microfluidic device are shown in detail in **Figure 15**.

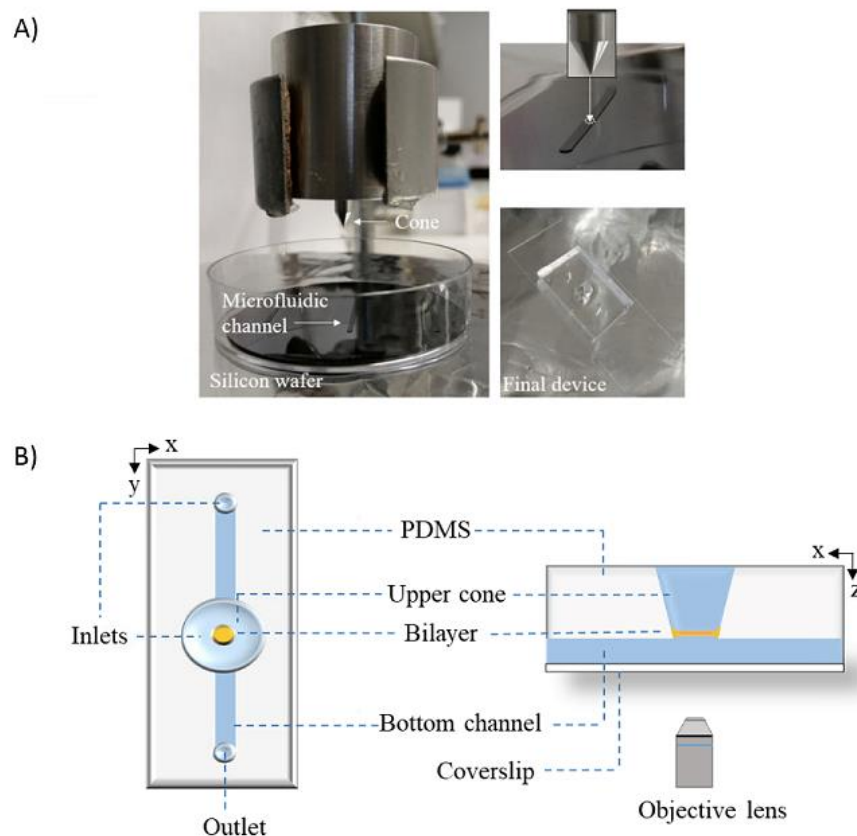


Figure 15 Combination of Aluminum based cone and channel on silicon wafer (left). Positioning the cone at the middle of the channel (upper right image). Final device (lower right image) (A). Schematic representation of the device from top (left) and side (right) view (B). The two inlets are used to introduce the components for the experiments.

#### 4.2.2 Bilayer Formation

The produced microfluidic platform as described in the previous section is used to create an artificial free-standing bilayer. The system characterization was performed by fluorescence microscopy connected to a path-clamp device. The microfluidic device is placed on an inverted confocal microscope (Nikon Ti-Eclipse) with the light source of Intensilight Epi-Fluorescence illuminator. The microscope is equipped with Yokogawa spinning disk heads (CSU-W1; Andor Technologies) and FRAP (Andor Technology) modules. All the units were controlled by Nikon NIS Software. To follow the formation kinetics, the electrodes were positioned directly to the upper cone and bottom channel (**Figure 16**).

The simply designed structure of the device consists of a channel linked to a cone at the middle of the channel as introduced in the previous section. The intersection point of the channel and the cone is the position where the lipid bilayer is formed. The formation of the lipid bilayer is

simply based on sandwiching (or trapping) the oil and lipid mixture between two water phases. For that, the bottom channel was filled with the buffer (0.1 M NaCl). After filling the bottom channel with the buffer, a 4  $\mu\text{L}$  drop of oil and lipid mixture was added from the upper cone using a pipette. Then the top of this droplet was covered again with water by introducing 6  $\mu\text{L}$  of the buffer from the upper cone. When the film thickness approaches a few hundred Angstroms, two phospholipid monolayers form at the oil/water interface and a lipid bilayer spontaneously forms by the zipping of these two monolayers as a result of van der Waals forces [4]. Therefore, a circle appears in the middle surrounded by a Plateau-Gibbs border due to this organization. The area outside the bilayer, which is called annulus, is the lipid oil mixture that is remaining. As the circle enlarges toward the walls of the cone, the oil is absorbed by the walls of PDMS. This process continues until the bilayer area reaches the limits of the aperture. This means that the two monolayers are completely zipped, and an oil-free lipid bilayer is formed at the intersection of the channel and the cone (**Figure 16**). Further modification of the bilayer is possible by adding other components like lipid droplets and proteins to the system.

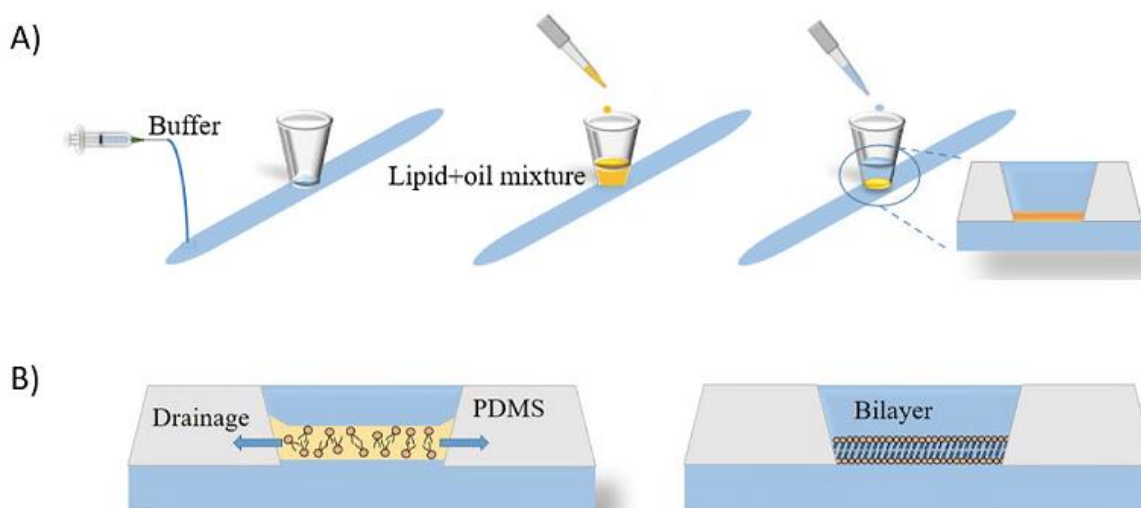


Figure 16 Steps of bilayer formation (A). Oil drainage by the walls of PDMS before the bilayer is formed (B). Reproduced by permission of publisher [6].

#### 4.2.3 Formation of Lipid Droplets

The lipid droplets are formed for the insertion experiments. Lipids and BODIPY (493/503) were used from the chloroform stock solutions with a concentration of 10 mg/mL. 1 mg of the mixture (which is in total 200  $\mu\text{L}$ ) consisting of of DOPC : DOPE : Triolein : BODIPY (35:35:28:2 mol%) was



deposited in a glass vial and the chloroform is evaporated under vacuum for 1 h. This dried film was dispersed in 0.1 M NaCl buffer prior to the formation of the droplet. The lipid-triolein droplets were shaped by sonicating the solution in an ultrasonic bath for 5 min. The optical visualization by fluorescence microscopy was used to examine the resulting size of the lipid droplets, which are typically around 5  $\mu\text{m}$ . Prior to the experiments, the solution was diluted (1:4 (vol/vol)) to limit the coalescence of lipid droplets. The lipid droplets stayed stable during the experiments for around 3 hours.

#### 4.2.4 Formation of PLDs containing UBXD8 Protein

UBXD8<sub>71-132</sub> is a fusion protein consists of a hydrophobic hairpin domain. It contains an N-terminal GST-tag chased with a PreScission Protease cleavage site, and a S-peptide-tag ahead the peptide sequence. The purification of the proteins and the preparation of liposomes were done in the lab of *Jun.Prof.Dr.Bianca Schrul, Medical Biochemistry and Molecular Biology, Saarland University* [6].

The prepared liposomes are composed of POPC and DOPS (9:1 molar ratio) reconstituted with (UBXD8<sub>71-132</sub>Atto488). The proteo-liposome containing fraction was used for the generation of proteo-LDs. To prepare the Proteo-LDs, 10  $\mu\text{L}$  of Triolein (from a chloroform stock solution) was added to an empty vial to evaporate the chloroform. Following, a biphasic was created by adding 180  $\mu\text{L}$  of the buffer that is used to store proteoliposome solution, and 20  $\mu\text{L}$  of ready to use proteoliposomes were mixed by this biphasic. The solution was stored overnight at 4°C, afterwards it was sonicated until a LD size of 15  $\mu\text{m}$  was achieved. These Proteo-LDs were directly added to the microfluidic system during the experiments (**Figure 17**).

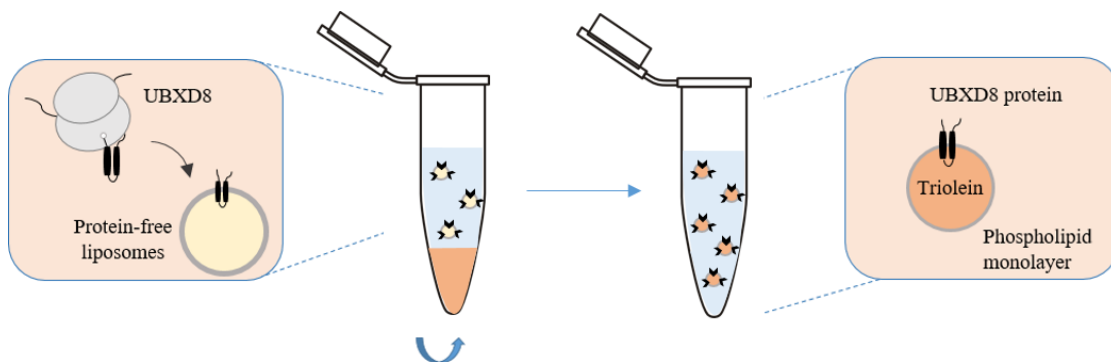


Figure 17 In vitro translated UBXD8 proteins are reconstituted in the protein-free liposomes composed of POPC:DOPS (1:9 mol%). A biphasic of triolein/buffer is formed and sonicated. The product is protein containing lipid droplets.

#### 4.2.5 Formation of PLDs containing Cav1<sub>1-17</sub> Peptides

The Cav1<sub>1-17</sub> peptide is introduced as a potential hairpin-like structure by Abcam (ab4928) with an amino acid sequence MSGGKYVDSEGHLYTVP, which is a short sequence of the N-terminal domain of full-length Cav1 protein. The peptide has a purity >95% and consists of first 17 amino acids in N-terminus of the full-length human Cav1 which has 178 amino acids. The crude hydrophobic/hydrophilic analysis of the sequence shows the structure as globally neutral with 29.41% of hydrophobic amino acids, 11.76% acidic, 11.76% basic, and 47.06% neutral (Peptide 2.0), which is also predicted by the AlphaFold2 IA and QUARK Algorithm, and provided in this thesis by courtesy of *JB Fleury* (**Figure 18**). The AlphaFold2 IA Protein Structure Database ranks the model based on a score called “Predicted Local Distance Difference Test (pLDDT) to choose the best model. While a model is scored greater than 90, it is considered as a high accuracy model with characterized binding sites. The pLDDT between the scores 70 and 90 are expected to be modelled with a well prediction [111], [112].

By assuming the helix type as alpha (Heli Quest Analysis tool), the hydrophobicity of the sequence is calculated as 0.346 (+20.80 Kcal/mol) with the net charge (z) of -1. The polar residues are 55.56% and the nonpolar residues are 44.44%, which also confirms the neutral structure. The helical wheel diagram in **Figure 18** shows all the residues by color coding. The hydrophobic residues (methionine (M), valine (V), tyrosine (Y), leucine (L)) are shown in yellow, the acidic residues (aspartic acid (D), glutamic acid (E)) in red, serine (S) and threonine (T) in purple, proline (P) in green, alanine (A) and glycine (G) in gray and histidine (H) in light blue circles. The circles marked with ‘N’ and ‘C’ are the N-terminal and C-terminal ends of the amphipathic helix. The arrow direction at the center shows the direction of the hydrophobic affinity. Thus, this hairpin-like protein shows affinity to both hydrophilic and hydrophobic residues, and it is thus expected to show affinity to the bilayer.

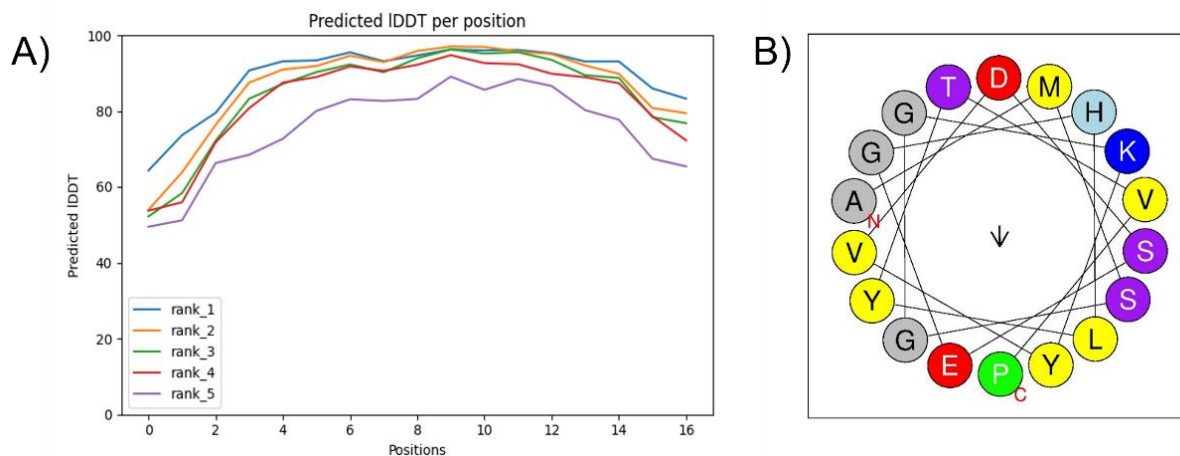


Figure 18 Predicted IDDT per position for Cav1<sub>1-17</sub> by AlphaFold2 IA (A). Sequence by Heli Quest analysis (B).

To follow the dynamics of Cav1<sub>1-17</sub> by fluorescence microscopy, it should be conjugated first. Prior to the conjugation of Cav1<sub>1-17</sub>, the concentration of the peptide was adjusted in the range of (0.03-0.1) mg/ml and 0.065 mg/ml was used. 1 µL of modifier reagent from the conjugation kit was added to 1.3 µL of Cav1<sub>1-17</sub> peptide solution and mixed gently. The sample (modifier reagent and peptide) was mixed with AlexaFluor dye (either AlexaFluor 488 (ab236553) or AlexaFluor 647 (ab269823)) and mixed gently once or twice. This mixture kept in dark at room temperature for 15 min. After that, 1 µL of quenching agent was added and the conjugated Cav1 peptide was ready after 5 minutes of waiting. To create the Proteo-liposomes (PLDs) containing Cav1<sub>1-17</sub>, first a solution composed of DOPC : DOPE : Triolein : BODIPY (493/503) with the molar ratio (33:33:32:2 mol%) was prepared. Here all the components were used from their chloroform stock solutions (10 mg/ml) and in total 30 µL was deposited in a glass falcon. After drying the chloroform for 1 hour under vacuum, 200 µL of PBS were added to the falcon. 1 µL of the conjugated peptide solution was diluted with PBS to ratio of 1:10 (vol/vol) at the same time. This diluted peptide was added to the falcon and stored in 4 °C overnight. Later, it was sonicated for 5 minutes to obtain the Proteo-LDs (Cav1<sub>1-17</sub>-LD). The approximate size of the PLDs measured as 5 µm. For the experiments, this Proteo-LDs were further diluted to avoid their possible coalescence which would result in a disruption of the bilayer.

#### **4.2.6 Formation of PLDs containing ADRP Proteins**

The ADRP is a full-length protein made of 437 amino acids, self-assembled in several  $\alpha$ -helices, with a secondary structure available from the AlphaFold OpenIA database. A stock solution of 0.5 mg/mL is prepared for the recombinant human ADRP proteins (Abcam-ab181932) by mixing it with ultra-pure water (Thermo Fischer). For the labelling of proteins, the AlexaFluor 488 conjugation kit (Abcam-ab236553) is used. First, 5 µg of the proteins are mixed gently with 1 µL of the modifier agent. This mixed sample is pipetted into the AlexaFluor dye and kept standing in dark for 15 minutes. After that, it is mixed with 1 µL of the quenching agent and the conjugated proteins are ready to after 5 minutes of waiting. The Proteo-liposomes containing ADRP proteins are prepared by first depositing in total 30 µL of DOPC:DOPE (1:1 molar ratio) with Triolein by the same protocol mentioned in the section 4.2.5. During the experiments these Proteo-LDs are dispersed around the bilayer and their insertion kinetics are observed using the confocal microscopy.

#### **4.2.7 Artificial Lipid Monolayer Formation**

A simple microfluidic approach is previously reported by *Asfia et.al,2022* to mimic the surface of a lipid droplet [113]. The fabrication of the device was based on positioning of a 3D printed cone at the center of a petri dish, and pouring the degassed PDMS into the mold until the resulting

layer thickness will be around 3 mm. The PDMS was cured at 60 °C for 6-7 hours and bonded to a PDMS coated glass coverslip [113]. The resulting device is composed of a cylindrical hole with 3 mm diameter in a PDMS matrix that is bonded to a glass substrate (**Figure 19**).

The working principle of this device is based on creating a phospholipid monolayer at the buffer-triolein interface composed of the same phospholipid composition as the bilayer. To produce the triolein-lipid mixture, first DOPC:DOPE (1:1 mol%) with a composition of 2% in total weight ratio are dissolved in chloroform and dried under vacuum. The dried phospholipids, triolein and DOPE-Cy5 fluorescent probe (2% in molar ratio) are mixed in an ultrasonic bath. To form the artificial monolayer, 6  $\mu$ L of the triolein-lipid mixture placed in the cylindrical opening of the PDMS device, and then 20  $\mu$ L of KCl solution which is already consist of 1  $\mu$ M conjugated ADRP is added to the top. Within seconds, phospholipid monolayer is spontaneously formed at the triolein-buffer interface. The platform is suitable for performing FRAP experiments (which will be introduced in Section 4.3.2) on this monolayer. Hence, this microfluidic set-up is used to investigate the dynamics of the phospholipids and ADRP proteins on the lipid droplet surface, to make proof of the results obtained in 3D microfluidic device.

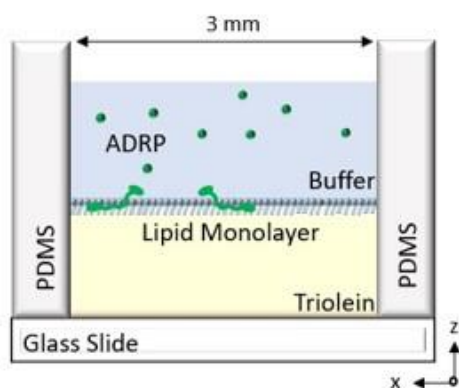


Figure 19 Scheme of the microfluidic device to form the artificial LD monolayer by decorating the phospholipids on the triolein-buffer interface. Reproduced by permission of publisher [114].

#### 4.2.8 Droplet Interface Bilayer (DIB) Formation

The DIB experiments are included in this thesis in courtesy of *JB Fleury* to confirm the presented results obtained by the microfluidic technique, and to assess various bilayer compositions for studying the effect of lipid packing in the bilayer on the regulation of Cav<sub>1-17</sub> proteins. First, the Proteo-SUVs are made by sonication [5]. Here, the buffer of Proteo-SUVs contains same molar concentration of Cav<sub>1-17</sub> peptides used for preparing PLDs. A hydrophobized (octadecyltrichlorosilane, OTS-coated) cylindrical glass container with 7 cm diameter and 1 cm height is

filled with triolein. Two nearly equal size droplets of the buffer containing Proteo-SUVs are injected into the triolein by two micropipettes and let at rest. The Proteo-SUVs in the buffer solution diffuse to the buffer/oil interface and decorate it with lipids by time. Two droplets brought into contact with a needle after 30 minutes, and a bilayer spontaneously appeared between these droplets as shown in **Figure 20** [115].

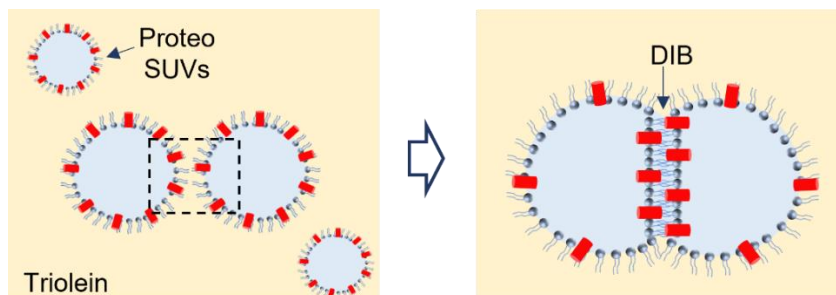


Figure 20 Schematic representation of DIB experiments.

## 4.3 MICROSCOPY

### 4.3.1 3D Imaging

A spinning disk confocal microscopy is used to visualize the system during the experiments. Confocal microscopy offers excellent advantages to achieve more detailed images compared to the wide-field (epifluorescence) microscopes when used in the appropriate area of application. The main feature is to block the out-of-focus light to visualize the specific section chosen in the sample. A shallow focus depth reduces background effects and thus increases signal-to-noise ratio that helps revealing more details, and high-contrast fluorescence images. The main components from the sample towards the detector are respectively: the objective lens, laser-beam splitter, pin-hole lens, and the pinhole. For a confocal microscope with one pinhole i.e., scanning confocal microscope, as the confocal laser collects fluorescence only from one focal point at a time, an image is created pixel by pixel. An alternative for imaging fast dynamics is the spinning disk confocal microscope which illuminates the sample using an array of pinholes arranged on a spinning disk, which is creating hundreds of focused beams [116], [117].

For the experiments to distinguish the positions of each component, distinct fluorophores in different emission wavelengths have been used. Confocal imaging was conducted using the excitation wavelengths of 481 nm and 647 nm, and emission filters of 447/60, 525/30, 607/36, and 685/40 (wavelengths/bandwidths) to distinguish bilayer area, lipid droplets, and proteins. For the quantification of the sample in all directions (x,y and z), 3D images were created by doing

a z-stack through the entire thickness of the sample. Also, by performing optical sectioning, only the section of interest can be quantified with remarkably high spatial precision. Eventually, the resolution of the spinning disk microscope was good enough to evaluate the shapes of the lipid droplets to study the wetting phenomenon, and to track the position of the proteins in the bilayer or lipid droplet.

#### 4.3.2 FRAP

The very first studies about the kinetics of FRAP were performed in the early 80s on cell membranes to investigate the long-range lateral diffusion and coefficient of lipids and proteins [118]–[121]. FRAP technique is applied to model lipid bilayer systems including free-standing or supported bilayers as the distribution of membrane lipids and their interaction with neighboring molecules are important to be understood for the further investigation of membrane organization and signal transduction [122]–[124]. Even if supported bilayers are suitable platforms to mimic the asymmetry of biological membranes, the presence of underlying substrate leads to a decrease in diffusion and mobility [125]. By using free-standing bilayers and GUVs, following the interactions of lipids and proteins within and across the bilayer became more promising [121], [126]. For a free-standing bilayer, a diffusion coefficient of  $\sim 10 \mu\text{m}^2 \text{s}^{-1}$  is reported in the literature [5]. This value is like the value for giant vesicles and is approximately three times faster than supported membranes [127].

Due to its properties, confocal microscopes with FRAP modules are widely used to measure molecular dynamics and interactions quantitatively. Selecting the right emission filter due to the fluorescence probe used in the sample and selecting the objective with the right working distance and numerical aperture can help to improve the image quality as much as possible. The area to bleach can be focused precisely and bleached efficiently with high laser power. For the samples like lipid bilayers, one needs to focus on one single focal plane to get the precise fluorescence signal from the right focus plane. To investigate the dynamic state of a lipid membrane, lipid molecules covalently linked to fluorophores are widely used for specific applications [128]. For a FRAP experiment on a membrane, several steps need to be followed to achieve the diffusion coefficient at the end. The region of interest should be fluorescently labeled in the membrane for the measurements. For the FRAP experiments, a pinhole size of  $50 \mu\text{m}$  was used when a circular area with a diameter of  $50 \mu\text{m}$  is aimed to be bleached. The imaging is performed either with a 40x oil immersion objective ( $\text{WD}=220 \mu\text{m}$ ) or long distance 60x water immersion objective ( $\text{WD}=310 \mu\text{m}$ ). For imaging the system, an EMCCD camera (Hamamatsu) was used.

During the FRAP experiments performed, being at the right focus is key to eliminate the signal from lower or higher focus points. In this way, the right quantitative data to calculate the diffusion coefficient can be measured. Typically, first, the fluorescent intensity of the selected area ( $I_{\text{ROI}}$ ) in the membrane is recorded for a brief period prior to the bleaching. Here, it shows

that there is a continuous signal coming from the sample, and there is no self-quenching of the fluorescence due to the exposed laser. Afterwards, the sample is exposed to an intense laser light (100% power) until the fluorescence molecules are bleached. When the selected area is bleached by high-intensity illumination, that region goes into the dark with a minimum intensity ( $I_0$ ) (intensity value should be 0) due to the elapse of fluorescence molecules. After this brief period of bleaching, the recovery dynamics on this bleached area is observed. Here, the diffusion of the non-bleached neighboring molecules into the bleached region and the diffusion of the bleached molecules outside the region are govern the recovery kinetics. So, this recovery happens due to the replacement of non-fluorescent probes with fluorescent probes by Brownian motion (free diffusion). During the recovery, intensity increases with an exponential trend and fits into the new maximum intensity value. After the recovery is completed, this curve can be fitted to the proper equation to obtain the diffusion coefficient value. Sketched curve of a bilayer with full recovery is shown in **Figure 21**.

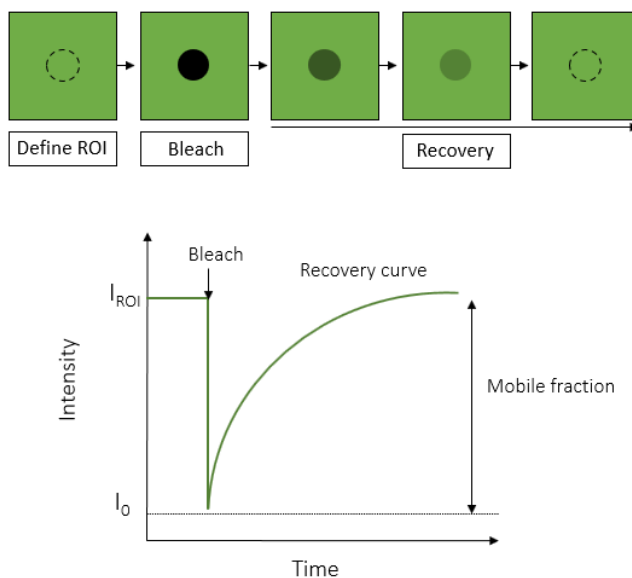


Figure 21 Representation of the principle of FRAP experiments and explanation of the steps by schematic drawing and graph.

To subtract the diffusion coefficient value, the membrane is assumed as a uniformly distributed infinite plane. By taking this assumption, for a simple lateral diffusion calculation, the following “ideal” conditions are assumed to analyze FRAP data: (a) The bleaching laser beam has a Gaussian profile (b) single diffusion coefficient is assumed for recovery (c) there is flow in membrane [118],

[129], [130]. The fitting of the fluorescence recovery curve is expressed by the equation [120], [131]:

$$I(t) = I_0 + \left\{ \sum_{n=1}^{+\infty} \left( (I_{n\infty} - I_0) e^{-2\left(\frac{r}{t}\right)} \left( J_0 \left( 2\frac{r}{t} \right) + J_1 \left( 2\frac{r}{t} \right) \right) \right) \right\} \quad (6)$$

Where  $I_0$  is the initial fluorescence intensity ( $t=0$ ) just after the bleaching,  $J_0$  and  $J_1$  are modified Bessel functions of the 0<sup>th</sup> and 1<sup>st</sup> order,  $I_{n\infty}$  is the intensity of  $n$  number of species at  $t=\infty$  and  $\tau$  is the characteristic diffusion time, respectively [131]. This equation is simplified to calculate the diffusion of molecules within a membrane by Soumpasis in 1983 and the diffusion coefficient ( $D$ ) is theoretically described as follows:

$$D = \frac{r^2}{4\tau} \quad (7)$$

where  $r$  is the radius of the beam, and  $\tau$  is the characteristic diffusion time obtained from the recovery curve [131], [132]. Due to the chosen bleaching area, the radius of the bleaching disk is set as  $r=25 \mu m$  for all the FRAP measurements to characterize the bilayer fluidity. Equation 7 is fitted to the experimental data and used to obtain the diffusivity of lipid molecules and proteins in the bilayer. By this method, transfer rate and protein partitioning can be proved quantitatively. In the current thesis, provided the bilayer is in the fluid state, mobility of lipids and proteins in the bilayer and lipid droplet monolayer are investigated by FRAP technique. The mobility of the lipids and proteins in bilayer and lipid droplet surrounding are determined. The obtained mobility of proteins is guided to the studies to clarify the mechanism behind partitioning.

#### 4.4 PATCH CLAMP RECORDINGS

Patch-clamp is a widely used electrophysiological method to measure membrane thickness and ion channel activity. In this thesis, patch-clamp method is used to confirm the bilayer formation and to measure the thickness of the bilayer. Each membrane behaves as an electrical capacitor separated by a dielectric material for a one-membrane equivalent circuit. The technique can be applied in two diverse ways called "Voltage clamping" and "Current clamping." For voltage clamping, a voltage is applied to a patch of the membrane to measure the resulting current. For current clamping, a current is applied to measure the voltage. With the voltage clamping method, ion flow can be measured in voltage-gated ion channels such as  $Na^+$ ,  $K^+$ ,  $Ca^{+2}$ , and  $Cl^-$  channels



[133]. The patch clamp measurements are also widely used to determine the formation of a bilayer. By applying the technique of “Current Clamping”, the voltage difference across the membrane is detected while applying constant current. The microfluidic device was connected to a patch-clamp amplifier (EPC 10 USB, Heka Electronics) by Ag/AgCl electrodes before forming the bilayer. The two electrodes were prepared by inserting 5-cm-long silver wires into a 100 mM NaCl electrolyte solution applying 3 V for 20 min. The two electrodes were positioned in the channel and the cone respectively to measure the capacitance value, and the optical imaging is also performed simultaneously by a standard inverted microscope (Axio Observer Z1 Zeiss). A detailed description of the system can be found in **Figure 22**. The capacitance of the bilayer is measured using the lock-in function, applying a 10 mV sinusoidal wave with a frequency of 10 kHz. The area of the conductive plates is equal to the area of the bilayer and the thickness of the bilayer is calculated depending on the following equation:

$$C = \frac{\epsilon_0 \epsilon_m}{d} A_m \quad (8)$$

where C is the capacitance,  $A_m$  is the area of the membrane.  $\epsilon_0$  is the dielectric permittivity ( $8.8 \times 10^{-12}$  F/m),  $\epsilon_m$  is the relative dielectric constant of the membrane (2.2) and d is the thickness of the membrane. The thickness of the bilayer is a key parameter to understand if the bilayer formation is completed or not.

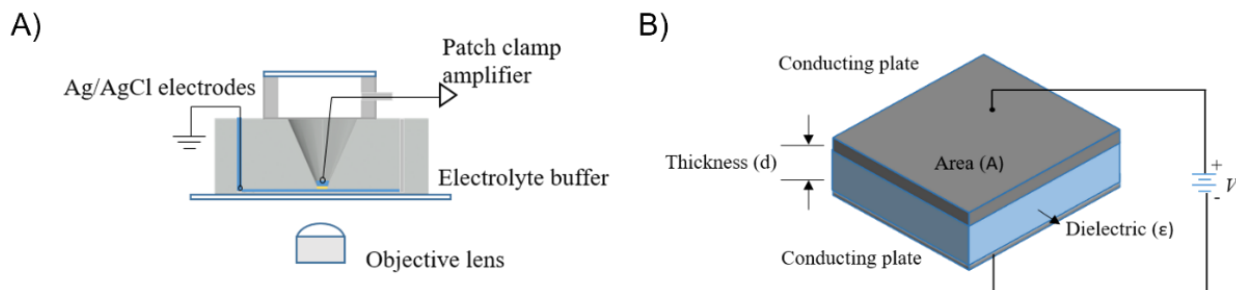


Figure 22 Positioning of Ag/AgCl electrodes into the microfluidic device (A) and the principle of patch clamp measurements of the bilayer (B).

## 4.5 INTERFACIAL TENSION MEASUREMENTS

The interfacial tension was determined by the pending drop method using a contact angle measurement device OCA 20 (DataPhysics, Germany). The phospholipid-oil mixtures were prepared at the same composition that is used for the experiments. The method was applied by filling a transparent cuvette by squalene-phospholipid mixture ( $\rho_{oil} = 0.858 \text{ g/cm}^3$ ) and injecting the buffer solution ( $\rho_{buffer} = 0.998 \text{ g/cm}^3$ ) with a defined volume to create a droplet. The droplet volume was set to  $(2.0 \pm 0.5) \mu\text{l}$  for all the measurements. By this optical method, the shape of the droplet hanging from the needle was determined by imaging the cross-section of the droplet. The geometry of the droplet was automatically extracted by the SCA20 Software based on a Young-Laplace equation [134] which defines the pressure difference between the inside and outside of the droplet with a radius of curvature  $R_i$  as follows:

$$\Delta P = (P_{int} - P_{ext}) = \gamma \left( \frac{1}{R_1} + \frac{1}{R_2} \right) \quad (9)$$

Where  $R_1$  and  $R_2$  are the principal radii of curvature which is shown in **Figure 23**. After a certain time, the surface tension value was fixed and the measurements were continued until the droplet succumbed to the gravity due to the Laplace pressure across the z-axis which is  $\Delta P(z) = (\Delta P_0 \pm \Delta \rho g z)$  where  $\Delta P_0$  is the Laplace pressure of the reference plane. Subsequently, the droplet is ruptured due to the limit of the size with respect to the surface tension. In our case, the liquid-liquid interface is decorated with lipid molecules, and the obtained surface tension value was used to calculate the bilayer tension. After getting the surface tension value, the bilayer contact angle  $2\theta$  was obtained from optical micrographs, and the bilayer tension was calculated using the Young equation,  $\Gamma = 2\gamma \cos(\theta)$  as schematically described by **Figure 5** in **Section 3.2.2**.

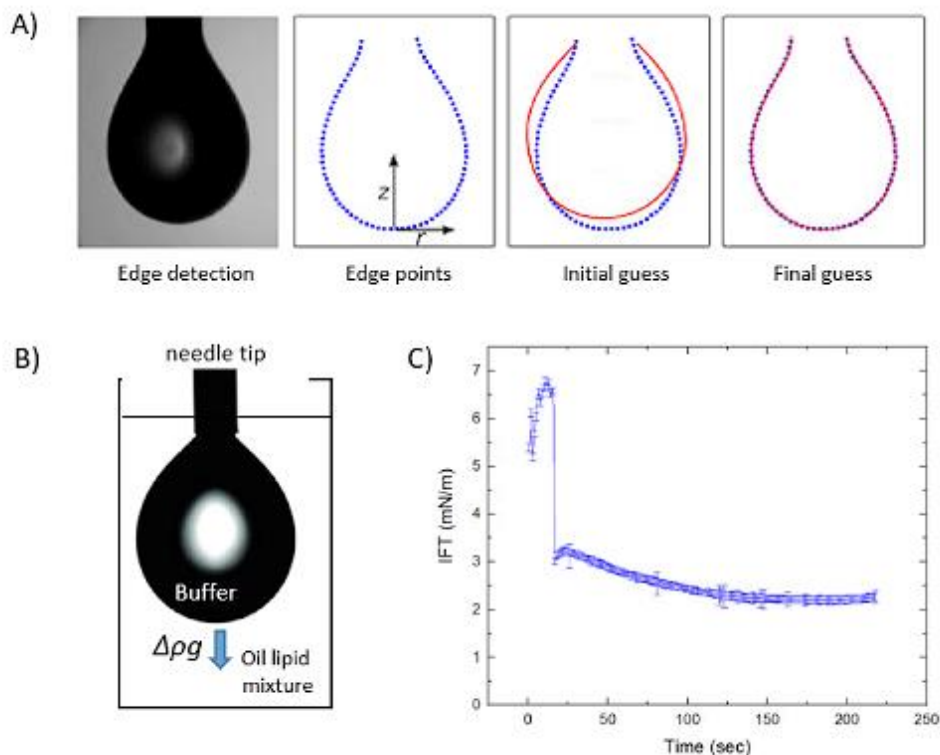


Figure 23 A typical drop image and schematic description of how the geometry of the droplet is fitted to obtain surface tension value (A). Reproduced by permission of publisher [134]. A typical drop image where the buffer phase (0.1 M NaCl) is formed in a mixture of squalene and phospholipids DOPC:DOPE:DOPS (60:30:10 mol%) (B). Corresponding change of IFT (Interfacial tension) by time until the fixed surface tension value is obtained (C).

## 4.6 MOLECULAR DYNAMICS SIMULATIONS

The MD Simulations have been carried out by the group of *Prof. Dr. Jochen Hub, Experimental Physics, Saarland University* to study the lipids localization on the lipid droplets. The Gromacs simulation software (version 2020.4) was used to run the simulations [135]. Characterization of the molecular interactions were completed by Martini 2.0 coarse-grained force field [136]. Verlet algorithm was performed to update the neighbor lists. The bilayer was made of 5000 lipids with a lipid composition of DOPC:DOPC:DOPS (50:40:10). There were 126478 water and 244 sodium beads around the bilayer. To constitute the triacylglycerol lipids in between two monolayers, a gap of 5.8 nm was created by moving them apart in z-direction normal to the membrane. This cylindrical gap with a radius of 8nm (axis is parallel to the z-axis) was filled with 529 triacylglycerol (TAG) lipids. The set-up provide an LD inserted in the bilayer with a well-defined insertion angle [6].

## **RESULTS AND DISCUSSION**

---

## 5 RESULTS AND DISCUSSION

---

### 5.1 BILAYER CHARACTERIZATION

To conduct the experiments with the lipid bilayer, it is important that the bilayers are formed in the microfluidic device behave similarly to an ER membrane in a cell. For that reason, in the following, a full characterization including the formation of the bilayer and its properties is discussed. Details about the formation technique can be found in the “Materials and Methods” section. The formation of the bilayer in the microfluidic set-up is confirmed by electrophysiological measurements (Patch-Clamp) and FRAP.

For the electrophysiological measurements of the bilayer formation, the microfluidic set-up is connected to a Patch-Clamp device by inserting two Ag/AgCl electrodes in the NaCl buffer (0.1 M) containing channel and the cone, and the formation is simultaneously monitored by bright-field microscopy. In this microfluidic geometry, the phospholipid mixture in oil is sandwiched between the buffer phases, and the lipids organize spontaneously to form two oil-water interfaces composed of monolayers of lipid molecules [137]. Optical imaging shows that, once the two interfaces meet between the bottom channel and the upper cone, a disk-like shape appears at the center of the opening which is also shown in literature [5]–[7], [138]. At this point, the formation starts and phospholipids in the oil organize to form a bilayer (**Figure 24**). The sudden appearance of this bright disk-like shape is a result of the draining of the oil from center area, thus changed thickness. The formation process continues until the area reaches the limits of the aperture and the bright ring disappears.

The simultaneous capacitance measurements of the bilayer show that, in the beginning, the capacitance value “ $C$ ” is measured around zero, indicating that the two interfaces are far away from each other. The capacitance value starts to increase by slow thinning of the oil layer between two monolayers. Subsequently, the oil-free bilayer starts forming as the zipping of the two monolayers take place. Therefore, once the formation starts ( $t=47$  s), the capacitance signal increases until meeting a stable value ( $t=55$  s) as shown in **Figure 24**. After this point, the bilayer has reached the size of the aperture, and the constant capacitance value shows that the formation is completed. The formation of an oil-free bilayer is confirmed by calculating the thickness of the bilayer which is calculated by the measured value of the capacitance is 1.3 nF and the diameter of the bilayer (550  $\mu\text{m}$ ). By using *Equation 8* and assuming dielectric permittivity  $\epsilon_0$  as  $8.8 \times 10^{-12}$  F/m and is the relative dielectric constant ( $\epsilon_m$ ) of the membrane as 2.2, the thickness of the lipid bilayer is calculated as  $\approx 3.2$  nm. In the literature, the thickness of a cell membrane is reported as 3-5 nm, which is compatible with the measured value of the lipid bilayer formed in the microfluidic device [139]. These results show that the bilayer is oil-free after the

formation, and the thickness of the bilayer is similar to the reported values for oil-free free-standing and GUV bilayer systems [5], [140], [141].

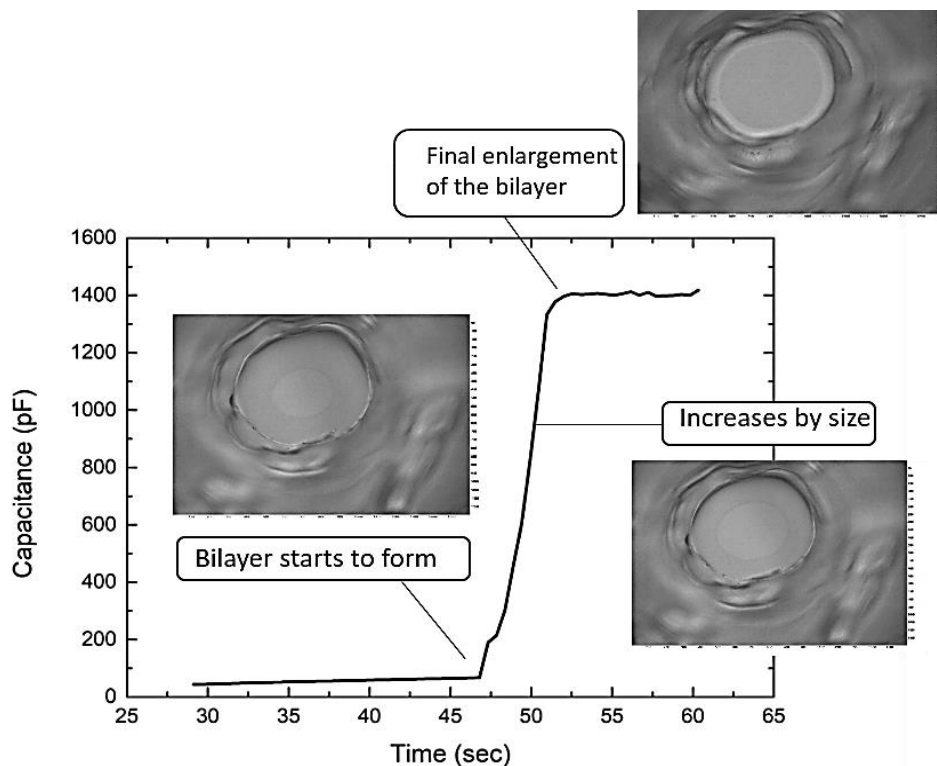


Figure 24 Capacitance measurement of a bilayer formation with bright-field images.

It is necessary to form a free-standing phospholipid bilayer in the fluid state to mimic the biological membrane. To check this membrane property, the physical state of the bilayer is characterized by the FRAP technique to measure the mobility of the lipids, which is the most common technique used to measure the mobility of cellular membrane components like lipids and proteins. For this aim, DOPE lipids in the bilayer are first labeled with the fluorescence dye. Three equivalent-size areas are bleached, and the recovery kinetics are recorded until the intensity approaches a plateau (**Figure 25**) as detailed in the Methods section. To obtain the diffusion coefficient, first, all the intensity value data are normalized due to the maximum value before the bleaching. The Soumpasis equation is fitted to the data to obtain the characteristic diffusion time ( $\tau$ ). From the diffusion time, the diffusion coefficient value for the phospholipids in the bilayer is calculated using **Equation 7** as  $D \approx 10 \mu\text{m}^2/\text{s}$ . This value shows that the lipids are freely diffusing in the bilayer, and the bilayer is in a fluid state. This extracted diffusion coefficient value is remarkably similar to the values reported for all bilayer systems as GUVs [142] and free-

standing bilayers in literature [5], which is three to four times more mobile than a supported bilayer [143].

All the characterization of the free-standing bilayer shows that this microfluidic approach is suitable to produce a free-standing bilayer with good optical and electrophysiological accessibility. Moreover, the bilayer could be produced in the fluid state and with a thickness similar to an ER membrane. These features indicate that this bilayer can be used as a model system to investigate more on the lipid droplets and associated proteins with a reasonable ER membrane composition.

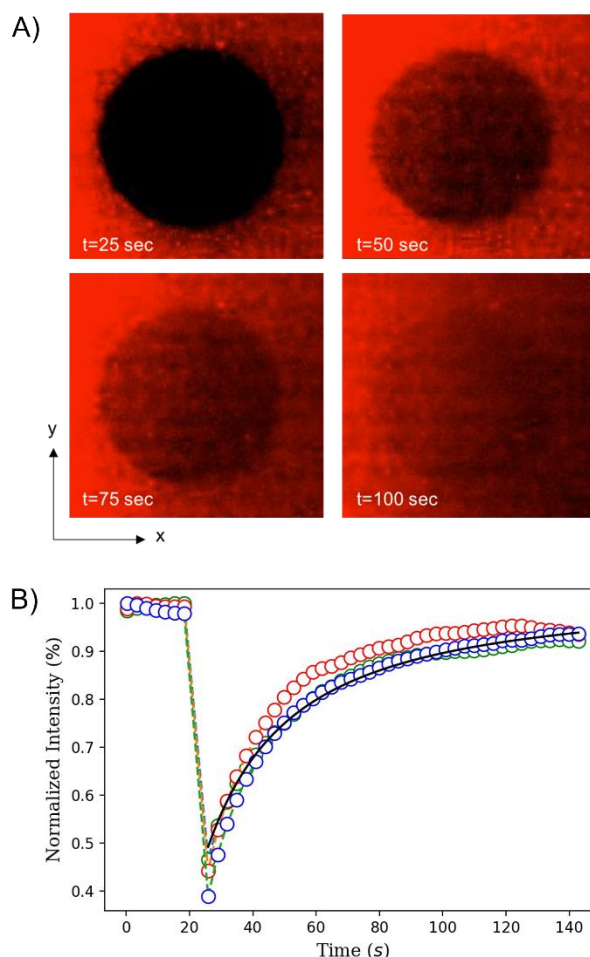


Figure 25 FRAP experiments on the bilayer for the bilayer composition DOPC:DOPE:DOPS (60:30:10 mol%) labelled with Atto DOPE-647N. Scale bars with arrows denote 15  $\mu\text{m}$  for x and y (A). FRAP data for three equivalent areas presented with dots in green, blue and red. The Soumpasis equation fitted to the data presented by the black line (B). Reproduced by permission of publisher [6].

## 5.2 INSERTION OF LDS AND PROTEO-LDS

In the previous subchapter it was demonstrated that the formed free-standing bilayer is a good model system with desirable properties that makes it also suitable to explore the behavior of model lipid droplets (LDs). Insertion kinetics of lipid droplets into the bilayer is one of the most important points to be clarified to investigate the diffusion dynamics of the LDs in the bilayer at the beginning of the studies with LDs. For this aim, the lipid bilayer lipid droplets are prepared with the compositions comparable with the literature [57], [62], [144], [145]. The preparation methods for bilayer and LDs are given in detail in the “Materials and Methods” section. Primary experiments to follow the insertion of LDs are performed by following only the lipid droplet signal by a laser system. Once a free-standing stable bilayer is formed in the microfluidic device, the artificially formed LDs are introduced to the system from the upper cone by pipetting a small volume of the emulsion. After a few minutes, once LDs immobilize at the bilayer area, the fluorescent intensity of the bilayer area increased simultaneously (**Figure 26**) due to the LDs labelled with BODIPY. This quite simple study showed that these LDs are positioned on or into the bilayer but the exact lateral position could not be determined. Therefore, the shape and position of LDs are determined by spinning-disk confocal microscope by using high numerical aperture objectives.

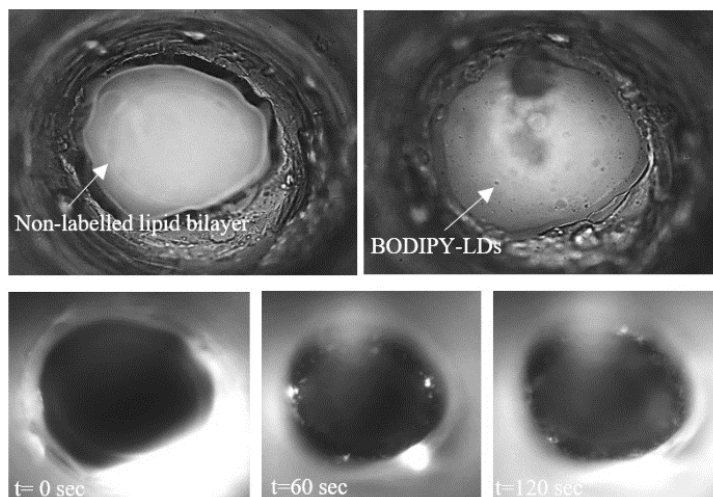


Figure 26 Lipid droplets labelled with BODIPY 493/503 on a non-fluorescent bilayer with a composition of DOPC:DOPE:DOPS (60:30:10 mol%).

Triolein-LDs are expected to encapsulate between two monolayers of the bilayer [50], [64], [101], [146], as the hydrophobic molecules can be encapsulated between two amphiphilic leaflets of the bilayer. These molecules either spread evenly in the bilayer or form droplets. Considering the



mechanics of membrane fusion, the fusion of the LD monolayer with the bilayer can be described as a stalk-like intermediate state upon very close contact of the two layers with a negative curvature through the stalk rim. The LDs with 5  $\mu\text{m}$  diameter imply a diffusion coefficient of 0.1  $\mu\text{m}^2/\text{s}$  in the bulk via the Einstein relation [147]. The insertion of a lipid droplet with a monolayer lipid composition of PC:PE (1:1 mol%) takes 10-15 min after introduction from the cone. For the LDs with a monolayer lipid composition of PC only, the insertion takes at least one hour. The accumulation of cone-shaped PE lipids may stabilize the pore rim by advocating the negative curvature [148], [149]. This shows that the presence of PE in the LD monolayer reduces the insertion energy barrier and facilitates the insertion of LDs into the bilayer.

For this system, the LD insertion and shape are confirmed by the position of the triolein that is visible as green due to BODIPY sandwiched between the two leaflets of the bilayer that are visible as red due to Atto647N. Overall, the z-stacks with a step size of 300 nm give a clear 3D image of how the lipid droplets have reached the bilayer, and how they are inserted (**Figure 27**). The LD does not spread after embedding into the bilayer but takes a characteristic lens shape with a well-defined insertion angle and does not move afterward [150]. The obtained 3D shape of an LD inserted in the bilayer is defined as highly symmetric as shown in **Figure 28**.

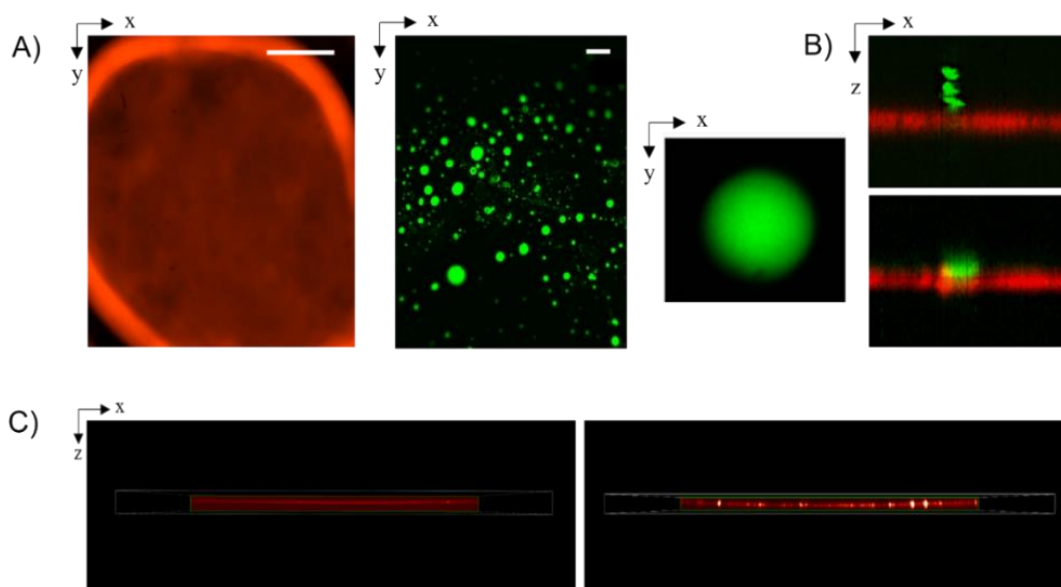


Figure 27 Fluorescence microscopy images of the lipid bilayer (left image) and LDs (middle two images) in bulk. Scale bars are 100  $\mu\text{m}$ , 10  $\mu\text{m}$ , and 1  $\mu\text{m}$  for bilayer, LDs, and single LD images, respectively (A). z-stack images of LD before (upper image,  $t \approx 5$  min) and after (bottom image,  $t \approx 10$  min) touching the bilayer (B). Lipid bilayer before and after LD insertion (C). Scale bars with arrows, 5  $\mu\text{m}$  for x and z. Reproduced by permission of publisher [6].

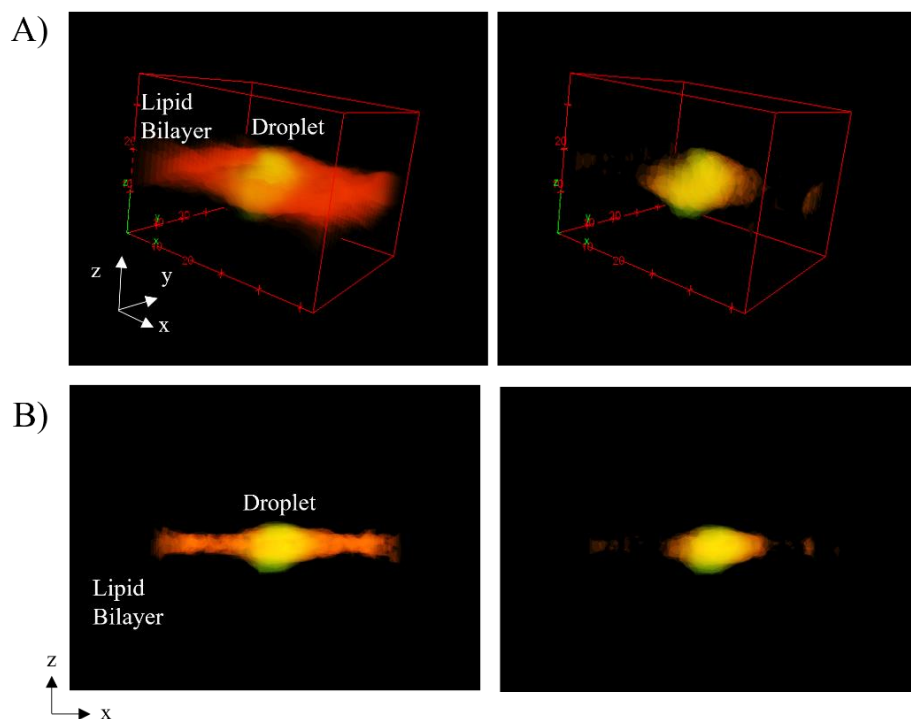


Figure 28 3D representation of a lipid droplet (in yellow) inserted in the 40 mol% cholesterol including bilayer (in red). Scale bars with arrows show 10  $\mu\text{m}$  in the upper panel (A). The xz plane of a lipid droplet insertion. Scale bars for the lower panel; 10  $\mu\text{m}$  for x and 2  $\mu\text{m}$  for z (B). Reproduced by permission of publisher [6].

The partitioning of several type of proteins that insert into the membrane are also studied to investigate the insertion kinetics of lipid droplets in presence of proteins. The first study is done by the Proteo-LDs (PLDs) consisting of the peptides of UBXD8 proteins, UBXD8<sub>71-132</sub>, which includes a hairpin region. After the bilayer formation, these PLDs labelled with fluorescent probes are introduced to the system from the upper cone following the same strategy as LD insertion before (**Figure 29**). From the bilayer core ( $z=0$ ) through the top of the PLD, the fluorescence signal transforms from a green ring ( $z=0$ ) to a spot ( $z=700$  nm). The green ring demonstrates the UBXD8<sub>71-132</sub> peptides are covering the interface. The spot at the top of the PLD shows a large area covered with proteins on the monolayer.

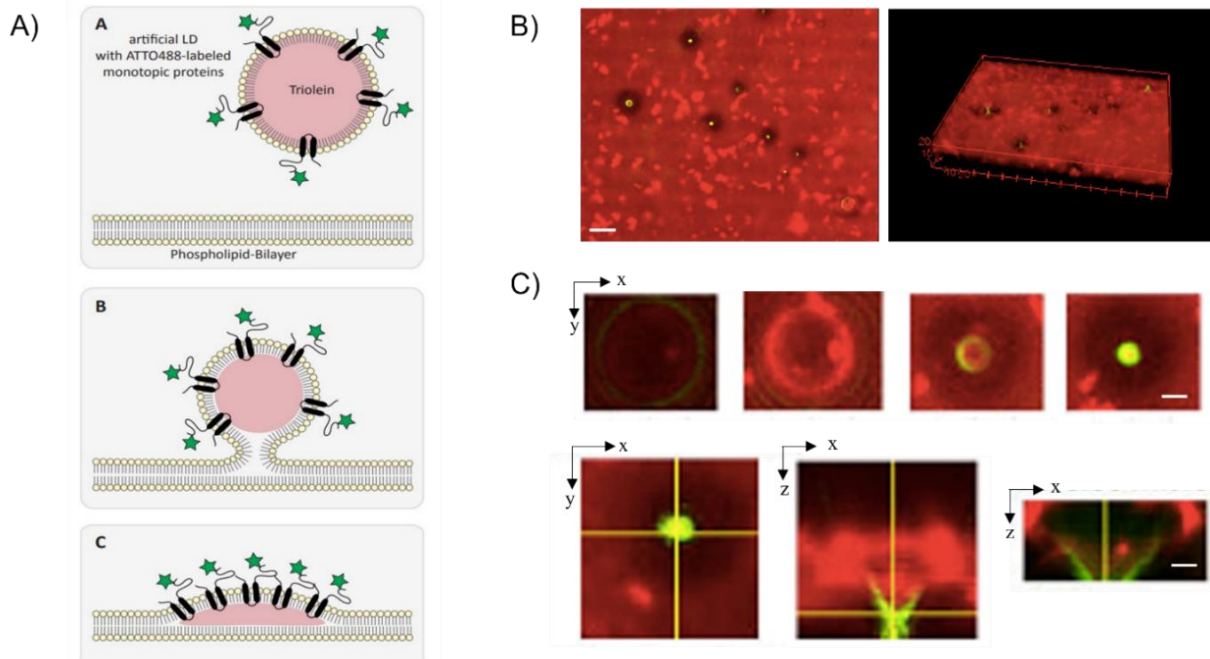


Figure 29 Schematic representation of the PLD-UBXD8 insertion pathway (A). Fluorescence images of the bilayer (red signal, Atto DOPE) containing PLDs (green signal, Atto488). The scale bar shows 15  $\mu\text{m}$  (B). z-stacks from the bilayer core through the PLD top (upper row). Scale bars denote 15  $\mu\text{m}$  and 10  $\mu\text{m}$  (x,y) for upper and lower rows, and z-arrows show 1  $\mu\text{m}$  for the lower left two images and 700 nm for the right image (C). Reproduced by permission of publisher [6].

Here, the 3D images have shown that the insertion of PLDs differs from LDs due to their positioning after the immobilization as the proteins are present only in the LD monolayer which indicates that these monotopic hairpin proteins are only localized in the monolayer leaflet on the side of insertion with their hydrophobic domain and changed the surface tension of the monolayer. Even after monitoring for 30 minutes, the proteins do not partition by freely diffusing from the monolayer through the bilayer. As a result, the localization of the proteins on one side of the LD breaks the symmetry and changes the monolayer composition, which ends up with an asymmetric LD shape as a bulge toward the protein-containing leaflet.

To explore the insertion kinetics of a hairpin-like protein, Cav1<sub>1-17</sub> is introduced to the system. During the insertion, first, the LD takes an asymmetric shape for a few minutes. Then a transition state takes place and once the LD completely embeds into the bilayer core. After insertion of the PLDs into the bilayer, the mixing of the LD monolayer phospholipids occurs as well as the mixing of proteins. When the system is equilibrated, the proteins are redistributed between the bilayer and LD monolayer and become visible in both areas. The shapes examined by the confocal

microscopy show that the LDs resulted in a symmetrical lens shape as shown in **Figure 30** [6], [50], [102], [146]. To achieve a symmetric LD shape like this after insertion in presence of proteins, the proteins should be also distributed equally in both leaflets. If the surface tensions for the cases with and without proteins are compared, the results show that the surface tension of LDs covered with PC/PE (1:1 mol%) monolayer ( $\approx 2$  mN/m) is very similar to the surface tension of LDs with  $1 \mu\text{M}$  of Cav1<sub>1-17</sub> ( $\approx 1.3$  mN/m). This means that the proteins are surface active, and they have a role in the achievement of remarkably close surface tensions in two monolayers surrounding the LDs. Hence, the symmetry of inserted lipid droplets is not destroyed in presence of Cav1<sub>1-17</sub> proteins which can be explained by the spontaneous diffusion of these proteins through the droplet core until both of the monolayers contain equivalent protein concentrations. This experimental result is in line with the literature about spontaneous diffusion of the Cav1<sub>1-17</sub> proteins which have been found in the LD core in our model system, as seen in the cell [82].

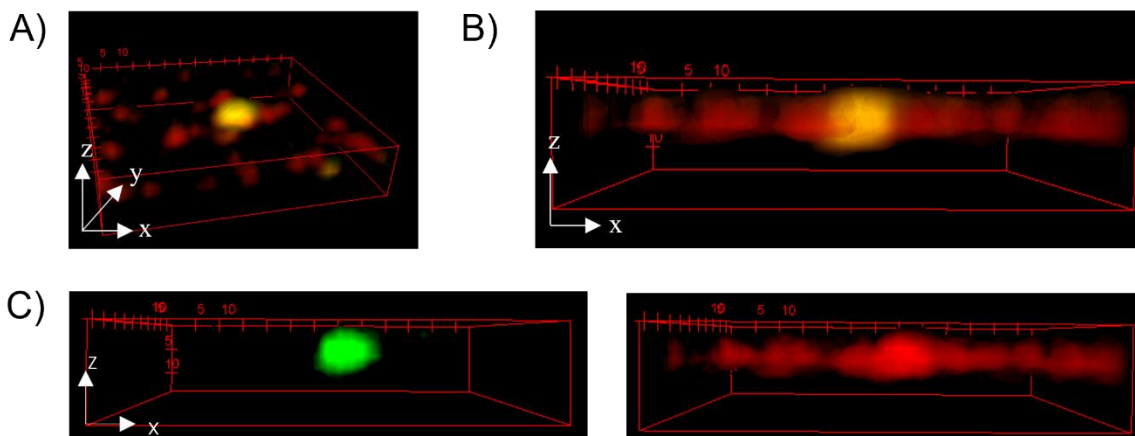


Figure 30 3D confocal images of an bilayer inserted PLD containing Cav1<sub>1-17</sub>. Channels are shown for LD and proteins in green and red colors, respectively. Scale bars with arrows denote  $5 \mu\text{m}$  (x,y, and z) (A) and  $5 \mu\text{m}$  (B) and  $2 \mu\text{m}$  (C) for (x and z).

To investigate the shape of the lipid droplets inserted in the bilayer in presence of a protein with an affinity to lipid droplet, the Proteo-LDs consisting of the ADRP proteins which has a cytoplasmic lipid droplet binding domain are studied. The surface tension measurements show that ADRP proteins are highly surface active as a triolein/buffer interface in presence of  $1 \mu\text{M}$  ADRP has a surface tension of  $\approx 10$  mN/m which is three times less than the surface tension of the interface without any surface-active molecules. So, these proteins are free to move on the lipid droplet surface as well as the core. The 3D confocal scans are performed on the inserted droplets to determine their shapes after the insertion of PLDs by following the same steps introduced previously for LDs and Proteo-LDs including UBXD8 and Cav1<sub>1-17</sub>. The fluorescence

images reveal that after the lipid droplets including ADRP proteins inserted into the bilayer, they have a diameter of about 20  $\mu\text{m}$  and a height of about 5  $\mu\text{m}$ , which shows that the shape of the droplets slightly escape from the ideal lens-shape with spherical interfaces which have been previously shown for the lipid droplets without proteins (**Figure 31**). These pancake shapes might be a result of inhomogeneous distribution of the surface active ADRP molecules, which might be accumulated more at the circumference of the LD and lowered the local surface tension as the measured surface tension values are very close to the value of surface tension of a pure triolein-water interface.

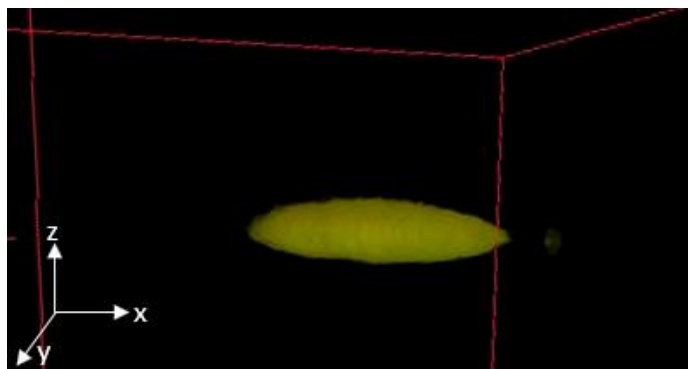


Figure 31 The typical pancake shape of Proteo-LDs containing ADRP proteins inserted into the bilayer. Scale bar denotes 5  $\mu\text{m}$  for x,y, and z.

Even if the hairpin structure and surface activation of UBXD8 protein allows the accumulation of the protein on one leaflet of the lipid droplet, the freely-diffusing protein ADRP with lipid droplet binding domains (PAT) are localized on the lipid droplet as expected [151], and lipid droplets with ADRP proteins resulted in a quasi-symmetric pancake shape. This shape is like the symmetric shape of the lipid droplets in presence of Cav<sub>1-17</sub> peptides and in contrast to the asymmetric shape of UBXD8 containing PLDs.

### 5.3 STUDYING WETTING PHENOMENON FOR LDS AND PLDS

The wetting of inserted LDs and PLDs are studied once the bilayer with the desired composition is completely stable. Characterization of the 3D shape of the bilayer-embedded LDs without proteins show a highly symmetric lens shape as previously mentioned in Section 5.2, which is like the lens shape of an LD in ER membrane before biogenesis. Bilayer tension is one of the main factors to change the shape of a LD by tuning the insertion angle of the LD. The wetting properties of the membrane are investigated depending on the cholesterol content in the bilayer by varying the amount from 20% to 40% (mol%) in the bilayer. Two-dimensional surface plot projections are created for each LD to measure the insertion angles both for the upper and lower leaflets as shown in **Figure 32**.

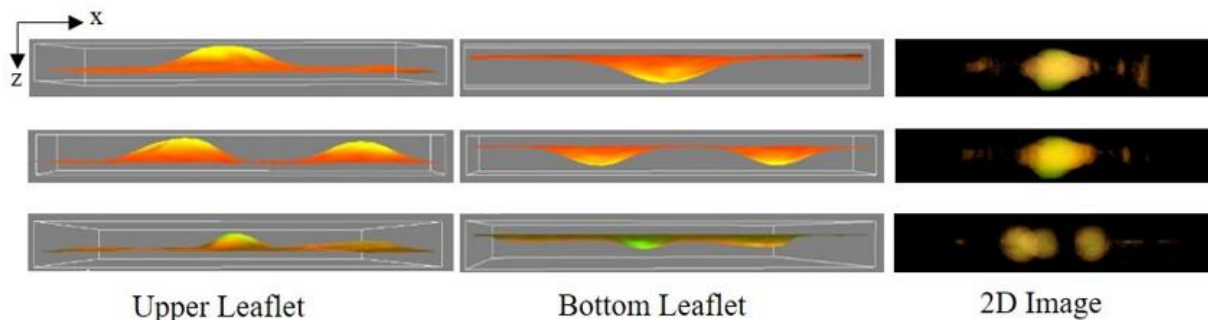


Figure 32 2D surface plot projections (left two rows) and corresponding confocal images (right rows) of LDs for bilayer-cholesterol compositions 40%, 30%, and 20% from top to bottom. Scale bars denote 5  $\mu\text{m}$  and 200 nm for x and z planes, respectively. Reproduced by permission of publisher [6].

To understand the dependence on cholesterol content of the bilayer, the measured insertion angles of LDs and PLDs are compared with the wetting theory [50], [63], [101], [146]. By using the 3D shapes of the lipid droplets, angles are measured, and surface tension values for bilayer and lipid droplets were obtained by the pendant drop method. According to the wetting theory, the balance of the bilayer tension ( $\Gamma$ ) and lipid droplet tension determines the shape of the LD. Here for a lipid droplet, the tension applied by the horizontal components of the upper leaflet surface tension is defined as  $\Gamma_{ULD} = \gamma_{ULD} \cdot \cos(\alpha_U)$ , and the lower leaflet surface tension is defined as  $\Gamma_{LLD} = \gamma_{LLD} \cdot \cos(\alpha_L)$  where  $\alpha_U$ ,  $\alpha_L$  are the measured angle and  $\gamma_{ULD}$ ,  $\gamma_{LLD}$  are the surface tensions (**Figure 33**).

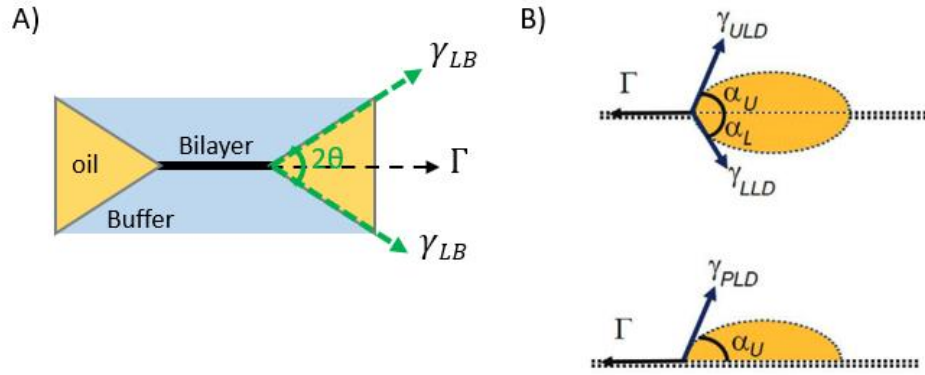


Figure 33 Schematic representation of surface forces acting on the bilayer (A) on a LD in the bilayer for the symmetric (upper) and asymmetric (lower) case (B). Reproduced by permission of publisher [6].

The lipid droplet tension considering both leaflets can be written as:

$$\Gamma_{LD} = \gamma_{ULD} \cdot \cos(\alpha_U) + \gamma_{LLD} \cdot \cos(\alpha_L) \quad (10)$$

Due to the Young-Dupre law, in equilibrium, the bilayer tension is defined as  $\Gamma = 2 \gamma_{LB} \cos(\theta)$  which is shown in **Figure 33** [50]. Here,  $\gamma_{LB}$  is the surface tension of one of the monolayers which are forming the bilayer,  $2\theta$  is the contact angle of the plateau border. For a symmetric bilayer the equation becomes:

$$\frac{\gamma_{LB}}{\gamma_{LD}} = \frac{\cos(\alpha_U) + \cos(\alpha_L)}{2\cos(\theta)} \quad (11)$$

For mirror symmetric lipid droplets with respect to the bilayer, we can simply assume  $\alpha_U = \alpha_L = \alpha_U$  and simplify Equation 11 to

$$\frac{\gamma_{LB}}{\gamma_{LD}} = \frac{\cos(\alpha)}{\cos(\theta)} \quad (12)$$

The extracted values (shown in **Table 1**) fit **Equation 12** and are compared with the wetting theory as plotted in **Figure 34**. The results demonstrate that when the cholesterol amount increased from 20% to 40%, the lipid bilayer contact angle of an LD decreases from  $(49\pm 3)^\circ$  to  $(29\pm 2)^\circ$ . Here, even if the angle changes, the characteristic lens shape of a LD is not affected by that. As the cholesterol amount in the bilayer increases, a reduction of the measured angle is observed due to the increased bilayer tension. In line with the literature, the displayed results are indicating that the lens shapes of the LDs are comparable with an equilibrium wetting theory for different amounts of cholesterol which is consistent with the literature [152], [153].

Table 1 Characterization of a bilayer including embedded LDs and PLDs containing UBXD8 protein.

<b>Lipid Droplets</b>					
<b>Cholesterol</b>	LB Surface Tension $\gamma_{LB}$ mN/m	LB Contact Angle $\theta$	Lipid Bilayer Tension $\Gamma$ mN/m	Lipid Droplet Tension $\gamma_{LD}$ mN/m	Lipid Droplet Contact Angle $\alpha$
<b>20%</b>	2.9±0.2	$(49\pm 3)^\circ$	3.8 ±0.2	1.7±0.2	$(33\pm 3)^\circ$
<b>30%</b>	3.0±0.3	$(41\pm 3)^\circ$	4.5±0.3	1.8±0.2	$(27\pm 2)^\circ$
<b>40%</b>	2.5±0.3	$(29\pm 3)^\circ$	4.3±0.3	1.9±0.3	$(24\pm 2)^\circ$
<b>PLDs</b>					
<b>Cholesterol</b>	LB Surface Tension $\gamma_{LB}$ mN/m	LB Contact Angle $\theta$	Lipid Bilayer Tension $\Gamma$ mN/m	Lipid Droplet Tension $\gamma_{LD}$	Proteo-LD Contact Angle $\alpha$
<b>0%</b>	0.78±0.2	$\approx 0$	3.2±0.2	1.6±0.2	$(40\pm 3)^\circ$



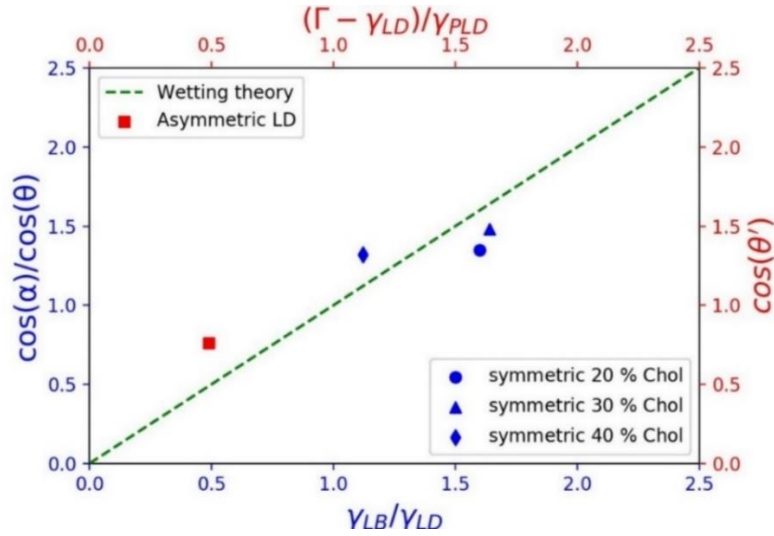


Figure 34 Comparison with the wetting theory for bilayer embedded LDs for 20%,30% and 40% cholesterol, and PLDs containing UBXD8 protein for 0% cholesterol. Reproduced by permission of publisher [6].

The asymmetric shapes of inserted Proteo-LDs are also analyzed by wetting theory. As it is already shown, when a Proteo-LD including UBXD8 peptides is embedded into the bilayer, the UBXD8<sub>71-132</sub> proteins are coated only on one side of the LD surface, which eventually created an asymmetric distribution on LDs. An asymmetric shape of a PLD with UBXD8 proteins in equilibrium fulfills the subsequent equation based on the wetting theory:

$$\Gamma_{PLD} = \gamma_{PLD} \cdot \cos(\alpha_U) + \gamma_{LD} \cdot \cos(\alpha_L) \quad (13)$$

Here the upper leaflet contains the protein, and due to the strong asymmetric shape, we can assume that  $\alpha_L$  of the droplet side which does not contain any proteins is approximately zero, so the lower leaflet tension can be written as  $\gamma_{LD} \cos(\alpha_L) = \gamma_{LD}$  and Equation 13 becomes:

$$\frac{\Gamma_{PLD} - \gamma_{LD}}{\gamma_{PLD}} = \cos(\alpha_U) \quad (14)$$

From the measured angles and calculated bilayer and lipid droplet tensions (**Table 2**), it can be concluded that the surface tension of one of the leaflets is adjusted by the proteins which causes the difference between the two leaflets, which resulted by an asymmetric bulged shape of the LD.

To investigate the wetting of lipid droplets in presence of proteins with high affinity to lipid droplets, PLDs consisting of ADRP (Adipose-differentiation related protein) proteins are investigated by using different cholesterol amounts in the bilayer. The contact angle values are extracted from the fluorescence images of PLDs inserted in the bilayers. The extracted values of surface tensions and contact angles (**Table 2**) of lipid droplet and bilayer fit to **Equation 11** and compared with the wetting theory as plotted in **Figure 35**. The results show that in presence of surface active ADRP proteins, increasing cholesterol amount results in an increased LD surface tension and also increased contact angle of inserted LDs. However, the already reported quasi-symmetric pancake-like shape remains and even more pronounced the increased the cholesterol concentration (from 0% to 40%), respectively the larger the contact angle (**Figure 35**).

Table 2 Characterization of a bilayer including embedded LDs and PLDs containing ADRP protein by using the values obtained by Interfacial Tension measurements.

Protein ( $\mu\text{M}$ )	Cholesterol	Bilayer Tension $\Gamma$ mN/m	LB Contact Angle $\theta$	LD Tension $\gamma_{\text{LD}}$ mN/m	LD Contact Angle $\alpha_{\text{U}}$	LD Contact Angle $\alpha_{\text{L}}$
1	0%	2 $\pm$ 0.2	(64 $\pm$ 3) $^\circ$	1.1 $\pm$ 0.2	(42 $\pm$ 3) $^\circ$	(35 $\pm$ 3) $^\circ$
1	20%	2.4 $\pm$ 0.3	(67 $\pm$ 3) $^\circ$	2 $\pm$ 0.3	(65 $\pm$ 3) $^\circ$	(55 $\pm$ 3) $^\circ$
1	40%	3.1 $\pm$ 0.3	(69 $\pm$ 2) $^\circ$	3.9 $\pm$ 0.2	(75 $\pm$ 3) $^\circ$	(65 $\pm$ 3) $^\circ$
0	0%	2 $\pm$ 0.2	(63 $\pm$ 2) $^\circ$	1.6 $\pm$ 0.2	(49 $\pm$ 3) $^\circ$	(51 $\pm$ 3) $^\circ$

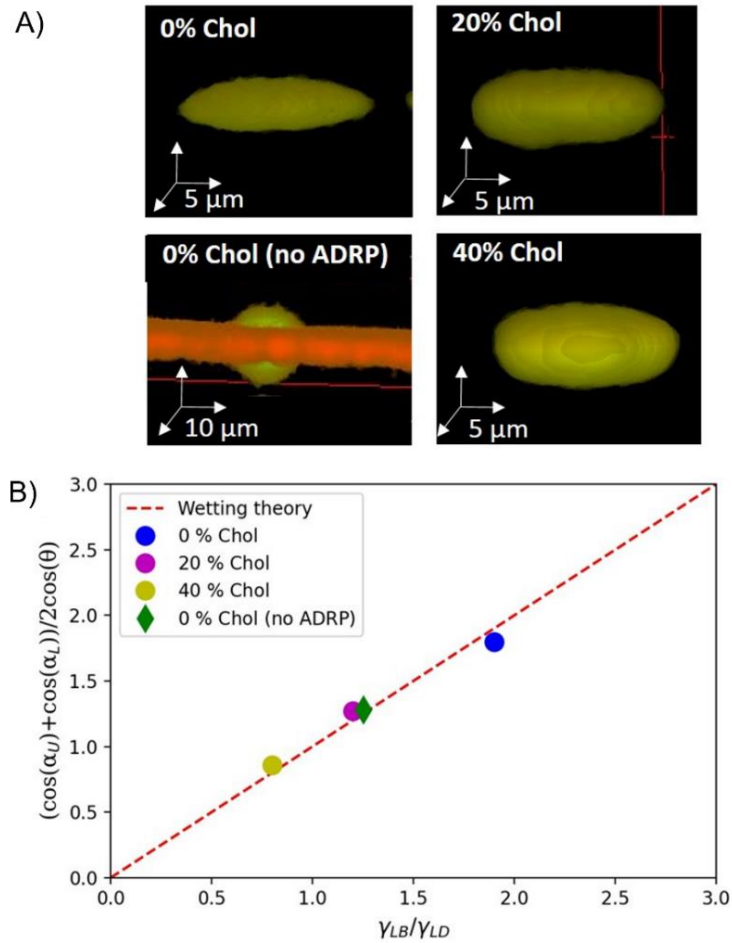


Figure 35 3D confocal images of bilayer embedded PLDs for 0%, 20% and 40% cholesterol, and bilayer embedded LD for 0% cholesterol (A). Comparison with the wetting theory (B).  
Reproduced by the permission of publisher [8].

The results of both lipid droplet and PLD studies have shown that the droplet shapes can be described by equilibrium wetting theory by using the insertion angles and surface tension values for the symmetric or asymmetric case. Depending on the type of the protein, the symmetry of lipid droplets without proteins can either be broken (as shown by UBXD8 containing PLDs) or the lipid droplet can take a specific shape like a pan-cake due to the non-homogeneous distribution of surface-active proteins (as shown by ADRP containing PLDs). This means that the distribution of the proteins due to their functional elements and types, is a controlling mechanism on the shape of the bilayer-embedded PLDs.

## 5.4 LIPID DIFFUSION BARRIER

As the microfluidic device is suitable for high-resolution optical imaging of LDs as detailed in Section 5.1, it also can be used to investigate the exchange rate of phospholipids and proteins between the lipid droplet and the bilayer. For this aim, either the phospholipids and proteins in the lipid droplet area or in bilayer area are bleached depending on the aim of the experiment as sketched in **Figure 36**.

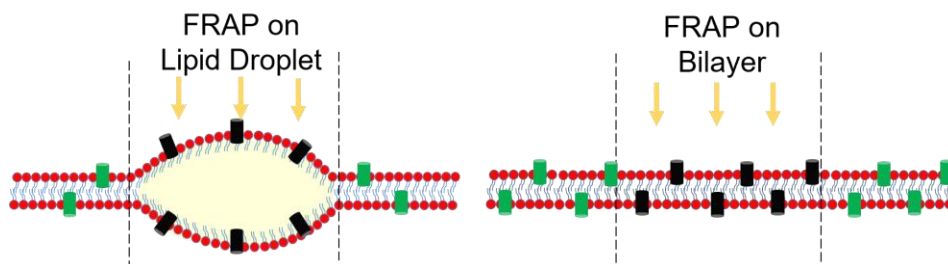


Figure 36 Area selection in the area of lipid droplet and bilayer. For bleaching the molecules on LD surface, entire surface of the lipid droplet, and for the bilayer, a bleaching area at the center of the entire bilayer is selected.

First FRAP experiments were performed on BODIPY-labeled neutral lipids in the LD core inserted into a non-fluorescent bilayer to explore the neutral lipid exchange between the lipid droplet core and the surrounding bilayer area. The results show that once the neutral lipid is bleached, there is no recovery, which indicates that an inserted LD is isolated from the surrounding without any spreading of neutral lipids inside the two leaflets of the bilayer (**Figure 37**). This means that the lipid droplets inserted in the bilayer are separated from the bilayer with a boundary around the LD rim, which will be studied in the following experiments to investigate the exchange rate of phospholipids between the bilayer and lipid droplet.

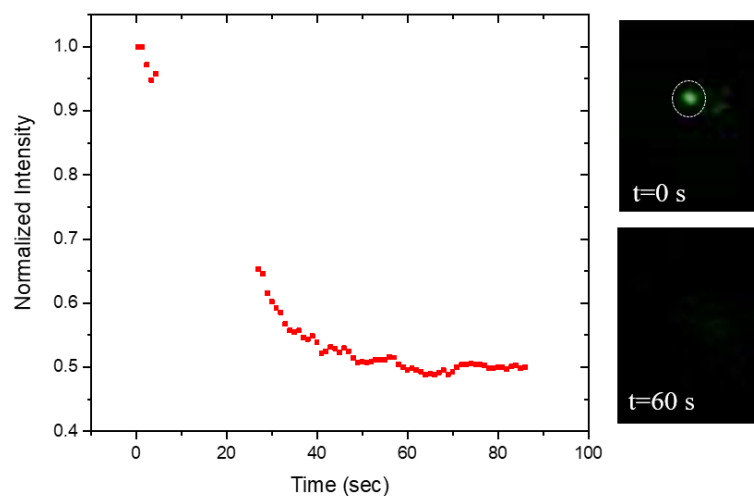


Figure 37 FRAP measurements on the neutral core of the lipid droplet with a size of 5  $\mu\text{m}$  inserted into a bilayer. The area is bleached for 20 seconds. Reproduced by permission of publisher [6].

For the phospholipid exchange rate experiments, the DOPE phospholipids in the bilayer are labeled with Atto-DOPE. The phospholipids in the LD monolayer are not labeled (invisible) until the LD is inserted into the bilayer. After the insertion of LDs, LD monolayer starts to fluorescent with the same intensity. This shows that these phospholipid molecules could exchange between the lipid droplet and the bilayer. When the phospholipids in the selected bilayer area without LDs are bleached, the recovery is observed after 30 seconds as shown in **Figure 38**. This area is completely recovered by the neighbor fluorescence molecules in 120 seconds. The experiments are continued by bleaching the phospholipids in the area of lipid droplets. On contrary, when only the area of the LD is bleached, a reduced recovery of the phospholipids is observed. The recovery is started from the intersection points through the center, and the area is never fully recovered.

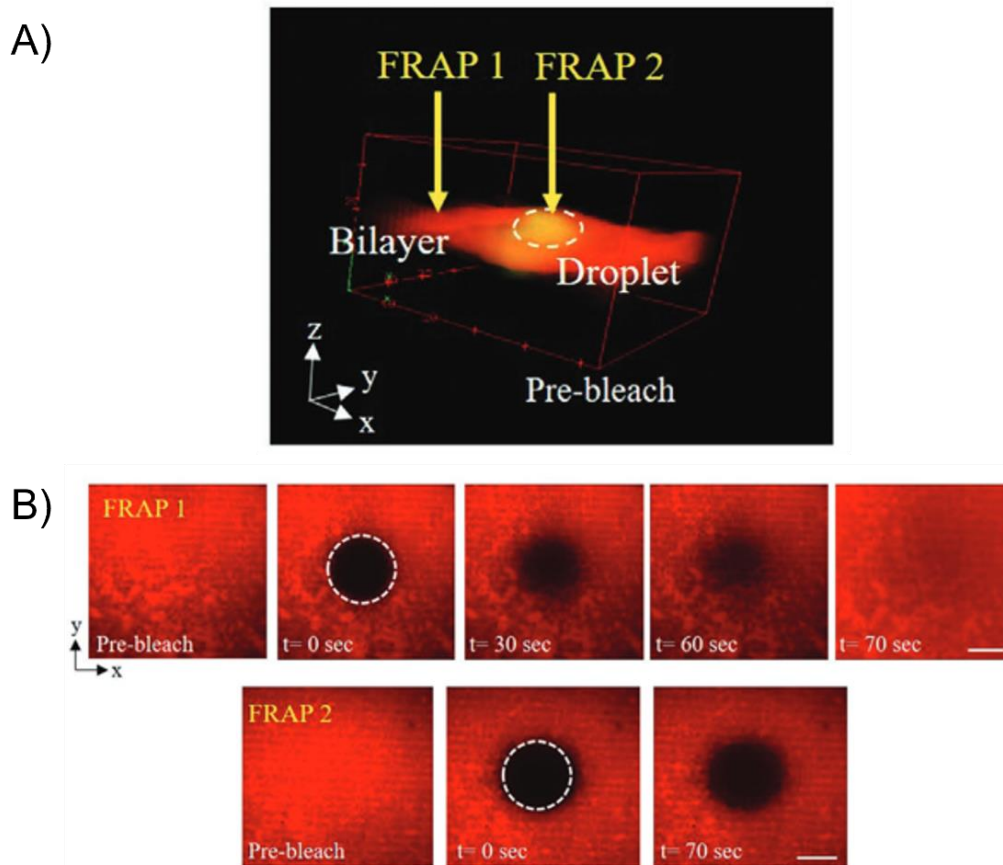


Figure 38 3D representation of the selection of areas for LD and bilayer before bleaching. Scale bars are  $10\ \mu\text{m}$  for all directions (A). FRAP experiments on the bilayer (upper row) and the entire LD (lower row) for the bilayer composition DOPC/DOPE/DOPS (60:30:10 mol%) labelled with Atto DOPE-647N. The scale bar shows  $25\ \mu\text{m}$  and  $10\ \mu\text{m}$ , respectively (B). Reproduced by permission of publisher [6].

The results show that even if there is 85%-100% recovery with respect to the initial value (before bleaching) in the bilayer, the recovery in the LD area is limited to a maximum of 10% with respect to the initial value of the LD area. Namely in the LD area, the recovery is slowed down from the sides through the center of the lipid droplet and stopped when the fluorescently labeled phospholipids are reached the lipid droplet area. The intensity values are extracted from measurements as in Figure 38 and plotted as recovery curves in **Figure 39**. The Soumpasis equation is fitted to these data to obtain the recovery time, thus, finally a diffusion coefficient. Due to that, the diffusion coefficient value obtained for the bilayer is  $\approx 10\ \mu\text{m}^2/\text{s}$ . However, the corresponding results of the LD area reveal a remarkably diminished motility of the phospholipids from the surrounding bilayer onto the LD surface (**Figure 39**). If the Soumpasis equation is fitted to the recovery curve of LD area, the suggested diffusion coefficient is calculated as  $0.1\text{-}0.5\ \mu\text{m}^2/\text{s}$  which points out diminished mobility of phospholipids on the lipid droplets by approximately one order of magnitude compared to the phospholipids in the bilayer. However, when assuming a

diffusion barrier for the lipids, the Soumpasis equation is not valid anymore. Based on the invalidity of Soumpasis equation in presence of a diffusion barrier, it is considered that the exchange of phospholipids can be quantified due to the transport rate between two membranes in contact, here LD monolayer and one leaflet of the bilayer. At  $t=0$  sec, one leaflet of the bilayer contains fluorescence molecules, and the LD monolayer does not contain them. When they are in equilibrium, they could exchange the molecules reversibly. The exchange of these molecules can be written as:



Where  $[A]$  and  $[B]$  are the concentration of fluorescent lipids in the donor and acceptor membranes, respectively. By using this one-stage first-order reversible reaction model, the lipid transfer rate can be differentiated as follows:

$$\frac{d[A]}{dt} = -\frac{d[B]}{dt} = k_{-1}[B] - k_1[A] \quad (16)$$

Here,  $k_1$  and  $k_{-1}$  are the transport rates for  $A$  and  $B$ . At the beginning ( $t=0$ ), the donor membrane has a number of molecules, " $N$ ", and the acceptor membrane has no molecules, assuming  $k_{-1}=k_1=k$ , the Equation 16 can be expressed as:

$$B = \frac{N}{2} (1 - e^{-2kt}) \quad (17)$$

$$\Delta I = \frac{N\alpha}{2} (1 - e^{-2kt}) \quad (18)$$

Where  $\Delta I$  is the fluorescence intensity change,  $\alpha$  is the scaling factor which is the efficiency of certain number of molecules result in fluorescent signal, and  $N\alpha/2$  is the final plateau value. Fitting Equation 18 to the recovery data on the LD surface, a transport rate of  $0.25 \text{ min}^{-1}$  is extracted. If the equation is fitted to the recovery data of a pure bilayer, the estimated transport rate is around  $3 \text{ min}^{-1}$ , which is one order of magnitude higher than that for the LD surface. These results confirm that there is a diffusion barrier for PE phospholipids, as there was a very reduced recovery in the lipid droplet area.

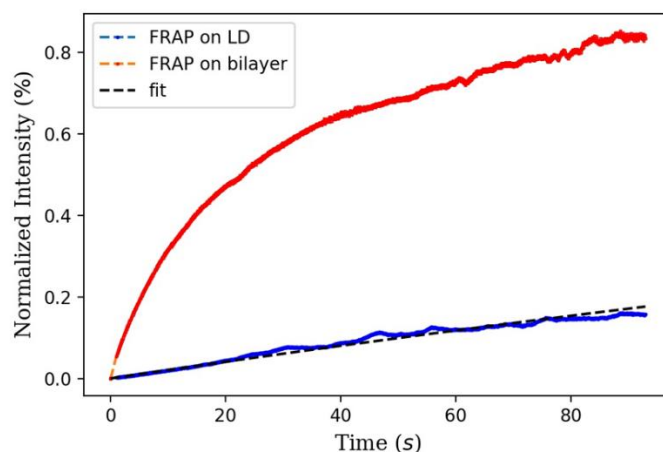


Figure 39 FRAP curves for LD and bilayer after bleaching an area labelled with Atto-DOPE with a diameter of  $30 \mu\text{m}$  for 20 sec. Reproduced by permission of publisher [6].

As only the PE molecules were probed, this raised a question of, if this barrier is specific to PE, or could be also measured for PC molecules which will be done in the following. For this aim, the experiments are repeated by replacing the dye with Cy5-PC, and the obtained fluorescence recovery data are fitted to Equation 18. The results show that the obtained transport rates for PC are remarkably similar to the transport rates of PE, which implies that the diffusion barrier is not specific to a phospholipid type and exists for both lipids as shown in **Figure 40**.



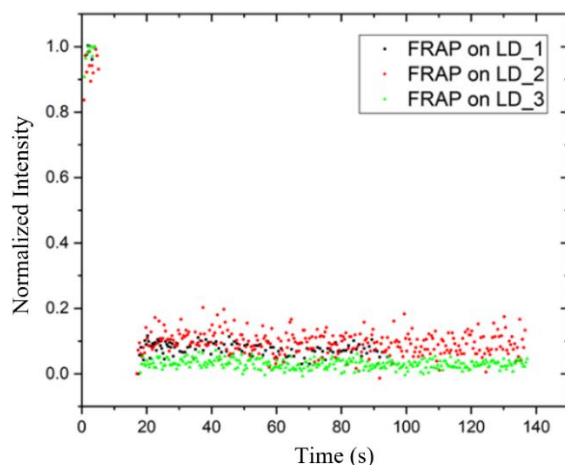


Figure 40 FRAP curves after bleaching an area labelled with Cy5-PC with a diameter of 30  $\mu\text{m}$  for 20 sec in the LD monolayer. Reproduced by permission of publisher [6].

## 5.5 MOLECULAR DYNAMIC SIMULATIONS

To explore more about the origin of this biophysical phenomenon of the experimentally observed lipid diffusion barrier, molecular dynamics simulations of LDs by using a coarse-grained MARTINI model (see Materials and Methods) were performed by the group of *Prof. Dr. Jochen Hub, Theoretical Physics, Saarland University* [136]. The bilayer composition is selected as DOPC/DOPE/DOPS (60:30:10), and the results were obtained on a nanometric lipid droplet inserted in the bilayer with a well-defined insertion angle. The components of the model are shown for an equilibrated coarse-grained simulation system in **Figure 41**.

The simulations disclosed that PE molecules concentrated at the interface in a ring structure (**Figure 42**). Lipids accumulate due to the structure of DOPE, while they balance the negative curvature around the lipid droplet due to their cone-shaped geometry [31], [154]. This raises the question of whether the origin of the diffusion barrier for both of the phospholipids is because of the negative curvature of DOPE lipids at the LD rim or not. To evaluate this hypothesis by simulations and confirm the experimentally established diminished diffusion, the mean first passage times (MFPTs) for all the bilayer phospholipids are computed with the same composition used for the experiments.

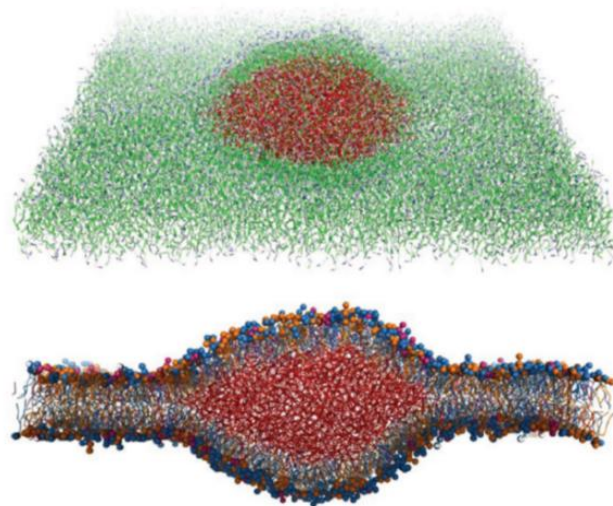


Figure 41 Equilibrated CG simulation of an LD. The red color is the neutral lipids and phospholipids are shown as green/blue/white sticks in the simulations. The detailed simulation of the side view consists of DOPC in blue, DOPE in orange, and DOPS in pink. Reproduced by permission of publisher [6].

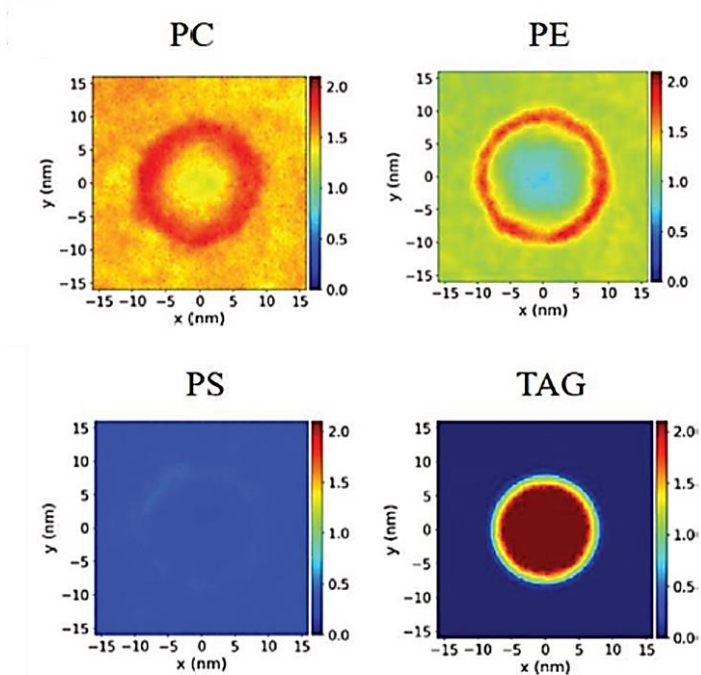


Figure 42 Coarse-grained numerical simulations representing the lateral lipid densities on a LD monolayer and surrounding bilayer. The lipid composition is set to DOPC:DOPE:DOPS (60:30:10 mol%) for bilayer. TAG composition is set to 537 triacylglycerol. Reproduced by permission of publisher [6].

The computed MFPTs show that the lateral diffusion in a pure bilayer is faster than that across the bilayer and lipid droplet boundary, by revealing that PE and PC molecules are accumulate in a ring structure at the interface of the lipid droplet and the bilayer. This result is confirming the existence of the diffusion barrier, but the key difference between the experimental results and the simulations observed is the impact of the diffusion barrier, which can be explained by the relative increase of the MFPTs. As shown in **Table 3**, the MFPTs are systematically larger in the LD-bilayer simulations compared to the pure bilayer simulations with a relative increase between 23% to 39%. This result indicates that the diffusion barrier is much weaker than the barrier obtained in experiments. This effect can potentially be explained by the differences in scales and thermal fluctuations of the simulations and experiments. It should be noted that the simulations are performed on the nanometric scale, where the LDs in the experiments have a size of a few micrometers. Under thermal fluctuations, the nanoscopic regions are expected to be more unstable, which results in an unstable PE ring. On the contrary, the increased thermal stability of phospholipids might influence the diffusion barrier and makes it more stable and enhanced. Such different spatial dimensions could cause a reduced effect of the barrier for simulations compared to the reported experimental results. Although the results clearly show that there is a visible diffusion barrier both in micrometric and nanometric scales.

Table 3 Comparison of lateral diffusion of lipids from the LD surface to the bilayer and in pure lipid bilayer by coarse-grained MD simulations.

	Pure bilayer simulation		LD simulation		Rel. increase
	$N_{trans}$	MFPT [ $\mu$ s]	$N_{trans}$	MFPT [ $\mu$ s]	
DOPC	7346	0.44	2025	0.61	39%
DOPE	5733	0.44	1600	0.54	23%
DOPS	1399	0.45	423	0.57	27%

## 5.6 PROTEIN PARTITIONING DUE TO LIPID PACKING

The protein structure and bilayer composition are the main factors for the partitioning as explained in detail in Section 3.3. The insertion of PLDs containing UBXD8<sub>71-132</sub> shows that proteins due to their structure can accumulate on one LD monolayer without partitioning. Compared to the UBXD8 protein, an integral membrane protein Caveolin-1 can show a dynamic partitioning by diffusing freely in the bilayer and the LD in living cells is employed [82]. The truncated peptide Cav1<sub>1-17</sub> is a short sequence of the N-terminal domain of Caveolin-1, and as also detailed in the Materials and Methods section, it has affinities with hydrophilic and hydrophobic residues. By using this hairpin-like protein, the mechanism behind dynamic protein partitioning is aimed to be further investigated in this model bilayer-lipid droplet system. The LD

core is labelled with BODIPY 493/503, Cav<sub>1-17</sub> protein and bilayer are labelled with Alexa Fluor 647 and Rhodamine-PE, respectively. The lipid droplets are decorated with Cav<sub>1-17</sub> peptides and introduced right after the bilayer formation, which is carried out similarly to the previous study. For this set of experiments, it has been waited at least for 20-30 minutes until the lipid droplets inserted in the bilayer, and proteins organized their distribution between the bilayer and the lipid droplets (**Figure 43**). The detailed regulation of the proteins as observed by fluorescence imaging will be explained in the following section.

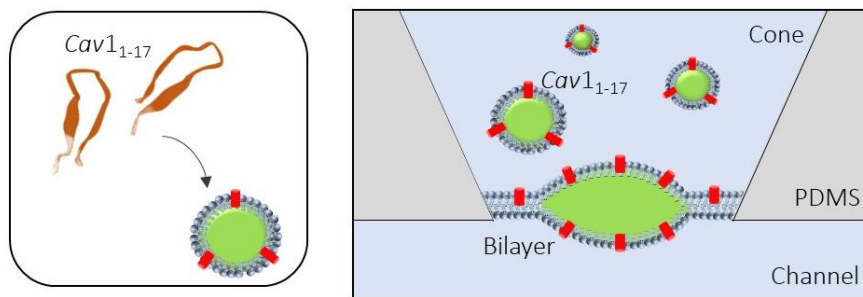


Figure 43 Schematic description of the insertion of PLDs consist of Cav<sub>1-17</sub> into the bilayer

Increasing the PE amount in the bilayer to alter the localization of proteins from bilayer through the LD monolayer has been reported for monotopic proteins previously by using DIBs [31]. This preference is explained by the packing defects caused by increased PE amount in the bilayer, which creates more area for the proteins to bind to the neutral lipids. To investigate the effect of lipid packing on the partitioning of a hairpin-like protein, the bilayer composition is changed by tuning the PE amount in the bilayer to vary the lipid packing by choosing a composition close to ER membrane [31]. The composition of the PC/PE (either DOPC/DOPE or POPC/POPE) in the bilayer is tuned between 2:1 to 1:3 in molar ratio. Depending on the composition of the bilayer, Cav<sub>1-17</sub> proteins are either distributed homogeneously or form visible clusters up to a few micrometers (**Figure 44**). Moreover, the distribution of the protein between the lipid droplet monolayer and bilayer is changed according to the composition of the bilayer.

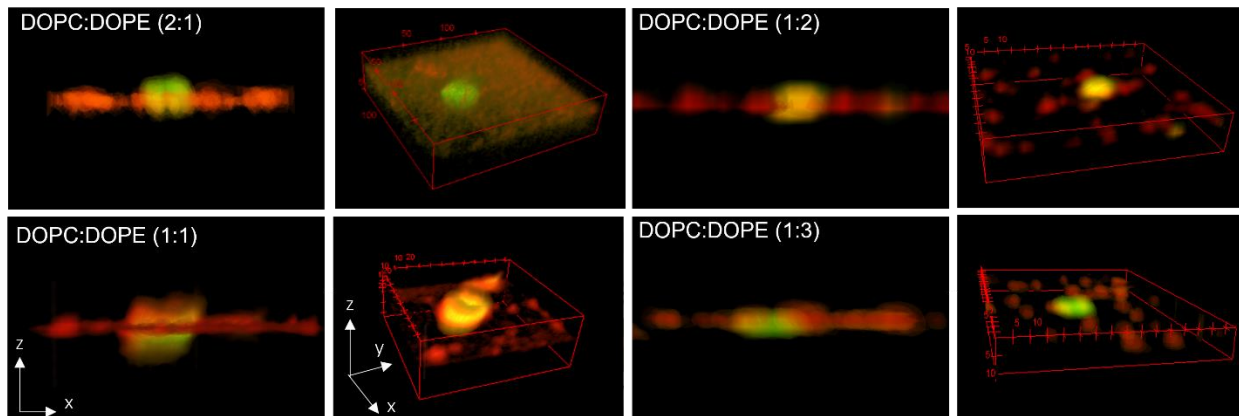


Figure 44 Confocal images of the lipid droplets inserted on the bilayer by 2D and 3D representations. Scale bars with the arrows are 5  $\mu\text{m}$  for x,z (2D images) and 10  $\mu\text{m}$  for x,y and z (3D images) for DOPC/DOPE experiments. Lipid droplet core and the Cav1<sub>1-17</sub> proteins are shown in green and red, respectively.

To investigate the regulation of proteins between the lipid droplet and bilayer, intensity values are obtained by processing the z-stack images. For this aim, the center of the bilayer is set to  $z=0$  position, and z-stack imaging is performed between the upper leaflet (z-top) and the bottom leaflet (z-bottom) positions. The distribution of the proteins is investigated by comparing the fluorescence intensity in the LD monolayers and the bilayer after. From the corresponding fluorescent intensities of two LD monolayers and the bilayer, the partition coefficient ( $P$ ) is calculated as follows:

$$P = \frac{2I_b}{I_{um} + I_{lm}} \quad (1)$$

where  $I_b$  is the bilayer intensity over the entire bilayer area including clusters,  $I_{um}$  is the intensity of the upper monolayer and  $I_{lm}$  is the intensity of the lower monolayer. Two different wavelengths have been used to define the lipid droplets and proteins to obtain a 3D shape, and only the channel detecting the proteins are processed to obtain the partition coefficient value. When  $P \gg 1$ , the proteins prefer to be in the bilayer, while they are slightly localizing in the LD monolayer in the case of  $P > 1$ . For the case where  $0 < P < 1$ , the proteins are distributed between the bilayer and on the LD monolayer, and they prefer to be on the LD monolayer for  $P = 0$  as sketched in **Figure 45**.

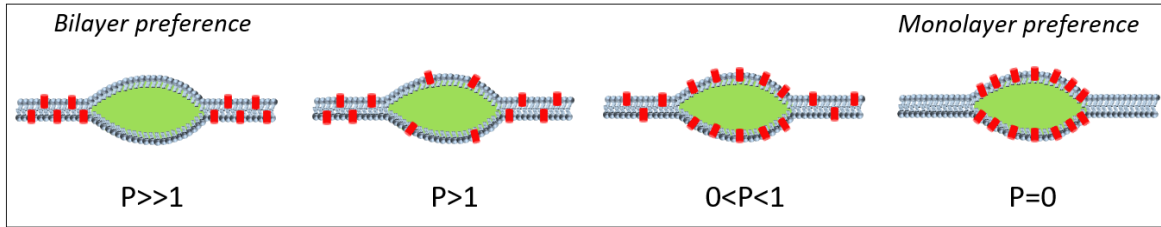


Figure 45 Schematic representation of how protein partitioning can be explained by the evaluated P value.

For the bilayer composition DOPC/DOPE (2:1), where the DOPC amount is two times larger than the DOPE amount in the bilayer, the proteins localized more in the bilayer ( $P \approx 2.2$ ). The proteins prefer to be in the monolayer when the bilayer ratio is increased to 1:1, 1:2 and 1:3. The value is evolved from  $P \approx 0.6$  to  $P \approx 0.3$  from PC/PE ratio of 1:1 to 1:3, where the localization is clearly shifted from the bilayer to the LD monolayer (**Figure 46**). This hypothesis is studied with another approach, by increasing the packing of the bilayer rather than increasing the packing defects. For this aim, the bilayer composition is changed from DOPC/DOPE to POPC/POPE with varying ratios of 1:1, 1:2, and 1:3. These two phospholipids ensure higher packing density with only one unsaturated fatty acid chain, where DOPC and DOPE are consisting of two unsaturated chains. The evaluated partition coefficient values for the POPC/POPE bilayers show that the preference of the proteins shifted through the bilayer. The ratios vary between 1:3 and 1:1 corresponding to  $P \approx 2.6$  to  $P \approx 2.4$ , and the preference is not shifted to the monolayer even for the case of considerable amounts of POPE in the bilayer (**Figure 46**). The results showed that increasing the PE amount in POPC/POPE bilayers did not show the same effect as in DOPC/DOPE bilayers. These result has shown that the distribution of the proteins is not directly related to the excess of PE in the bilayer, and there is another mechanism controlling this preference.

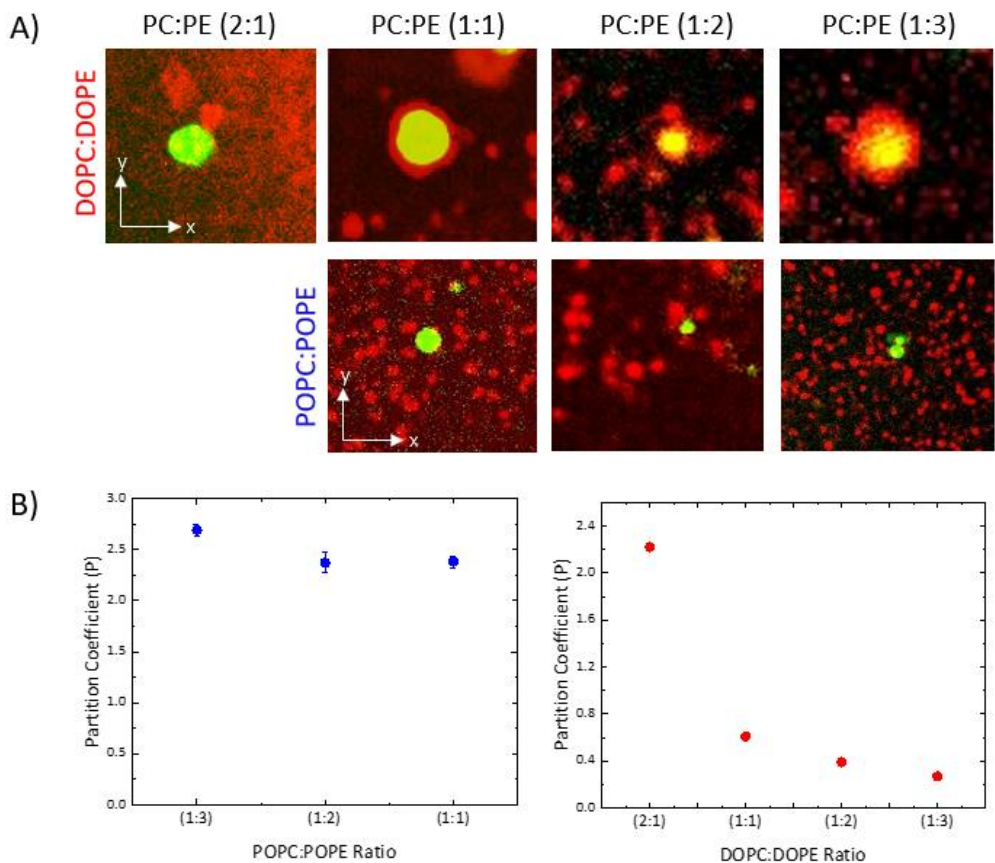


Figure 46 Confocal images of protein partitioning between the LD (in green) and bilayer (in red) to show the distribution of proteins with respect to increased lipid packing in the bilayer (A). Partition coefficients for the bilayers composed of DOPC/DOPE and POPC/POPE (B).

The results obtained with DOPC/DOPE bilayer compositions agree with the literature [31]. In this microfluidic system, the bilayer mimics the ER membrane, and the water-oil interfaces decorated with phospholipid monolayers mimic the two leaflets of LDs, which creates a much larger size of LDs compared to the bilayer. Besides, the curvature of the LDs significantly differs from an expected lens shape of an LD in the ER membrane. Therefore, to ensure that the results of POPC/POPE which showed the opposite trend compared to DOPC/DOPE do not depend on the chosen model system i.e. DiB or microfluidic technique, DiB experiments are included in courtesy of *JB Fleury* to confirm the presented results obtained by the microfluidic technique, and to assess various bilayer compositions for studying the effect of lipid packing in the bilayer on the regulation of proteins. The DiBs system is set up by dispersing Proteo-SUVs decorated with phospholipid monolayer in Triolein as detailed in Materials and Methods section.



As the Proteo-SUVS in the DIB system have equal protein concentrations, the bilayer fluorescent signal is measured, which means that the relative protein presence in the bilayer compared for each bilayer composition. When the DOPE amount in the bilayer is increased by changing the DOPC/DOPE ratio from 1:1 to 1:3, the relative bilayer intensity is slightly decreased (**Figure 47**). The regulation for the bilayers composed of DPhPC/DPhPE also confirms the same trend, where the signal reduction of the bilayer becomes less evident for the compositions of POPC/DOPE and POPC/POPE. The results for DOPC/DOPE bilayers are in line with the results obtained from the free-standing bilayer system and show that the PC/PE ratio does not determine the partitioning of a hairpin-like protein Cav1<sub>1-17</sub>, but rather its influence on lipid packing regulates the partitioning. When the lipid packing increases due to the molecular interactions of highly-packed phospholipids, the hairpin-like proteins prefer to be in the bilayer independent of the experimental approach.

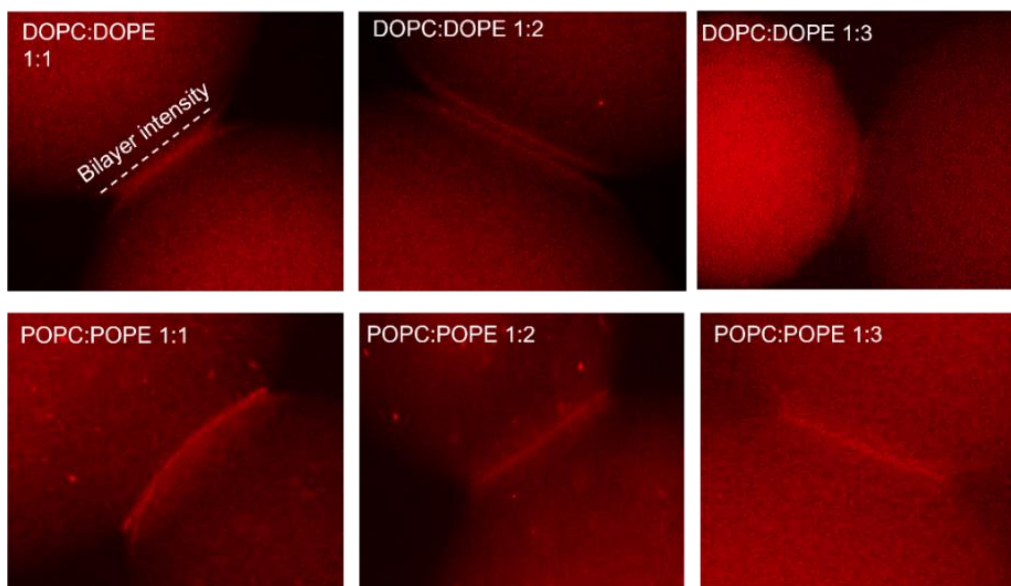


Figure 47 DIB examples of bilayer intensities for DOPC/DOPE and POPC/POPE for the molar ratios 1:1, 1:2 and 1:3.

Lipid packing defects in the membrane originate due to the geometry of specific lipids, such as PE [23], [31], [155]–[157]. PC phospholipid molecules are presenting cylindrical shapes which create compact structures in the bilayer. Compared to cylindrical shape PC lipids, PE lipids have truncated cone shapes [14], [158], which creates packing defects in the membrane. Hence, varying the PC/PE ratio in the membrane can strongly affect lipid packing. DOPE creates more lipid packing defects than POPE due to its molecular structure, while POPE has only one unsaturated chain (C-C double bond) and a fully saturated chain. This structure ensures more



rigidity than a structure consisting of two unsaturated chains [24], [30], [159]. Due to the degree of saturation, DOPC is also known to create bilayers with a lower area fraction than POPC. DPhPC, and DPhPE lipids are creating membranes with high defect density [160]. If we categorize the bilayers as a function of their lipid packing, from lowest to the highest packing: DPhPC/DPhPE → DOPC/DOPE → POPC/DOPE → POPC/POPE. Comparing the relative bilayer intensities from 20 DiBs, the results show that the protein organization is directly controlled by the bilayer lipid packing (**Figure 48**).

As mentioned before, the hairpin-like protein Cav<sub>1-17</sub> shows affinity to the bilayer, which has both hydrophobic and hydrophilic parts. The dependence of Cav<sub>1-17</sub> partitioning can be rationalized based on the interaction of non-polar residue of the protein, which is necessary for the insertion of the protein into the bilayer, with the hydrophobic core of the bilayer. In presence of packing defects in the bilayer, some hydrophobic residues of the protein interact more with the aqueous buffer, which is energetically unfavorable. Considering the energetic argumentation, the protein recruitment into the bilayer could be explained due to the packing defects in the bilayer. If we consider the bilayer composition of DOPC/DOPE, with ratios from 1:1 to 1:3, the distribution of the proteins is changed from homogenous to clustered. In addition to these few micron-size clusters in higher PE ratios in the bilayer, the proteins also cover the monolayers of LDs. This organization also shows that the lipid packing in the bilayer is a controlling mechanism of the partitioning of Cav<sub>1-17</sub> proteins.

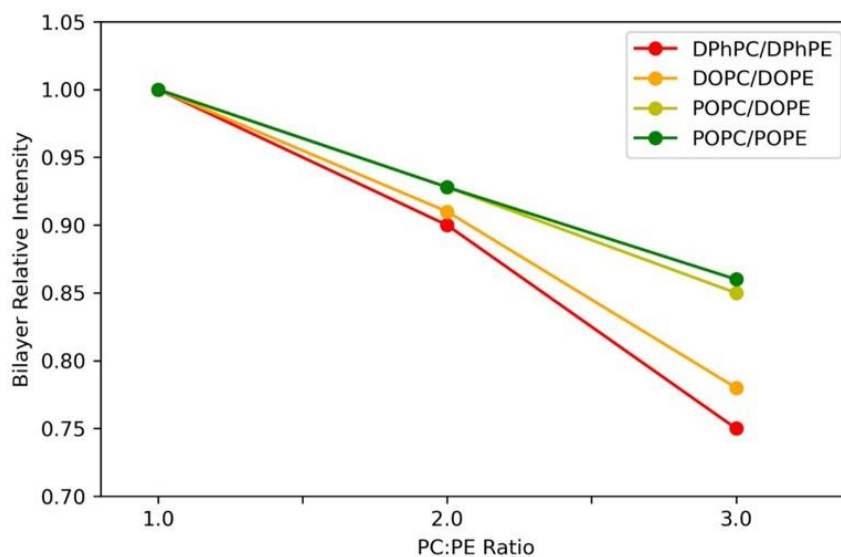


Figure 48 Relative bilayer intensity due to PC/PE ratio for all bilayer compositions for DIB experiments.

## 5.7 EXCHANGE KINETICS OF PROTEINS AND PHOSPHOLIPIDS

In this thesis, FRAP measurements are performed on Cav<sub>1-17</sub> and ADRP proteins to investigate how proteins with different binding characteristics are diffusing in the bilayer and monolayer, and how the mobility of phospholipids gets affected by proteins. The bilayer is composed of DOPC/DOPE with a ratio of 1:1 is formed as the partitioning studies have already shown that the proteins present almost equally both in the bilayer and monolayer (Section 5.6) for this bilayer composition. Hence, the mobility of the proteins for each case could be measured. To perform the FRAP experiments, the bilayer and Cav<sub>1-17</sub> are labeled with Atto647N-DOPE and Alexa Fluor 488, respectively. The diffusion coefficients are extracted from the Soumpasis equation fit to the measured recovery data [131]. The obtained phospholipid diffusion coefficient of 10  $\mu\text{m}^2/\text{s}$  shows that the bilayer is fluid in presence of the proteins [5], [6]. The obtained diffusion coefficients of the Cav<sub>1-17</sub> proteins are in the range of (2.8-4.6)  $\mu\text{m}^2/\text{s}$ , which is in line with the reported values for peripheral and transmembrane proteins in literature [5]. Moreover, in cells Cav1 protein shows dynamic partitioning by freely diffusing in the bilayer, which is the feature to allow localization [76], [79], [82]. These results confirm that the Cav<sub>1-17</sub> protein diffuses freely in the model bilayer (**Figure 49**).

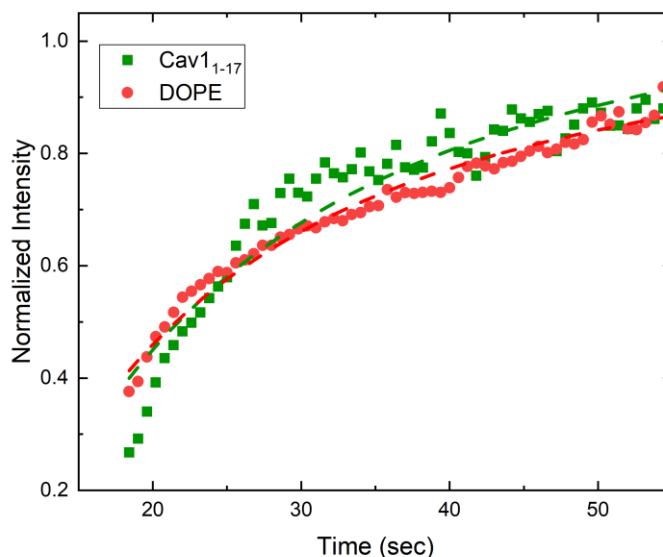


Figure 49 FRAP data obtained for Cav<sub>1-17</sub> proteins and DOPE lipids in the bilayer with a composition DOPC:DOPE:DOPS (60:30:10 mol%).

It has been reported in Section 5.4 that phospholipids do not move freely at the intersection of the bilayer and the monolayer and create a diffusion barrier [6]. To explore the effect of proteins on the existence of this diffusion barrier at the LD rim, the labeled Cav<sub>1-17</sub> proteins present on

the entire LD surface are bleached, as well as the phospholipids (**Figure 50A**). The fluorescent recovery of the monolayer covering the LD is measured. The recovery data of DOPE lipids at the intersection of the bilayer and monolayer in presence of Cav1<sub>1-17</sub> proteins are obtained to see if the same DOPE barrier exists for these proteins. The calculated transport rate  $k = (0.73-0.96) \text{ min}^{-1}$  shows that the diffusion barrier is weakened by around a factor of 4, which was previously reported as  $0.25 \text{ min}^{-1}$  in the absence of proteins [6]. For the proteins at the interface, a transport rate ( $k$ ) of  $(0.7-1.5) \text{ min}^{-1}$  is extracted, which is 3 to 10 times smaller than the transport rate of a protein freely diffusing in the bilayer. These results indicate that proteins show reduced mobility at the interface compared to their mobility in the bilayer (**Figure 50B**). This can be explained by the still-existing diffusion barrier which possibly slows down the re-localization of proteins between the bilayer and monolayer. Although it is not strong enough to affect the partitioning of the proteins over 10 minutes. Therefore, once the measurements are performed 20-30 minutes after the insertion of PLDs, the effect of the diffusion barrier on the partitioning can be neglected safely.

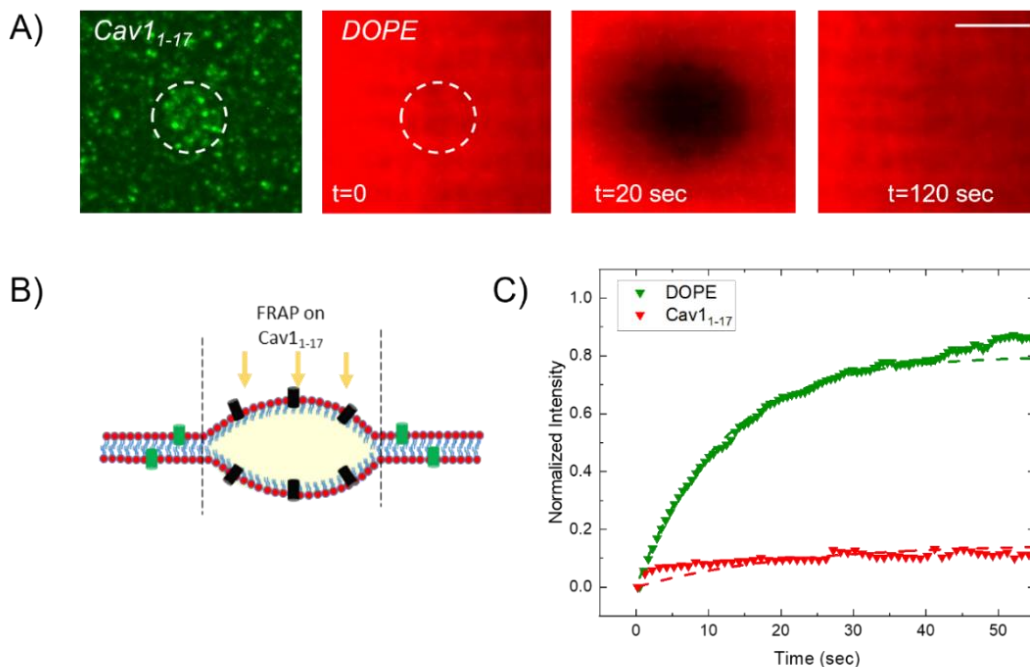


Figure 50 (A) Area of Cav1<sub>1-17</sub> proteins on LD area (dashed circle) and DOPE in the bilayer area composed of DOPC:DOPE:DOPS (60:30:10 mol%) for FRAP experiments. Scale bar shows 10  $\mu\text{m}$ . (B) Schematic of FRAP in the LD area (C) FRAP data obtained for proteins and lipids in the LD monolayer.

The impact of ADRP protein, which shows high affinity to the lipid droplet, on the existence of the diffusion barrier is also tested by following the same steps previously explained for phospholipids and Cav1<sub>1-17</sub> peptides. Although the ADRPs have a known binding affinity to the LD surface, it is unknown how the presence of ADRP affects the hypothetical diffusion barrier. For this aim, a bilayer is formed with a composition of DOPC:DOPE (3:1) and labeled with DOPE-Cy5, where the PLDs are labeled with Atto-488 to distinguish the components (See Materials and Methods). After the PLDs are inserted into the bilayer and equilibrated, selected areas in the bilayer and the entire surfaces of several LDs are bleached. The Soumpasis equation fitted to the data have shown that the diffusion coefficient of the phospholipids in the LD monolayer is about 8  $\mu\text{m}^2/\text{s}$  which is very close to the diffusion coefficient of PE in the bilayer (10  $\mu\text{m}^2/\text{s}$ ). The LD monolayer could include a potential diffusion barrier and thus indicates that this barrier can only have a small influence.

For evidence, the microfluidic system created to mimic the surface of a LD is used to create a phospholipid monolayer at the buffer-triolein interface composed of the same phospholipid composition as the bilayer. The details of the platform can be found in Materials and Methods section. The extracted diffusion coefficient of the LD monolayer is calculated as  $\approx 8 \mu\text{m}^2/\text{s}$  which is identical to the value extracted from the bilayer-embedded PLDs (**Figure 51**). These findings show that the presence of ADRP proteins destroyed the hypothetical PE ring which is the origin of the diffusion barrier. This can facilitate the molecular transport between the bilayer and LD monolayer through the LD rim. The free diffusing of all molecules proves that the pancake shape of the PLDs (introduced in Section 5.3) is not a result of diffusion related artifact but can be a consequence of ADRP molecules close to the LD perimeter. The motility of the ADRP proteins is also investigated on the artificial LD monolayer. The extracted diffusion coefficient for the ADRP protein is  $\approx 0.3 \mu\text{m}^2/\text{s}$ , which shows that the motility of the ADRP proteins is 20 times smaller than that of the phospholipids on the monolayer. Even if the proteins motility is slower, the diffusion of ADRP molecules along the LD surface is not negligible.

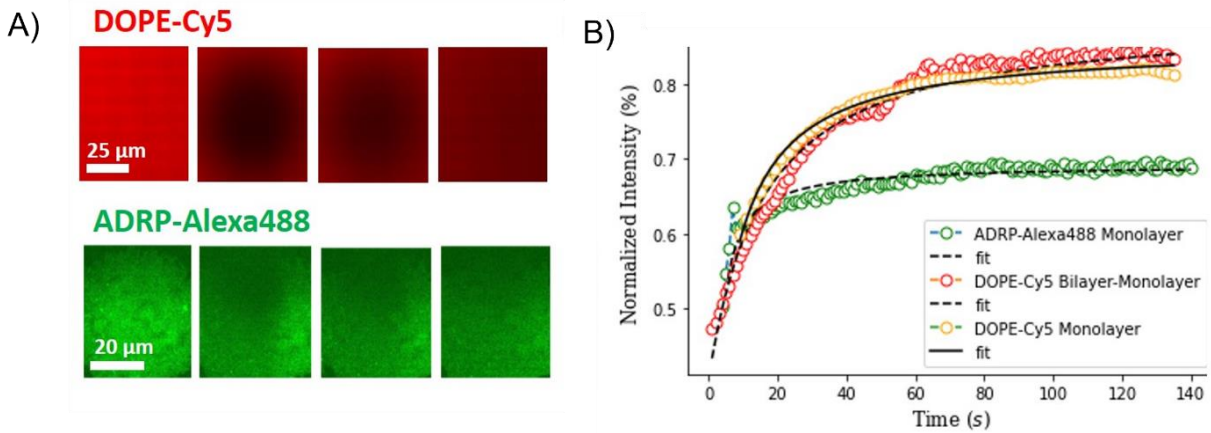


Figure 51 (A) FRAP experiments on the lipid monolayer with a composition of DOPC:DOPE (3:1). The images correspond to DOPE-Cy5 (2% mol) (upper row) and ADRP-Alexa488 (lower row). (B) FRAP data obtained for LD monolayer and bilayer embedded LD experiments. Reproduced by permission of publisher [8].

## **SUMMARY**

---

## 6 SUMMARY

---

The designed model bilayer system is able to mimic the relevant features of LDs inserted in the ER membrane and allow to study the lipid droplets and associated protein partitioning. One of the main advantages of the design is the height of the bottom channel, which allows a higher level of optical access, and gives the occasion for high-resolution imaging of the few micron size bilayer components. Besides, the cone connected to this channel gives easy access to the bilayer where new components such as LDs and proteins can be added to the system. The characterization of the bilayer by Patch-Clamp demonstrates that the bilayer is formed with an identical thickness to an ER membrane, and further characterization with the FRAP method indicates that the free-standing bilayer is in a fluid state. These two characterizations are showing that the properties of thickness and fluidity of the bilayer are similar to a biological membrane. After a thorough examination of the bilayer, the lipid droplets could be inserted after a free-standing bilayer is formed by the microfluidic technique and optically distinguished by fluorescently labeling each component individually. The contact angles of well-defined symmetric shaped bilayer-embedded lipid droplets are demonstrated depending on the changing bilayer tension. The data suggests that the symmetric lens shape, so the insertion angle of a lipid droplet is based on the balance between the bilayer and the two monolayers of the lipid droplet which is described by the equilibrium wetting theory. The study also displays a correlation between the cholesterol amount in the bilayer and the contact angle of the lipid droplet in line with the hypothesis of increasing the cholesterol amount increases the bilayer tension, so results in a reduced insertion angle for the lipid droplets [152], [153]. The data contribute to an understanding of how the lipid droplet shape is facilitated by the bilayer tension without proteins and in presence of diverse types of proteins. In presence of peptides including a hairpin region (here UBXD8<sub>71-132</sub>) with a known preference for lipid droplet monolayer, the symmetry is broken by the accumulation of the peptide in only one monolayer side, which is resulted in an asymmetric bulged-shaped lipid droplet. Besides, a smaller hairpin-like peptide (here Cav1<sub>1-17</sub>) with the feature of freely diffusing in the bilayer, does not break the symmetry due to its fusion through the lipid droplet core until the amount of the proteins in both monolayers is equivalent. Although, in presence of the surface active ADRP proteins, lipid droplets took a specific pancake-like shape, which is promoted in presence of cholesterol.

The dynamics of the lipids and proteins are investigated by a quantitative measurement technique, FRAP. The exchange kinetics of lipid molecules are studied both in the lipid droplet area and the bilayer. The data suggest that the transport rate of lipids at the intersection of the lipid droplet and the bilayer is reduced by a factor of 10, which call “diffusion barrier”. The existence of the barrier is studied by MD Simulations and the results show the diffusion barrier with a reduced intention. This could be based on the spatial dimensions used in the simulations,

as the thermal stability has more influence on the nanometer scale simulations compared to micron scale experiments, which results in a weaker diffusion barrier. Although the effects are different, the barrier is also reported by simulations in line with the hypothesis. The experiments about the diffusion barrier provide new insight into the transport of phospholipids at the intersection of the bilayer and lipid droplet area. In addition, the dynamics of the phospholipids in presence of a freely diffusing hairpin-like peptide (Cav1<sub>1-17</sub>) is investigated. The FRAP data supports the theory that Cav1<sub>1-17</sub> is freely diffusing in the bilayer with a similar diffusion coefficient of peripheral and transmembrane proteins reported in the literature [5]. The existence of a lipid diffusion barrier in presence of proteins is studied, and the results show that phospholipids have a reduced transport rate at the LD rim with 4 times weaker impact, whereas the proteins also have a slower transport compared to bilayer. These results should be taken into account when considering how the transport rate of lipids changes in presence of proteins through the LD rim. Even if the barrier still exists, it is not strong enough to block the partitioning of the peptides over 10 minutes. Hence, all the measurements in presence of proteins are performed just after the system is fully equilibrated, where the barrier is neglected safely. The motility measurements in presence of ADRP protein have shown that the mobility of phospholipids in the LD monolayer is very similar to the bilayer. Therefore, the hypothesized diffusion barrier is diminished when the lipid droplet area is covered with the ADRP proteins. These results show that proteins can have a high impact on diminishing the possible diffusion barrier at the LD rim depending on their class and type.

To investigate the mechanism behind the partitioning of hairpin-like proteins between the lipid droplet and bilayer, the bilayer packing was systematically changed by tuning the PE amount in the bilayer. The results show that increasing the DOPE amount in the bilayer changes the direction of the preference from the bilayer to the LD monolayer. In the continuation, the bilayer structure is changed from a less-packed to high-packed composition by changing the lipid types. It has been found that the partitioning is controlled by the lipid bilayer packing, rather than only the PE amount. This finding is supported by the DIB experiments, to make evidence that the difference is not based on the microfluidic technique used. The data show that the partitioning of a hairpin-like protein highly dependent on the lipid bilayer packing, whereas for the bilayers with high-packing defects, the preference is for the lipid droplet surface.



## **CONCLUSION AND OUTLOOK**

---

## 7 CONCLUSION AND OUTLOOK

---

### *Conclusion*

In this thesis, the research aimed to improve the understanding of the mechanisms behind lipid droplet insertion into the bilayer, and how the dynamics of lipids and proteins are influenced in presence of lipid droplets in the bilayer. The lipid droplet experiments with the model bilayer have shown that this approach is advantageous to study lipid droplet-associated proteins in such a microfluidic device by combining with techniques like FRAP and Patch-Clamp. The characterization results of the artificial bilayer show that the model bilayer is close to the ER membrane with its phospholipid composition and fluidity. Besides, the bilayer with inserted lipid droplets is promising in sum to study different classes of lipid droplet-associated proteins with high-resolution imaging. This design strategy may provide inspiration for new proteins or distinct types of membranes to be studied in such a microfluidic setup.

Based on the quantitative analysis of the lipid droplets in the model ER membrane, it can be concluded that one main factor determining the shape of the droplet is the balance between bilayer tension and the tension created by two monolayers of an LD. The bilayer tension has been changed by tuning the bilayer composition, which has governed the insertion angle of the lipid droplets based on the equilibrium wetting theory. By analyzing the 3D images, it has been shown that the symmetry of the lipid droplet is broken depending on the accumulation of surface-active protein (here UBXD8<sub>71-132</sub>) on one leaflet, which is resulted in an asymmetric shape in equilibrium. This result clearly illustrated the case where protein is located only on one lipid droplet monolayer, but it also raised the question of how the proteins partition in the system. This approach has been studied in this thesis by adding a freely diffusing hairpin-like protein Cav1<sub>1-17</sub> and ADRP protein which has an affinity to the lipid droplet separately, and the dynamics of these proteins are followed.

By using FRAP measurements, the transfer rate of lipids and proteins in the bilayer and in the area of lipid droplets are investigated. On lipid droplets in absence of proteins, it can be concluded that the transfer rate of phospholipids is weakened at the LD rim which indicates a diffusion barrier. Even if the hairpin-like peptide Cav1<sub>1-17</sub> can freely diffuse in the bilayer and lipid droplet, the diffusion barrier still exists in presence of these proteins in a reduced manner and has no significant effect on the localization of the proteins from the bilayer through the LD core. Moreover, the experiments with ADRP proteins show that this diffusion barrier could almost disappear in presence of ADRP proteins located on the LD surface. This effect has been demonstrated for the first time with a model system by using several types of proteins.

## *Outlook*

Using the established bottom-up approach to explore protein partitioning between LD and bilayer, the developed microfluidic model system allows to study more complex situations by adding more proteins that might lead to understand biochemical and enzymatic reactions in cells. The approach followed in this thesis is focused on studying the specific types of proteins individually. Thus, studying the combination of distinct proteins and enzymes will make the system closer to the interactions and dynamics in a cell, which can be done by several set of experiments.

Even if the effect of PE amount on the partitioning of monotopic proteins is as previously reported, it is new to study the driving mechanism of partitioning for hairpin-like peptides in a free-standing bilayer system. In addition to the existing literature for monotopic proteins, the results have shown that the partitioning of hairpin-like proteins is directly related to the bilayer packing. Hence, the results of lipid-packing dependent partition of hairpin-like peptides open a new perspective on the regulation phenomenon, which can be applied to other classes of proteins to understand the underlying mechanism controlling the dynamic partitioning between ER membrane and the LDs in cells. Further, lipid-mediated parameters such as lipid packing and surface tension can be modulated by varying the composition of the bilayer in a wider range of lipid classes to determine their influence on bilayer-monolayer partitioning.

In this thesis, proteins are introduced to the system as Proteo-LDs, which are reconstituted to the lipid droplet surface before introducing to the microfluidic device. For further understanding of the proteins which are targeting the bilayer or lipid droplets directly from the cytosol, the proteins can be added individually after the lipid droplets are inserted into the bilayer.

The design of our system is optimized for imaging after the system is stable in 20-30 minutes. While the time scale of the event limits the trafficking of a protein from the stretch, the approach of using the FRAP method provides new insight into the transport rates of the lipids and proteins after the system is stabilized. Nevertheless, imaging the real-time partitioning of different types of proteins from the moment it touches the membrane and during the system is equilibrated could be an interesting research topic for future research.

This research clearly illustrates a diffusion barrier for the lipids at the LD rim, but it also raises the question if this barrier is existing for all types of proteins or in presence of specific protein-protein interactions. Based on the conclusions, the LD rim could be weakened in presence of hairpin-like peptides or could be destroyed by ADRP proteins. To better understand the implications of these results, future studies could address the existence of the diffusion barrier depending on the type of protein.

## REFERENCES

---

- [1] Y. Guo, K. R. Cordes, R. v Farese, and T. C. Walther, "Lipid droplets at a glance," *J Cell Sci*, vol. 122, pp. 749–752, 2009, doi: 10.1242/jcs.037630.
- [2] M. S. Khan, N. S. Dosoky, and J. D. Williams, "Engineering lipid bilayer membranes for protein studies," *International Journal of Molecular Sciences*, vol. 14, no. 11. pp. 21561–21597, Oct. 31, 2013. doi: 10.3390/ijms141121561.
- [3] J. N. Vargas, R. Seemann, and J.-B. Fleury, "Fast membrane hemifusion via dewetting between lipid bilayers †," 2014, doi: 10.1039/c4sm01577k.
- [4] H. Suzuki, K. v. Tabata, H. Noji, and S. Takeuchi, "Highly reproducible method of planar lipid bilayer reconstitution in polymethyl methacrylate microfluidic chip," *Langmuir*, vol. 22, no. 4, pp. 1937–1942, Feb. 2006, doi: 10.1021/la052534p.
- [5] P. Heo *et al.*, "Highly Reproducible Physiological Asymmetric Membrane with Freely Diffusing Embedded Proteins in a 3D-Printed Microfluidic Setup," 2019, doi: 10.1002/sml.201900725.
- [6] S. Puza *et al.*, "2106524 (1 of 12) Lipid Droplets Embedded in a Model Cell Membrane Create a Phospholipid Diffusion Barrier," 2022, doi: 10.1002/sml.202106524.
- [7] F. Nimmerjahn *et al.*, "Transport Properties of Gramicidin A Ion Channel in a Free-Standing Lipid Bilayer Filled With Oil Inclusions," 2020, doi: 10.3389/fcell.2020.531229.
- [8] S. Puza, S. Asfia, R. Seemann, and J.-B. Fleury, "Bilayer-Embedded Lipid Droplets Coated with Perilipin-2 Display a Pancake Shape," *Int J Mol Sci*, vol. 24, no. 3, p. 2072, Jan. 2023, doi: 10.3390/ijms24032072.
- [9] A. Baszkin and W. Norde, *Physical Chemistry of Biological Interfaces*. New York & Basel: Marcel Dekker, Inc., 2000.
- [10] A. 'Baszkin and W. 'Norde, *Physical Chemistry of Biological Interfaces*. Marcel Dekker, INC. , 2000.
- [11] S. J. Singer and G. L. Nicolson, "The Fluid Mosaic Model of the Structure of Cell Membranes experimental evidence in terms of the model; and (v) to show that the ftriid mosaic model suggests .new ways of thinking about membrane fUJ)ctions and membrane phenomena." [Online]. Available: <https://www.science.org>
- [12] G. L. Nicolson, "The Fluid - Mosaic Model of Membrane Structure: Still relevant to understanding the structure, function and dynamics of biological membranes after more than 40 years," *Biochimica et Biophysica Acta - Biomembranes*, vol. 1838, no. 6. Elsevier, pp. 1451–1466, 2014. doi: 10.1016/j.bbamem.2013.10.019.
- [13] J. Lombard, "Once upon a time the cell membranes: 175 years of cell boundary research," 2014, doi: 10.1186/s13062-014-0032-7.
- [14] G. van Meer, D. R. Voelker, and G. W. Feigenson, "Membrane lipids: Where they are and how they behave," *Nature Reviews Molecular Cell Biology*, vol. 9, no. 2. pp. 112–124, Feb. 2008. doi: 10.1038/nrm2330.

- [15] J. T. Groves and J. Kuriyan, "Molecular mechanisms in signal transduction at the membrane," *Nature Structural and Molecular Biology*, vol. 17, no. 6. pp. 659–665, Jun. 2010. doi: 10.1038/nsmb.1844.
- [16] "Gating of an organic transistor through a bilayer lipid membrane with ion channels," 2006, doi: 10.1063/1.2266250.
- [17] S. Anuytsel, J. Arniello, and M. I. Wallace, "Artificial Signal Transduction across Membranes", doi: 10.1002/cbic.201900254.
- [18] D. L. Daleke, "Phospholipid flippases," *Journal of Biological Chemistry*, vol. 282, no. 2. pp. 821–825, Jan. 12, 2007. doi: 10.1074/jbc.R600035200.
- [19] L. E. Hedin and A. Elofsson, "An Introduction to Membrane Proteins †," *J. Proteome Res*, vol. 10, pp. 3324–3331, 2011, doi: 10.1021/pr200145a.
- [20] H. Koldsø and M. S. P. Sansom, "Organization and Dynamics of Receptor Proteins in a Plasma Membrane," *J Am Chem Soc*, vol. 137, no. 46, pp. 14694–14704, Nov. 2015, doi: 10.1021/jacs.5b08048.
- [21] L. E. Hedin and A. Elofsson, "An Introduction to Membrane Proteins †," *J. Proteome Res*, vol. 10, pp. 3324–3331, 2011, doi: 10.1021/pr200145a.
- [22] M. Salim, H. Minamikawa, A. Sugimura, and R. Hashim, "Amphiphilic designer nano-carriers for controlled release: From drug delivery to diagnostics," *MedChemComm*, vol. 5, no. 11. Royal Society of Chemistry, pp. 1602–1618, Nov. 01, 2014. doi: 10.1039/c4md00085d.
- [23] M. Raja, "Do Small Headgroups of Phosphatidylethanolamine and Phosphatidic Acid Lead to a Similar Folding Pattern of the K<sup>+</sup> Channel?," 2011, doi: 10.1007/s00232-011-9384-4.
- [24] S. Vanni, H. Hirose, H. Ne Barelli, B. Antony, and R. Gautier, "ARTICLE A sub-nanometre view of how membrane curvature and composition modulate lipid packing and protein recruitment," 2014, doi: 10.1038/ncomms5916.
- [25] D. Snead, R. T. Wragg, J. S. Dittman, and D. Eliezer, "Membrane curvature sensing by the C-terminal domain of complexin," *Nat Commun*, vol. 5, 2014, doi: 10.1038/ncomms5955.
- [26] B. J. Peter *et al.*, "BAR Domains as Sensors of Membrane Curvature: The Amphiphysin BAR Structure." [Online]. Available: <https://www.science.org>
- [27] B. Antony, "Mechanisms of membrane curvature sensing," *Annu Rev Biochem*, vol. 80, pp. 101–123, Jul. 2011, doi: 10.1146/annurev-biochem-052809-155121.
- [28] G. Drin, J.-F. Casella, R. Gautier, T. Boehmer, T. U. Schwartz, and B. Antony, "A general amphipathic  $\alpha$ -helical motif for sensing membrane curvature," *Nat Struct Mol Biol*, vol. 14, 2007, doi: 10.1038/nsmb1194.
- [29] O. O. O O P O O Oh N, "Nature Reviews | Molecular Cell Biology," 2008. [Online]. Available: [www.nature.com/reviews/molcellbio](http://www.nature.com/reviews/molcellbio)

- [30] J. Bigay and B. Antonny, "Curvature, Lipid Packing, and Electrostatics of Membrane Organelles: Defining Cellular Territories in Determining Specificity," *Developmental Cell*, vol. 23, no. 5, pp. 886–895, Nov. 13, 2012. doi: 10.1016/j.devcel.2012.10.009.
- [31] L. Caillon *et al.*, "Triacylglycerols sequester monotopic membrane proteins to lipid droplets," *Nat Commun*, vol. 11, no. 1, Dec. 2020, doi: 10.1038/s41467-020-17585-8.
- [32] J.-F. Tocanne, L. Dupou-Ciżanne, and A. / Lopez, "LATERAL DIFFUSION OF LIPIDS IN MODEL AND NATURAL MEMBRANES," 1994.
- [33] S. Ramadurai, A. Holt, V. Krasnikov, G. van den Bogaart, J. A. Killian, and B. Poolman, "Lateral diffusion of membrane proteins," *J Am Chem Soc*, vol. 131, no. 35, pp. 12650–12656, Sep. 2009, doi: 10.1021/ja902853g.
- [34] I. M. Sokolov and J. Klafter, "From diffusion to anomalous diffusion: A century after Einstein's Brownian motion," *Chaos*, vol. 15, no. 2, 2005, doi: 10.1063/1.1860472.
- [35] P. G. Saffman and M. Delbrock, "Brownian motion in biological membranes (diffusion)," 1975. [Online]. Available: <https://www.pnas.org>
- [36] R. L. Schoch, F. L. H. Brown, and G. Haran, "Correlated diffusion in lipid bilayers," *BIOPHYSICS AND COMPUTATIONAL BIOLOGY*, vol. 118, 2021, doi: 10.1073/pnas.2113202118/-/DCSupplemental.
- [37] M. D. King, D. Marsh, and D. Marsh, "Free volume model for lipid lateral diffusion coefficients. Assessment of the temperature dependence in phosphatidylcholine and phosphatidylethanolamine bilayers," 1986.
- [38] M. H. Cohen and D. Turnbull, "Cite as," *Liquids The Journal of Chemical Physics*, vol. 31, p. 3038, 1959, doi: 10.1063/1.1730566.
- [39] R. Peters and R. J. Cherrytt, "Lateral and rotational diffusion of bacteriorhodopsin in lipid bilayers: Experimental test of the Saffman-Delbriick equations (fluorescence microphotolysis/lipid-protein interaction/phase transition)," 1982. [Online]. Available: <https://www.pnas.org>
- [40] H.-J. Galla, W. Hartmann, U. Theilen, and E. Sackmann, "On Two-Dimensional Passive Random Walk in Lipid Bilayers and Fluid Pathways in Biomembranes," 1979.
- [41] A. Kusumi *et al.*, "PARADIGM SHIFT OF THE PLASMA MEMBRANE CONCEPT FROM THE TWO-DIMENSIONAL CONTINUUM FLUID TO THE PARTITIONED FLUID: High-Speed Single-Molecule Tracking of Membrane Molecules," *Annu. Rev. Biophys. Biomol. Struct*, vol. 34, pp. 351–78, 2005, doi: 10.1146/annurev.biophys.34.040204.144637.
- [42] T. C. Walther and R. v Farese, "Lipid Droplets and Cellular Lipid Metabolism," 2012, doi: 10.1146/annurev-biochem-061009-102430.
- [43] J. A. Olzmann and P. Carvalho, "Dynamics and functions of lipid droplets", doi: 10.1038/s41580-018-0085-z.
- [44] T. C. Walther, J. Chung, and R. v Farese, "Lipid Droplet Biogenesis," *Annu Rev Cell Dev Biol*, 2017, doi: 10.1146/annurev-cellbio-100616.

- [45] H. Khandelia, L. Duelund, K. I. Pakkanen, and J. H. Ipsen, "Triglyceride blisters in lipid bilayers: Implications for lipid droplet biogenesis and the mobile lipid signal in cancer cell membranes," *PLoS One*, vol. 5, no. 9, pp. 1–8, 2010, doi: 10.1371/journal.pone.0012811.
- [46] V. Tozzini *et al.*, "To Bud or Not to Bud: A Perspective on Molecular Simulations of Lipid Droplet Budding," *Frontiers in Molecular Biosciences* | [www.frontiersin.org](http://www.frontiersin.org), vol. 6, p. 124, 2019, doi: 10.3389/fmolb.2019.00124.
- [47] S. G. Young *et al.*, "Seipin is required for converting nascent to mature lipid droplets," 2016, doi: 10.7554/eLife.16582.001.
- [48] G. Onal, O. Kutlu, D. Gozuacik, and S. Dokmeci Emre, "Lipid Droplets in Health and Disease," *Lipids in Health and Disease*, vol. 16, no. 1. BioMed Central Ltd., Jun. 29, 2017. doi: 10.1186/s12944-017-0521-7.
- [49] S. Xu, X. Zhang, and P. Liu, "Lipid droplet proteins and metabolic diseases," *Biochimica et Biophysica Acta - Molecular Basis of Disease*, vol. 1864, no. 5. Elsevier B.V., pp. 1968–1983, May 01, 2018. doi: 10.1016/j.bbadis.2017.07.019.
- [50] P. G. de Gennes, "Wetting: statics and dynamics," 1985.
- [51] A. R. Thiam and M. Beller, "The why, when and how of lipid droplet diversity," *Journal of Cell Science*, vol. 130, no. 2. Company of Biologists Ltd, pp. 315–324, 2017. doi: 10.1242/jcs.192021.
- [52] A. R. Thiam and L. Forêt, "The physics of lipid droplet nucleation, growth and budding," *Biochimica et Biophysica Acta - Molecular and Cell Biology of Lipids*, vol. 1861, no. 8. Elsevier B.V., pp. 715–722, Aug. 01, 2016. doi: 10.1016/j.bbalip.2016.04.018.
- [53] N. Jacquier, V. Choudhary, M. Mari, A. Toulmay, F. Reggiori, and R. Schneiter, "Lipid droplets are functionally connected to the endoplasmic reticulum in *Saccharomyces cerevisiae*," *J Cell Sci*, vol. 124, no. 14, pp. 2424–2437, Jul. 2011, doi: 10.1242/jcs.076836.
- [54] F. Wilfling *et al.*, "Arf1/COPI machinery acts directly on lipid droplets and enables their connection to the ER for protein targeting," *Elife*, vol. 2014, no. 3, Feb. 2014, doi: 10.7554/ELIFE.01607.
- [55] A. R. Thiam, R. v. Farese, and T. C. Walther, "The biophysics and cell biology of lipid droplets," *Nat Rev Mol Cell Biol*, vol. 14, no. 12, pp. 775–786, 2013, doi: 10.1038/NRM3699.
- [56] N. E. Hotrum, T. van Vliet, M. A. Cohen Stuart, and G. A. van Aken, "Monitoring entering and spreading of emulsion droplets at an expanding air/water interface: A novel technique," *J Colloid Interface Sci*, vol. 247, no. 1, pp. 125–131, 2002, doi: 10.1006/jcis.2001.8124.
- [57] K. Bersuker and J. A. Olzmann, "Establishing the lipid droplet proteome: Mechanisms of lipid droplet protein targeting and degradation," *Biochimica et Biophysica Acta - Molecular and Cell Biology of Lipids*, vol. 1862, no. 10. Elsevier B.V., pp. 1166–1177, Oct. 01, 2017. doi: 10.1016/j.bbalip.2017.06.006.
- [58] N. Kory, R. v. Farese, and T. C. Walther, "Targeting Fat: Mechanisms of Protein Localization to Lipid Droplets," *Trends in Cell Biology*, vol. 26, no. 7. Elsevier Ltd, pp. 535–546, Jul. 01, 2016. doi: 10.1016/j.tcb.2016.02.007.

- [59] A. Rachid Thiam, R. v. Farese, and T. C. Walther, "The biophysics and cell biology of lipid droplets," 2013, doi: 10.1038/nrm3699.
- [60] N. Kory, R. v. Farese, and T. C. Walther, "Targeting Fat: Mechanisms of Protein Localization to Lipid Droplets," *Trends in Cell Biology*, vol. 26, no. 7. Elsevier Ltd, pp. 535–546, Jul. 01, 2016. doi: 10.1016/j.tcb.2016.02.007.
- [61] M. Ingelmo-Torres *et al.*, "Hydrophobic and basic domains target proteins to lipid droplets," *Traffic*, vol. 10, no. 12, pp. 1785–1801, Dec. 2009, doi: 10.1111/j.1600-0854.2009.00994.x.
- [62] R. Dhiman, S. Caesar, A. R. Thiam, and B. Schrul, "Mechanisms of protein targeting to lipid droplets: A unified cell biological and biophysical perspective," *Seminars in Cell and Developmental Biology*, vol. 108. Elsevier Ltd, pp. 4–13, Dec. 01, 2020. doi: 10.1016/j.semcd.2020.03.004.
- [63] A. Chorlay and A. R. Thiam, "Neutral lipids regulate amphipathic helix affinity for model lipid droplets," *Journal of Cell Biology*, vol. 219, no. 4, Apr. 2020, doi: 10.1083/JCB.201907099.
- [64] A. Chorlay, A. Santinho, and A. R. Thiam, "Making Droplet-Embedded Vesicles to Model Cellular Lipid Droplets," *STAR Protoc*, vol. 1, no. 3, Dec. 2020, doi: 10.1016/j.xpro.2020.100116.
- [65] N. Kory, A. R. Thiam, R. v. Farese, and T. C. Walther, "Protein Crowding Is a Determinant of Lipid Droplet Protein Composition," *Dev Cell*, vol. 34, no. 3, pp. 351–363, Aug. 2015, doi: 10.1016/j.devcel.2015.06.007.
- [66] K. Römisch, "Cdc48p is UBX-linked to ER ubiquitin ligases," *Trends in Biochemical Sciences*, vol. 31, no. 1. Elsevier Ltd, pp. 24–25, 2006. doi: 10.1016/j.tibs.2005.11.004.
- [67] C. W. Wang and S. C. Lee, "The ubiquitin-like (UBX)-domain-containing protein Ubx2/Ubx8 regulates lipid droplet homeostasis," *J Cell Sci*, vol. 125, no. 12, pp. 2930–2939, Jun. 2012, doi: 10.1242/jcs.100230.
- [68] J. N. Lee *et al.*, "Identification of Ubx8 protein as a sensor for unsaturated fatty acids and regulator of triglyceride synthesis", doi: 10.1073/pnas.1011859107/-/DCSupplemental.
- [69] M. Suzuki *et al.*, "Derlin-1 and UBXD8 are engaged in dislocation and degradation of lipidated ApoB-100 at lipid droplets," 2012, doi: 10.1091/mbc.E11-11-0950.
- [70] J. K. Zehmer, R. Bartz, B. Biesel, P. Liu, J. Seemann, and R. G. W. Anderson, "Targeting sequences of UBXD8 and AAM-B reveal that the ER has a direct role in the emergence and regression of lipid droplets," *J Cell Sci*, vol. 122, no. 20, pp. 3694–3702, Oct. 2009, doi: 10.1242/jcs.054700.
- [71] H. Kim, H. Zhang, D. Meng, G. Russell, J. N. Lee, and J. Ye, "UAS domain of Ubx8 and FAF1 polymerizes upon interaction with long-chain unsaturated fatty acids," *J Lipid Res*, vol. 54, no. 8, pp. 2144–2152, Aug. 2013, doi: 10.1194/jlr.M037218.
- [72] B. Schrul and R. R. Kopito, "Peroxisome-dependent targeting of a lipid-droplet-destined membrane protein to ER subdomains," *Nat Cell Biol*, vol. 18, no. 7, pp. 740–751, Jun. 2016, doi: 10.1038/ncb3373.
- [73] A. Pol, R. Luetterforst, M. Lindsay, S. Heino, E. Ikonen, and R. G. Parton, "A Caveolin Dominant Negative Mutant Associates with Lipid Bodies and Induces Intracellular Cholesterol Imbalance 7," 2001. [Online]. Available: <http://www.jcb.org/cgi/content/full/152/5/1057>



- [74] G. Golani, N. Ariotti, R. G. Parton, and M. M. Kozlov, "Membrane Curvature and Tension Control the Formation and Collapse of Caveolar Superstructures," *Dev Cell*, vol. 48, no. 4, pp. 523-538.e4, Feb. 2019, doi: 10.1016/j.devcel.2018.12.005.
- [75] C. Matthaeus and J. W. Taraska, "Energy and Dynamics of Caveolae Trafficking," *Frontiers in Cell and Developmental Biology*, vol. 8. Frontiers Media S.A., Jan. 21, 2021. doi: 10.3389/fcell.2020.614472.
- [76] T. M. Williams and M. P. Lisanti, "The caveolin proteins," 2004. [Online]. Available: <http://genomebiology.com/2004/5/3/214>
- [77] J. C. Porta *et al.*, "Molecular architecture of the human caveolin-1 complex," 2022. [Online]. Available: <https://www.science.org>
- [78] S. Monier, R. G. Parton, F. Vogel, J. Behlke, A. Henske, and T. v Kurzchalia, "VIP21-Caveolin, a Membrane Protein Constituent of the Caveolar Coat, Oligomerizes In Vivo and In Vitro," 1995.
- [79] A. G. Ostermeyer, J. M. Paci, Y. Zeng, D. M. Lublin, S. Munro, and D. A. Brown, "Accumulation of Caveolin in the Endoplasmic Reticulum Redirects the Protein to Lipid Storage Droplets," 2001. [Online]. Available: <http://www.jcb.org/cgi/content/full/152/5/1071>
- [80] F. Â. de Â Ric Beaudoin, B. M. Wilkinson, C. J. Stirling, and J. A. Napier, "In vivo targeting of a sunflower oil body protein in yeast secretory (sec) mutants."
- [81] S. Turró *et al.*, "Identification and Characterization of Associated with Lipid Droplet Protein 1: A Novel Membrane-Associated Protein That Resides on Hepatic Lipid Droplets," *The Authors Journal compilation #*, vol. 7, pp. 1254–1269, 2006, doi: 10.1111/j.1600-0854.2006.00465.x.
- [82] M. J. Robenek *et al.*, "Lipids partition caveolin-1 from ER membranes into lipid droplets: updating the model of lipid droplet biogenesis.," *The FASEB journal : official publication of the Federation of American Societies for Experimental Biology*, vol. 18, no. 7, pp. 866–868, 2004, doi: 10.1096/fj.03-0782fje.
- [83] L. Lobos-González, L. Aguilar, G. Fernández, C. Sanhueza, and A. F. G. Quest, "Caveolin-1 in Melanoma Progression." [Online]. Available: [www.intechopen.com](http://www.intechopen.com)
- [84] H. Itabe, T. Yamaguchi, S. Nimura, and N. Sasabe, "Perilipins: a diversity of intracellular lipid droplet proteins," *Lipids in Health and Disease*, vol. 16, no. 1. BioMed Central Ltd., Apr. 28, 2017. doi: 10.1186/s12944-017-0473-y.
- [85] N. A. Ducharme and P. E. Bickel, "Minireview: Lipid droplets in lipogenesis and lipolysis," *Endocrinology*, vol. 149, no. 3. pp. 942–949, Mar. 2008. doi: 10.1210/en.2007-1713.
- [86] M. Giménez-Andrés *et al.*, "Exceptional stability of a perilipin on lipid droplets depends on its polar residues, suggesting multimeric assembly," *Elife*, vol. 10, 2021, doi: 10.7554/ELIFE.61401.
- [87] E. R. Rowe *et al.*, "Conserved amphipathic helices mediate lipid droplet targeting of perilipins 1-3," *Journal of Biological Chemistry*, vol. 291, no. 13, pp. 6664–6678, Mar. 2016, doi: 10.1074/jbc.M115.691048.

- [88] P. Targett-Adams *et al.*, “Live cell analysis and targeting of the lipid droplet-binding adipocyte differentiation-related protein,” *Journal of Biological Chemistry*, vol. 278, no. 18, pp. 15998–16007, May 2003, doi: 10.1074/jbc.M211289200.
- [89] L. Caillon *et al.*, “Triacylglycerols sequester monotopic membrane proteins to lipid droplets,” *Nat Commun*, vol. 11, no. 1, Dec. 2020, doi: 10.1038/s41467-020-17585-8.
- [90] R. Mani, S. D. Cady, M. Tang, A. J. Waring, R. I. Lehrer, and M. Hong, “Membrane-dependent oligomeric structure and pore formation of a-hairpin antimicrobial peptide in lipid bilayers from solid-state NMR,” 2006. [Online]. Available: [www.pnas.org/cgi/doi/10.1073/pnas.0605079103](http://www.pnas.org/cgi/doi/10.1073/pnas.0605079103)
- [91] R. B. Cornell, S. G. Taneva, M. K. Dennis, R. Tse, R. K. Dhillon, and J. Lee, “Disease-linked mutations in the phosphatidylcholine regulatory enzyme CCT impair enzymatic activity and fold stability,” *Journal of Biological Chemistry*, vol. 294, no. 5, pp. 1490–1501, Feb. 2019, doi: 10.1074/jbc.RA118.006457.
- [92] E. R. Rowe *et al.*, “Conserved amphipathic helices mediate lipid droplet targeting of perilipins 1-3,” *Journal of Biological Chemistry*, vol. 291, no. 13, pp. 6664–6678, Mar. 2016, doi: 10.1074/jbc.M115.691048.
- [93] D. Barneda *et al.*, “The brown adipocyte protein CIDEA promotes lipid droplet fusion via a phosphatidic acid-binding amphipathic helix,” *Elife*, vol. 4, Nov. 2015, doi: 10.7554/eLife.07485.
- [94] M. Hubert *et al.*, “Lipid accumulation controls the balance between surface connection and scission of caveolae,” *Elife*, vol. 9, pp. 1–31, May 2020, doi: 10.7554/eLife.55038.
- [95] A. Hayer, M. Stoeber, C. Bissig, and A. Helenius, “Biogenesis of caveolae: Stepwise assembly of large caveolin and cavin complexes,” *Traffic*, vol. 11, no. 3, pp. 361–382, Mar. 2010, doi: 10.1111/j.1600-0854.2009.01023.x.
- [96] C. M. Blouin *et al.*, “Lipid droplet analysis in caveolin-deficient adipocytes: Alterations in surface phospholipid composition and maturation defects,” *J Lipid Res*, vol. 51, no. 5, pp. 945–956, May 2010, doi: 10.1194/jlr.M001016.
- [97] P. Thomsen, K. Roepstorff, M. Stahlhut, and B. van Deurs, “Caveolae are highly immobile plasma membrane microdomains, which are not involved in constitutive endocytic trafficking,” *Mol Biol Cell*, vol. 13, no. 1, pp. 238–250, 2002, doi: 10.1091/mbc.01-06-0317.
- [98] P. F. Pilch, T. Meshulam, S. Ding, and L. Liu, “Caveolae and lipid trafficking in adipocytes,” 2011.
- [99] P. Thomsen, K. Roepstorff, M. Stahlhut, and B. van Deurs, “Caveolae are highly immobile plasma membrane microdomains, which are not involved in constitutive endocytic trafficking,” *Mol Biol Cell*, vol. 13, no. 1, pp. 238–250, 2002, doi: 10.1091/mbc.01-06-0317.
- [100] A. R. Thiam and I. Dugail, “Lipid droplet-membrane contact sites - From protein binding to function,” *Journal of Cell Science*, vol. 132, no. 12. Company of Biologists Ltd, Jun. 01, 2019. doi: 10.1242/jcs.230169.
- [101] A. Chorlay and A. R. Thiam, “An Asymmetry in Monolayer Tension Regulates Lipid Droplet Budding Direction,” *Biophys J*, vol. 114, no. 3, pp. 631–640, Feb. 2018, doi: 10.1016/j.bpj.2017.12.014.

- [102] A. Chorlay *et al.*, “Membrane Asymmetry Imposes Directionality on Lipid Droplet Emergence from the ER,” *Dev Cell*, vol. 50, no. 1, pp. 25–42.e7, Jul. 2019, doi: 10.1016/j.devcel.2019.05.003.
- [103] K. ben M’barek, D. Ajjaji, A. Chorlay, S. Vanni, L. Forêt, and A. R. Thiam, “ER Membrane Phospholipids and Surface Tension Control Cellular Lipid Droplet Formation,” *Dev Cell*, vol. 41, no. 6, pp. 591–604.e7, Jun. 2017, doi: 10.1016/j.devcel.2017.05.012.
- [104] V. Zoni, R. Khaddaj, P. Campomanes, A. R. Thiam, R. Schneider, and S. Vanni, “Pre-existing bilayer stresses modulate triglyceride accumulation in the er versus lipid droplets,” *Elife*, vol. 10, pp. 1–24, Feb. 2021, doi: 10.7554/eLife.62886.
- [105] A. Bacle, R. Gautier, C. L. Jackson, P. F. J. Fuchs, and S. Vanni, “Interdigitation between Triglycerides and Lipids Modulates Surface Properties of Lipid Droplets,” *Biophys J*, vol. 112, no. 7, pp. 1417–1430, Apr. 2017, doi: 10.1016/j.bpj.2017.02.032.
- [106] L. Vamparys *et al.*, “Conical lipids in flat bilayers induce packing defects similar to that induced by positive curvature,” *Biophys J*, vol. 104, no. 3, pp. 585–593, Feb. 2013, doi: 10.1016/j.bpj.2012.11.3836.
- [107] M. E. Haque and B. R. Lentz, “Roles of Curvature and Hydrophobic Interstice Energy in Fusion: Studies of Lipid Perturbant Effects †,” *Biochemistry*, vol. 43, p. 46, 2004, doi: 10.1021/bi035794j.
- [108] O. S. Ostroumova, S. S. Efimova, E. v Mikhailova, · Ludmila, and V. Schagina, “The interaction of dipole modifiers with amphotericin-ergosterol complexes. Effects of phospholipid and sphingolipid membrane composition,” *Eur Biophys J*, vol. 43, pp. 207–215, 2014, doi: 10.1007/s00249-014-0946-0.
- [109] N.-T. Nguyen, S. Wereley, and S. A. M. Shaegh, *Fundamentals and Applications of Microfluidics*, Third Edition. Artech, 2019.
- [110] G. M. Whitesides, “The origins and the future of microfluidics,” *Nature*, vol. 442, no. 7101, pp. 368–373, Jul. 27, 2006. doi: 10.1038/nature05058.
- [111] Y. Takei and T. Ishida, “How to select the best model from AlphaFold2 structures?,” doi: 10.1101/2022.04.05.487218.
- [112] V. Mariani, M. Biasini, A. Barbato, and T. Schwede, “IDDT: A local superposition-free score for comparing protein structures and models using distance difference tests,” *Bioinformatics*, vol. 29, no. 21, pp. 2722–2728, Nov. 2013, doi: 10.1093/bioinformatics/btt473.
- [113] R. Seemann, J.-B. Fleury, and S. Asfia, “Phospholipids Diffusion on the Surface of Model Lipid Droplets,” doi: 10.1101/2022.06.30.498225.
- [114] S. Puza, S. Asfia, R. Seemann, and J.-B. Fleury, “Bilayer-Embedded Lipid Droplets Coated with Perilipin-2 Display a Pancake Shape,” *Int J Mol Sci*, vol. 24, no. 3, p. 2072, Jan. 2023, doi: 10.3390/ijms24032072.
- [115] H. Bayley *et al.*, “Droplet interface bilayers,” *Mol Biosyst*, vol. 4, no. 12, pp. 1191–1208, 2008, doi: 10.1039/b808893d.

- [116] J. Jonkman, C. M. Brown, G. D. Wright, K. I. Anderson, and A. J. North, "Guidance for quantitative confocal microscopy," *Nat Protoc*, Mar. 2020, doi: 10.1038/s41596-020-0307-7.
- [117] H. C. Ishikawa-Ankerhold, R. Ankerhold, and G. P. C. Drummen, "Advanced fluorescence microscopy techniques-FRAP, FLIP, FLAP, FRET and FLIM," *Molecules*, vol. 17, no. 4. pp. 4047–4132, Apr. 2012. doi: 10.3390/molecules17044047.
- [118] J. Yguerabide, J. A. Schmidt, and E. E. Yguerabide, "Lateral mobility in membranes as detected by fluorescence recovery after photobleaching," *Biophys J*, vol. 40, no. 1, pp. 69–75, 1982, doi: 10.1016/S0006-3495(82)84459-7.
- [119] W. L. C. Vaz, D. Hallmann, R. M. Clegg, A. Gambacorta, and M. de Rosa, "European Biophysics Journal A comparison of the translational diffusion of a normal and a membrane-spanning lipid in La phase I-palmitoyl-2-oleoylphosphatidylcholine bilayers," 1985.
- [120] K. Braeckmans, K. Remaut, R. E. Vandenbroucke, B. Lucas, S. C. de Smedt, and J. Demeester, "Line FRAP with the confocal laser scanning microscope for diffusion measurements in small regions of 3-D samples," *Biophys J*, vol. 92, no. 6, pp. 2172–2183, 2007, doi: 10.1529/biophysj.106.099838.
- [121] G. Rayan, J.-E. Guet, N. Taulier, F. Pincet, and W. Urbach, "Recent Applications of Fluorescence Recovery after Photobleaching (FRAP) to Membrane Bio-Macromolecules," *Sensors*, vol. 10, pp. 5927–5948, 2010, doi: 10.3390/s100605927.
- [122] N. W. Goehring, D. Chowdhury, A. A. Hyman, and S. W. Grill, "FRAP analysis of membrane-associated proteins: Lateral diffusion and membrane-cytoplasmic exchange," *Biophys J*, vol. 99, no. 8, pp. 2443–2452, Oct. 2010, doi: 10.1016/j.bpj.2010.08.033.
- [123] J. Lippincott-Schwartz, E. L. Snapp, and R. D. Phair, "The Development and Enhancement of FRAP as a Key Tool for Investigating Protein Dynamics," *Biophysical Journal*, vol. 115, no. 7. Biophysical Society, pp. 1146–1155, Oct. 02, 2018. doi: 10.1016/j.bpj.2018.08.007.
- [124] F. Pincet *et al.*, "FRAP to characterize molecular diffusion and interaction in various membrane environments," *PLoS One*, vol. 11, no. 7, Jul. 2016, doi: 10.1371/journal.pone.0158457.
- [125] Y. H. M. Chan and S. G. Boxer, "Model membrane systems and their applications," *Current Opinion in Chemical Biology*, vol. 11, no. 6. pp. 581–587, Dec. 2007. doi: 10.1016/j.cbpa.2007.09.020.
- [126] M. Kang, C. A. Day, K. Drake, A. K. Kenworthy, and E. DiBenedetto, "A generalization of theory for two-dimensional fluorescence recovery after photobleaching applicable to confocal laser scanning microscopes," *Biophys J*, vol. 97, no. 5, pp. 1501–1511, Sep. 2009, doi: 10.1016/j.bpj.2009.06.017.
- [127] L. Zhang and S. Granick, "Lipid diffusion compared in outer and inner leaflets of planar supported bilayers," *J. Chem. Phys*, vol. 123, p. 211104, 2005, doi: 10.1063/1.2138699.
- [128] T. J. Pucadyil, S. Mukherjee, and A. Chattopadhyay, "Organization and Dynamics of NBD-Labeled Lipids in Membranes Analyzed by Fluorescence Recovery after Photobleaching," 2007, doi: 10.1021/jp066092h.
- [129] D. Blumenthal, L. Goldstien, M. Edidin, and L. A. Gheber, "Universal approach to FRAP analysis of arbitrary bleaching patterns," *Sci Rep*, vol. 5, Jun. 2015, doi: 10.1038/srep11655.

- [130] B. L. Sprague and J. G. McNally, "FRAP analysis of binding: Proper and fitting," *Trends in Cell Biology*, vol. 15, no. 2. pp. 84–91, Feb. 2005. doi: 10.1016/j.tcb.2004.12.001.
- [131] D. M. Soumpasis, "Theoretical analysis of fluorescence photobleaching recovery experiments," *Biophys J*, vol. 41, no. 1, pp. 95–97, 1983, doi: 10.1016/S0006-3495(83)84410-5.
- [132] D. Axelrod, D. E. Koppel, J. Schlessinger, E. Elson, and W. W. Webb, "Mobility measurement by analysis of fluorescence photobleaching recovery kinetics," *Biophys J*, vol. 16, no. 9, pp. 1055–1069, 1976, doi: 10.1016/S0006-3495(76)85755-4.
- [133] B. Sakmann and E. Neher, "PATCH CLAMP TECHNIQUES FOR STUDYING IONIC CHANNELS IN EXCITABLE MEMBRANES," 1984. [Online]. Available: [www.annualreviews.org](http://www.annualreviews.org)
- [134] J. D. Berry, M. J. Neeson, R. R. Dagastine, D. Y. C. Chan, and R. F. Tabor, "Measurement of surface and interfacial tension using pendant drop tensiometry," *Journal of Colloid and Interface Science*, vol. 454. Academic Press Inc., pp. 226–237, Sep. 05, 2015. doi: 10.1016/j.jcis.2015.05.012.
- [135] M. J. Abraham *et al.*, "Gromacs: High performance molecular simulations through multi-level parallelism from laptops to supercomputers," *SoftwareX*, vol. 1–2, pp. 19–25, 2015, doi: 10.1016/j.softx.2015.06.001.
- [136] S. J. Marrink, H. J. Risselada, S. Yefimov, D. P. Tieleman, and A. H. de Vries, "The MARTINI force field: Coarse grained model for biomolecular simulations," *Journal of Physical Chemistry B*, vol. 111, no. 27, pp. 7812–7824, Jul. 2007, doi: 10.1021/jp071097f.
- [137] J. N. Vargas, R. Seemann, and J. B. Fleury, "Fast membrane hemifusion via dewetting between lipid bilayers," *Soft Matter*, vol. 10, no. 46, pp. 9293–9299, Nov. 2014, doi: 10.1039/c4sm01577k.
- [138] J. B. Fleury, M. Werner, X. le Guével, and V. A. Baulin, "Protein corona modulates interaction of spiky nanoparticles with lipid bilayers," *J Colloid Interface Sci*, vol. 603, pp. 550–558, Dec. 2021, doi: 10.1016/j.jcis.2021.06.047.
- [139] A. Chen and V. T. Moy, "Cross-Linking of Cell Surface Receptors Enhances Cooperativity of Molecular Adhesion," 2000.
- [140] M. Garten, L. D. Mosgaard, T. Bornschlöggl, S. Dieudonné, P. Bassereau, and G. E. S. Toombes, "Whole-GUV patch-clamping," *Proc Natl Acad Sci U S A*, vol. 114, no. 2, pp. 328–333, Jan. 2017, doi: 10.1073/pnas.1609142114.
- [141] D. P. Nikolelis+ and U. J. Krull~, "RELIABLE AND FACILE METHOD FOR PREPARATION OF SOLVENTLESS BILAYER LIPID MEMBRANES FOR ELECTROANALYTICAL INVESTIGATIONS," 1992.
- [142] T. Wang, C. Ingram, and J. C. Weisshaar, "Model lipid bilayer with facile diffusion of lipids and integral membrane proteins," *Langmuir*, vol. 26, no. 13, pp. 11157–11164, Jul. 2010, doi: 10.1021/la101046r.
- [143] M. Przybylo *et al.*, "Lipid Diffusion in Giant Unilamellar Vesicles Is More than 2 Times Faster than in Supported Phospholipid Bilayers under Identical Conditions," 2006, doi: 10.1021/la061934p.
- [144] A. L. S. Cruz, E. D. A. Barreto, N. P. B. Fazolini, J. P. B. Viola, and P. T. Bozza, "Lipid droplets: platforms with multiple functions in cancer hallmarks", doi: 10.1038/s41419-020-2297-3.

- [145] K. Tauchi-Sato, S. Ozeki, T. Houjou, R. Taguchi, and T. Fujimoto, "The surface of lipid droplets is a phospholipid monolayer with a unique fatty acid composition," *Journal of Biological Chemistry*, vol. 277, no. 46, pp. 44507–44512, Nov. 2002, doi: 10.1074/jbc.M207712200.
- [146] M. J. Greenall and C. M. Marques, "Hydrophobic droplets in amphiphilic bilayers: a coarse-grained mean-field theory study", doi: 10.1039/c2sm07193b.
- [147] P. A. Ferrari, S. Goldstein, and J. L. Lebowitz, *Statistical Physics and Dynamical Systems: Rigorous Results*. Boston, MA: Progress in Physics, Birkhäuser, 1985.
- [148] C. S. Poojari, K. C. Scherer, and J. S. Hub, "Free energies of membrane stalk formation from a lipidomics perspective," *Nat Commun*, vol. 12, no. 1, Dec. 2021, doi: 10.1038/s41467-021-26924-2.
- [149] L. v. Chernomordik and M. M. Kozlov, "Mechanics of membrane fusion," *Nature Structural and Molecular Biology*, vol. 15, no. 7. pp. 675–683, Jul. 2008. doi: 10.1038/nsmb.1455.
- [150] V. Choudhary *et al.*, "Architecture of Lipid Droplets in Endoplasmic Reticulum Is Determined by Phospholipid Intrinsic Curvature," *Current Biology*, vol. 28, no. 6, pp. 915–926.e9, Mar. 2018, doi: 10.1016/j.cub.2018.02.020.
- [151] C. P. Najt *et al.*, "Structural and functional assessment of perilipin 2 lipid binding domain(s)," *Biochemistry*, vol. 53, no. 45, pp. 7051–7066, Nov. 2014, doi: 10.1021/bi500918m.
- [152] T. Takei, T. Yaguchi, T. Fujii, T. Nomoto, T. Toyota, and M. Fujinami, "Measurement of membrane tension of free standing lipid bilayers via laser-induced surface deformation spectroscopy," *Soft Matter*, vol. 11, no. 44, pp. 8641–8647, 2015, doi: 10.1039/c5sm01264c.
- [153] B. A. Brüning *et al.*, "Bilayer undulation dynamics in unilamellar phospholipid vesicles: Effect of temperature, cholesterol and trehalose," *Biochim Biophys Acta Biomembr*, vol. 1838, no. 10, pp. 2412–2419, 2014, doi: 10.1016/j.bbamem.2014.06.006.
- [154] V. Zoni, R. Khaddaj, P. Campomanes, A. R. Thiam, R. Schneiter, and S. Vanni, "Pre-existing bilayer stresses modulate triglyceride accumulation in the er versus lipid droplets," *Elife*, vol. 10, pp. 1–24, Feb. 2021, doi: 10.7554/eLife.62886.
- [155] L. Vamparys *et al.*, "Conical lipids in flat bilayers induce packing defects similar to that induced by positive curvature," *Biophys J*, vol. 104, no. 3, pp. 585–593, Feb. 2013, doi: 10.1016/j.bpj.2012.11.3836.
- [156] K. Murzyn, T. Róg, and M. Pasenkiewicz-Gierula, "Phosphatidylethanolamine-phosphatidylglycerol bilayer as a model of the inner bacterial membrane," *Biophys J*, vol. 88, no. 2, pp. 1091–1103, 2005, doi: 10.1529/biophysj.104.048835.
- [157] G. Cevc, *Phospholipids Handbook*. CRC Press, 1993.
- [158] O. G. Mouritsen, "Lipids, curvature, and nano-medicine," *European Journal of Lipid Science and Technology*, vol. 113, no. 10, pp. 1174–1187, Oct. 2011, doi: 10.1002/ejlt.201100050.
- [159] F. A. Heberle *et al.*, "Bilayer thickness mismatch controls domain size in model membranes," *J Am Chem Soc*, vol. 135, no. 18, pp. 6853–6859, May 2013, doi: 10.1021/ja3113615.

- [160] S. Kara, S. Afonin, O. Babii, A. N. Tkachenko, I. v. Komarov, and A. S. Ulrich, "Diphytanoyl lipids as model systems for studying membrane-active peptides," *Biochim Biophys Acta Biomembr*, vol. 1859, no. 10, pp. 1828–1837, Oct. 2017, doi: 10.1016/j.bbamem.2017.06.003.